DISSERTATION

BIOMIMETIC AND ANTIMICROBIAL SURFACES FOR ORTHOPEDIC IMPLANTS

Submitted by

Tara Wigmosta

School of Biomedical Engineering

In partial fulfillment of the requirements

For the Degree of Doctor of Philosophy

Colorado State University

Fort Collins, Colorado

Spring 2021

Doctoral Committee:

Advisor: Matt Kipper
Co-Advisor: Ketul Popat

Brian Giess
Susan DeLong
Alan Schenkel

ABSTRACT

BIOMIMETIC AND ANTIMICROBIAL SURFACES FOR ORTHOPEDIC IMPLANTS

The number of total knee and hip replacement surgeries is expected to continue to rise in the United States. As such, the number of revision surgeries is also expected to rise. The two most common causes of failure for these implants is aseptic loosening, caused by incomplete osseointegration, and infection. Therefore, preventing infection while increasing the osteogenic properties of the surfaces used in orthopedic implants could reduce the number of revision surgeries.

It is the goal of this work to create nanostructured surfaces that both increase mineralization and antimicrobial properties of titanium surfaces commonly used in orthopedic implants. To accomplish this, chitosan/heparin polyelectrolyte multilayers (PEMs), with the addition of either bone morphogenetic protein 2 (BMP-2) or gentamicin, were adsorbed onto titania nanotubes. BMP-2 has been used in clinical applications to increase osseointegration in spinal fusions, and gentamicin is effective against the most common pathogens found in infected orthopedic implants. Both heparin and chitosan are biocompatible and have antimicrobial properties. BMP-2 has a binding site for heparin that increases BMP-2's half-life *in vitro*.

The first chapter summarizes the motivation and previous strategies used to increase osseointegration and antimicrobial properties of nanostructured biomimetic orthopedic implant surfaces. The first chapter concludes with a shift in hypothesis testing, outlining three different hypotheses: 1) surface modification(s) increase cytocompatibility and the osteogenic properties of mammalian bone cells; 2) surface modification(s) reduce bacterial adhesion,

proliferation, and infection rate, without decreasing cytocompatibility; and 3) surface modification(s) provide a favorable environment in which mammalian cells can beat bacterial cells and colonize the surface first, thus increasing the osteogenic and antimicrobial properties of the surface. The testing of these hypotheses are explored in chapters 2 through 4. The second chapter explores hypothesis 1) by testing if BMP-2 released from chitosan/heparin PEM coated titania nanotubes surfaces induce an osteogenic response from rat bone marrow cells. Chapter 3 explores hypothesis 2) by testing if *iota*-carrageenan/chitosan and pectin/chitosan PEMs have antimicrobial properties against *Pseudomonas aeruginosa* (*P. aeruginosa*) and *Staphylococcus aureus* (*S. aureus*), and support rat bone marrow cell adhesion and proliferation. The last chapter explores hypothesis 3) by testing if gentamicin released from titania nanotubes coated with chitosan/heparin PEMs influences the "race to the surface" in favor of mammalian cells.

ACKNOWLEDGMENTS

I would like to thank all the amazing scientists, staff, students, and coworkers who helped me throughout my PhD. First I would like to thank my advisor Dr. Matt Kipper and co-advisor Dr. Ketul Popat. Dr. Kipper, thank you for being an exceptional mentor throughout my time at CSU. Your excitement and passion for research is something that has motivated me throughout my work here at CSU and is something I will take with me as I continue my career in research. Dr. Popat, thank you for your continued support here at CSU, from help with research to teaching. I have modeled some of my own teaching and mentorship based on your compassion and care for your students, both in the lab and in the classroom. Thank you both for your endless support and patience. My time at CSU would not have been as enjoyable, rewarding, and educational without your mentorship.

Next, I would like to thank my committee members. Thank you Dr. Brian Giess. You were the first faculty that I worked with at CSU. Working with you my first semester set a great first impression of graduate school while providing me with fundamental skills I used throughout my PhD. Dr. Susan De long, thank you for stepping in last minute before my preliminary exam. I enjoyed working with you as a TA, you taught me how to teach students laboratory techniques, both in the classroom and in the lab. These were valuable skills I still use to help mentor students and will carry with me. Thank you, Dr. Alan Schenkel, for your valuable feedback on my research plans. My research goals would not have been as successful without your help.

I would also like to thank all of the students I worked with during my time here. From the Kipper lab, thank you, Dr. Hasan Hedayati, Jessi Vlcek, Dafu Wang, and Dr. Liszt Yeltsin. From

the Popat lab, thank you, Roberta Maia Sabin and Vignesh Manivasagam. All of you have helped me tremendously in the lab, both with research and emotional support. My time here at CSU would not have been as enjoyable or fulfilling without your continued support, friendship, and advice. Thank you as well, to all the other students who helped me throughout my PhD.

Lastly, I would like to thank my family, especially my parents and Jacob Garritson, for continued your love and support throughout this journey.

The following akcnoledgements are for the financial support for each chapter. Chapter 2: This work was supported by the National Institutes of Health under award numbers 5R01HL135505 and 5R21HL139208. Chapter 3: A.F. Martins thanks "National Council for Scientific and Technological Development – CNPq" for financial support (protocol 0008678964988973). Chapter 4: This work was supported by the National Institutes of Health under award numbers 5R01HL135505 and 5R21HL139208.

DEDICATION

My family

TABLE OF CONTENTS

CHAPTER 1: PREVENTING TOTAL KNEE AND HIP IMPLANT FAILURE: CURRENT TECHNOLOGIES AND RECENT ADVANCEMENTS

Overview

Complete joint replacement surgeries, such as knee and hip replacements, are widely used and effective treatment for joint disease. However, many of these implants fail and require revision surgery. The two most common causes of revision surgery are aseptic loosening and infection. Surfaces modifications, surface coatings, and drug delivery are common strategies used to prevent implant failure due to the two most common causes. This review focuses on the motivation and strategies used to develop dual-functioning drug-delivering nanostructured surfaces. The strategies summarized here represent the testing of three main hypotheses: 1) surface modification(s) increase cytocompatibility and the osteogenic properties of mammalian bone cells; 2) surface modification(s) reduce bacterial adhesion, proliferation, and infection rate, without decreasing cytocompatibility; and 3) surface modification(s) provide a favorable environment in which mammalian cells can beat bacterial cells and colonize the surface first, thus increasing the osteogenic and antimicrobial properties of the surface.

1.1 Introduction

1.2 Overview of Orthopedic Implants

Complete joint replacement is a widely used and effective treatment for patients with injured or diseased joints. Those with end-stage joint deterioration due to osteoarthritis or rheumatoid arthritis make up the largest group of those considered for surgery.[1] Total joint replacement causes a substantial improvement in physical health, including a reduction in chronic

pain and improved physical functioning.[1] There are currently over 1 million total knee and hip implants performed annually in the United States.[2] Elderly patients suffering from joint deterioration due to osteoarthritis or rheumatoid arthritis make up the majority of these surgeries.[3] It is projected that the population of people aged 65 years or older in the US will more than double from 40.2 million in 2010 to 88.5 million by 2050.[4] As a result, the number of complete joint replacement surgeries is expected to increase to over 4 million by 2030.[5]

While most complete joint replacement surgeries are successful, over 60,000 revision surgeries due to implant failure are performed annually.[6] Revision surgeries are costly and expose patients to risks associated with infection and anesthesia. Patients that undergo revision surgery also experience significant decreases in physical functioning compared to those that have only a primary surgery.[1] The most common cause of orthopedic implant failure is aseptic loosening of the implant from the surrounding bone tissue, followed by failure of the implant due to infection.[5,7]

1.3 Implant Loosening and Osteointegration

In cementless arthroplasties, one of the key determinants of risk of aseptic loosening is the degree of osseointegration of the surface to the bone.[3] Implant loosening is caused by the inability of an implant surface to integrate with the adjacent bone and other tissues due to physiological loads giving rise to implant-bone relative micromovements.[8] To prevent loosening it is essential to have materials that promote the integration of the implant with the surrounding bone.[9] Osseointegration is the stable anchorage of an implant achieved by direct bone-to-implant contact.[10] The higher the degree of osseointegration that takes place, the higher mechanical stability and the lower the probability of implant instability.[9] Surface chemistry, roughness, and topography all play an important role in good osseointegration of the implant.[9]

Mineralization is one of the first steps to osseointegration. The cells responsible for new bone formation and mineralization are osteoblasts. Mineralization occurs in two phases (**Figure 1.1**). The first phase, phase one, of mineralization takes place in matrix vesicles released from osteoblasts. At the start of mineralization alkaline phosphatase (ALP) increases the generation of inorganic phosphate and internal transport into the vesical.[11–13] After ALP activity peaks, calcium, and inorganic phosphate are internalized into the vesical. In the vesical, they form non-crystalline amorphous CaP that is then converted into octa-CaP crystals, and then eventually into insoluble hydroxyapatite crystals. After this, the next phase, phase 2, of mineralization occurs. During phase two of mineralization, hydroxyapatite is released from the vesicle, and extra-vesicular Ca^{2+} and P_i increases.[14] With the increase of extra-vesicular Ca^{2+} and P_i, binding proteins including osteocalcin regulate the continued nucleation of hydroxyapatite crystals and the formation of new bone.[13] The above-mentioned markers are all used as markers for osseointegration and new bone formation.

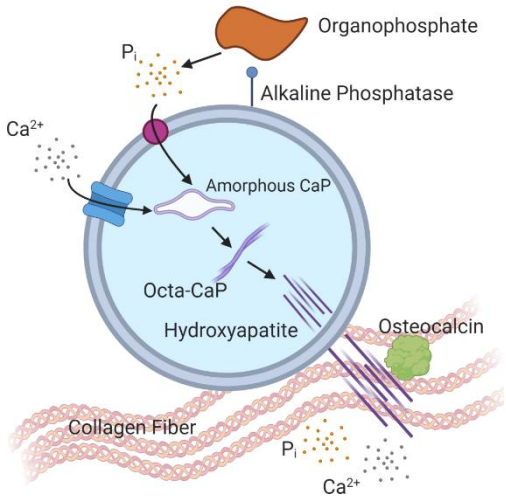

Figure 1.1: A representative schematic of a matrix vesical during mineralization. Phase I is the increase of ALP activity and the uptake of P_i and Ca^{2+} into the matrix vesical. The ions then form non-crystalline amorphous CaP, which is then converted into octa-CaP crystals and then into hydroxyapatite crystals. Phase II hydroxyapatite is released from the vesicle and extra-vesicular Ca^{2+} and P_i and binding proteins, including osteocalcin, regulate the continued nucleation of hydroxyapatite crystals and the formation of new bone. *Created with BioRender.com*

1.3.1 Changes in Surface Roughness and Topography Increase Osteogenic Properties of Cells

Surface roughness has been shown to affect both osteoblast adhesion and differentiation.[3,15–17] Rough surfaces, created by wet-grinding of pure titanium and Ti-6A1-4V alloy, increased ALP activity and osteocalcin production when compared to smooth surfaces.[16] While surface roughness increases osteogenic properties of osteoblast-like cells, roughness has also been shown to inhibit the cells responsible for bone removal, osteoclasts.[3,15,18] A study done by Bjursten *et al.*[19] implanted rabbits with titania disks with either nanotube or grit-blasted surfaces. After four weeks of implantation in the tibias, pull-out testing showed a significantly increased bone-bonding strength in nanotube surfaces by nine-fold compared to grit-blasted surfaces. Histological analysis confirmed greater bone-implant contact area, new bone formation, and calcium and phosphorus levels on the nanotubes surfaces compared with the grit-blasted surfaces.[19] This study suggests that nanotubes enhance bone bonding to implants *in vivo*. Currently, there are multiple implants in clinical use that contain surface micro-pits and depressions. These surfaces show an increase in osteointegration when compared to smooth implants *in vivo*.[3]

Bone cements composed of polymethyl methacrylate (PMMA) are primarily used to transfer forces from bone to prosthesis; however, these cements have poor cytocompatibility and osteointegration.[10,20,21] The incorporation of multi-walled carbon nanotube powders into PMMA bone cement increased cell adhesion and proliferation of rat bone marrow mesenchymal stem cells *in vitro*.[21] *In vivo* it was found that when implanted in rabbits PMMA containing carbon nanotubes had significantly more bone integration by 12 weeks compared to PMMA controls.[21]

Nanotopographical structures enhance bone formation both *in vitro* and *in vivo*.[18,19,22–25] Our group has fabricated novel nanotubular titania surfaces using an anodization process. This

process uniformly modifies titanium surfaces with titania nanotubes.[26] The nanotube formation starts when a dense layer of titanium-oxide (titania) forms on the surface. Then small pores form. Adjacent small pores integrate and become large pores, and at the same time, small tubes are formed. These small tubes continue to integrate into larger tubes until the main tubes are formed (**Figure 1.2**).[27] Our group has demonstrated that titania nanotube surfaces provide a favorable template for bone cell growth and differentiation. Nanotube surfaces support higher cell adhesion, proliferation, and viability for up to 7 days in culture compared to titanium surfaces. Cells cultured on nanotube surfaces demonstrate higher alkaline phosphatase (ALP) activity, and improved calcium and phosphorus accumulation. This suggests that osteoblast activity can be significantly enhanced using controlled nanotopographies such as nanotubes.[26] Further studies on bone formation on nanotube surfaces have been conducted. A study by Ballo *et al.* histologically evaluated bone growth on implants after 7 and 28 days.[18] Implants had topographical nanostructures with well-defined semispherical protrusions and variable sizes (60nm, 120 nm, and 220 nm). Surfaces with 60 nm features had significantly higher bone-implant contact compared to 120 nm and 220 nm surfaces.

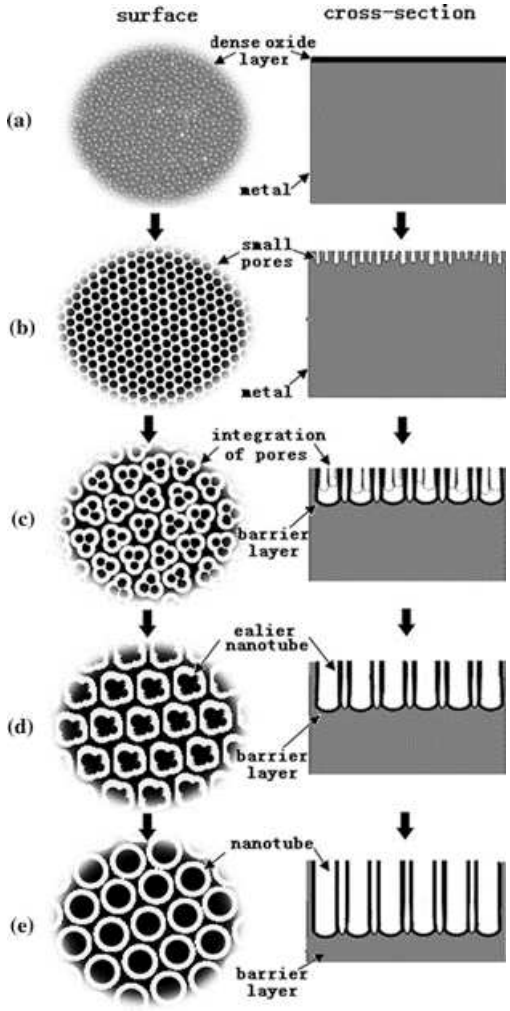

Figure 1.2: Schematic diagram of the evolution of straight nanotubes at a constant anodization voltage, as follows: (a) dense oxide layer formation, (b) pore formation and deepening, (c) integration of some adjacent small pores into a big one, (d) earlier nanotube arrays formation, and (e) perfect nanotube arrays formation. *Reproduced with permission from* [27] *copyright 2008, Journal of Material Science*

1.3.2 Surface Modifications and Coatings to Increase Osteointegration

Materials currently used for implants include 316L stainless steel, cobalt-chromium (Co-Cr) alloys, titanium and titanium alloys. A major problem with stainless steel and Co-Cr alloys are the toxic effects of nickel (Ni), cobalt (Co), and chromium (Cr) metals released from implants due to corrosion in the environment of the body.[9,28] Furthermore, these materials usually do not have a biologically active surface that encourages osseointegration. To increase the osseointegration

properties of these surfaces there has been increasing research on developing surfaces with various coatings.[3]

Hydroxyapatite (HA) is an integral part of bone mineral.[13] HA as a coating and as a porous surface, has been shown to increase osteogenic markers both *in vitro* and *in vivo*.[29–31] MC3T3-E1 osteoblasts showed a significant increase in ALP activity and messenger RNA (mRNA) transcripts for early-stage osteoblast markers, when grown on HA compared to plastic surfaces.[29] These coatings have also been studied in human clinical trials.[32–35] An article by Voigt *et al.* reviewed 14 studies on primary total knee implants between 1990 and 2010. It was found that in patients 65 years of age and older HA-coated tibial implants may provide better durability than other forms of tibial fixation.[34] Conversely, a review by Goosen *et al.*, which looked at eight studies compared uncemented HA-coated primary total hip arthroplasty to non-coated uncemented implants. Radiological data revealed equal endosteal bone ingrowth in the surface of the prosthesis, showing no difference between the two implants.[35]

Metal implants that have not been modified usually have a bio-inert hydrophobic surface. Therefore, to overcome this problem, surfaces can be functionalized with hydroxyl groups (−OH), to impart hydrophilicity.[3,36,37] To determine the role of functional groups on titanium implants, a study by Lu *et al.* used self-assembled monolayer (SAM) technique to introduce various functional layers onto the titanium surfaces. They showed that HA could be deposited on surfaces with $-PO_4H_2$ and −COOH functional group, but not those with $-CH{=}CH_2$ and -OH. By adding just −OH groups did not decrease the contact angle of the surfaces by more than one % where $-PO_4H_2$ and −COOH decreased the contact angle compared to Ti by over 20 %.[36] The addition of calcium hydroxide ($Ca(OH)_2$) to porous Ti created a complete carbonated apatite coating after 14 days soaking in modified simulated body fluid (m-SBF).[37] Calcium, phosphorous, magnesium and

fluoride ions have also been incorporated into surfaces and shown promise at promoting osteointegration.[3,38–40]

1.3.3 Growth Factors

Growth factors have been incorporated into scaffolds for bone tissue engineering; however, these techniques use super-physiological amounts of growth factors with inconsistent growth factor release. The use of large amounts of growth factor can result in nonspecific delivery and overgrowth of the tissue with the potential for unsafe side effects.[41]

Bone morphogenic proteins (BMPs) have been extensively researched because of their ability to induce bone and cartilage development[42]. The first BMP was isolated in the 1980s with the crystal structure of human BMP-2 and BMP-7 published in the 1990s. BMPs are part of the transforming growth factor beta (TGF-β) superfamily and are multifunctional cytokines. BMPs are divided into four subfamilies depending on sequence and function: (1) BMPs 2 and 4, (2) BMPs 5, 6, 7, 8a and 8b, (3) BMPs 9 and 10, and (4) BMPs 12, 13 and 14. BMP-2, BMP-4, and BMP-7 have osteogenic potential.[43]

Bone morphogenic protein-2 (BMP-2) is useful for the treatment of critical-sized bone defects with results comparable to autologous bone grafts.[42] The use of BMP-2 for the treatment of tibial fractures was investigated by the Surgery for Tibial Trauma (BESTT-ALL) trial.[44] In this study, 450 patients with an open tibial fracture were randomized to receive either the standard of care, the standard of care, and an implant containing 0.75 mg/ml of rhBMP-2, or standard of care and an implant containing 1.50 mg/ml rhBMP-2. When patients were re-examined at 12 months post-surgery, the 1.50 mg/ml rhBMP-2 group had a 44% reduction in the risk of failure, significantly fewer invasive interventions, and significantly faster fracture true-healing, when compared with control patients.[44] Because of BMP-2's success in bone healing, it has been

approved by the Food and Drug Administration (FDA) and used in spinal fusions since 2002.[45] Two BMPs are currently available for clinical applications, recombinant human BMP-2 (rhBMP-2, (INFUSE); Medtronic Sofamor Danek, Memphis) and rhBMP-7 (osteogenic protein 1 (OP-1), Stryker Biotech, Hopkinton, MA).[42] Most products use a high dose of BMP-2 to compensate for the short half-life *in vivo* (1-4 hours).[41,46] The INFUSE product uses a high dose of BMP-2 (1.5mg/ml).[47] In June 2008 the FDA issued a Public Health Notification of life-threatening complications associated with rhBMP-2 use.[41] These complications included swelling of the neck and throat tissue, which resulted in compression of the airway and/or neurological structures of the neck, and some reports difficulty swallowing, breathing, or speaking.[41]

Because of the safety concerns associated with higher doses of BMP-2, work has been done on incorporating lower concentrations of it into scaffolds for use in bone tissue engineering.[48–50] One solution is to use polyelectrolyte multilayers (PEMs) to provide tunable growth factor concentration and release.[51,52] Polyelectrolyte multilayers (PEMs) are prepared by layer-by-layer (LbL) assembly of polyelectrolytes to produce highly tunable thin-film polymer coatings.[52] PEMs self-assemble due to the electrostatic interactions between the oppositely charged and sequentially deposited polyelectrolytes.[53] BMP-2 has a binding site for heparin that modulates its bioactivity.[54] In the presence of heparin, degradation of BMP-2 was blocked and the half-life in culture media was prolonged by nearly 20-fold.[55] Our group has shown that chitosan-heparin polyelectrolyte multilayers (PEMs) and polyelectrolyte complexes can bind and stabilize growth factors, preserving growth factor activity for weeks in physiological pH and temperature, and enabling their presentation to cells in a context that enhances growth factor activity.[56–58] *In vitro* release results demonstrated that different biologically relevant amounts of heparin-bound

growth factors, FGF-2 and TGF-β1, can be delivered from chitosan-heparin polyelectrolyte multilayers.[59]

A previous study by Hu *et al.* incorporated BMP-2 into PEMs on titanium foil to increase osteogenesis.[60] Chitosan/gelatin multilayers were constructed onto Ti6Al4V surfaces. A loading amount of rhBMP-2 (273.83 ng/substrate) was added to the surfaces and showed an increase in ALP activity and mineralization *in vitro* and increased bone density and bone formation *in vivo* when implanted in rabbits.[60] Another study conjugated BMP-2 onto titania nanotube surfaces using dopamine.[61] Surfaces with conjugated BMP-2 saw an increase in ALP and mineralization after 7 and 14 days. The total concentration of BMP-2 onto surfaces was not reported, and samples were incubated in 50 ml of 80 ng/ml rhBMP-2.[61]

1.4 Implant Infection

While the leading cause of implant failure is loosening, the second most common cause of implant failure is infection.[7,62] In some cases, infection necessitates removal of the implant, followed by a delay in revision surgery to re-implant a new prosthesis. This causes the patients to have increased periods of immobility and a higher chance of reinfection and loosening associated with another surgery.[3] Infection occurs either at the time of the operation or later via the bloodstream.[63] Most infections occur when bacteria are introduced directly into the patient during, or soon after, surgery; individuals moving around the operating room contribute the largest portion of pathogenic bacteria in the wound.[63,64] The presence of clotted blood and compromised soft tissue in the surgical wound make it ideal for bacterial colonization.[64] Bacteria and adhesion and colonization occur in two phases (**Figure 1.3**).[65] Phase I occurs during the first 1-2 hours and Phase II occurs during the next 2-3 hours.[65] The most common pathogens in orthopedic implant-associated infections are *Staphylococcus epidermidis* (*S. epidermidis,* 32%) and *Staphylococcus*

aureus (*S.* aureus, 34%).[7] The prevalence of *S. epidermidis* as the pathogenic organism for infections of prosthetic joints is increasing.[63]

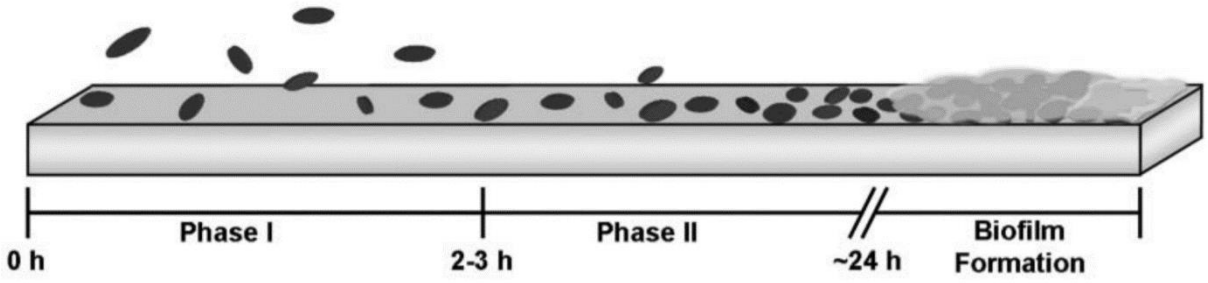

Figure 1.3: Representation of bacterial adhesion to a biomaterial substrate. Phase I adhesion involves reversible cellular association with the surface. During Phase II, bacteria undergo irreversible molecular bridging with the substrate through cellular surface adhesin compounds. After approximately 1 d, certain bacterial species are capable of secreting a protective exopolysaccharide matrix (biofilm) that protects the adhered bacteria from host defenses and systemically-administered antibiotics. *Reproduced with permission from* [76] *copyright 2006, The Royal Society of Chemistry*

1.4.1 Preventing Infection with coatings

There have been multiple studies on surface modification including coating of devices to prevent infection, using surfactants, proteins such as albumin, and polysaccharides such as heparin and chitosan.[66–68] The chemical structure of heparin is shown below (**Figure 1.4**).

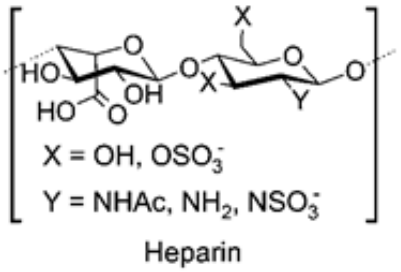

Figure 1.4: The chemical structure of heparin

Silver and silver coatings increase the antimicrobial properties of surfaces.[69–71] $AgNO_3$ causes the cytoplasm membrane to detach from the cell wall in both *E. coli* and *S. aureus*.[69] HA

coatings were S. doped with $AgNO_3$, which reduced the number of *S. aureus* and *E. coli* present on the surface while maintaining cell proliferation and differentiation of human embryonic palatal mesenchyme cells (HEPM).[70] Silver-coated titanium implants were implanted in rabbits and compared to normal titanium implants. There was a significant decrease in the infection rate of 47% in rabbits with titanium implants to 7% in rabbits with silver-coated implants.[71] While promising *in vitro* and in animal studies, there have been a few human trials with fixation pins, that have shown no significant difference in infection rate between titanium pins and silver-coated titanium pins.[72,73] One of the studies even had to be discontinued because there was a significant increase in silver serum levels of the patients, along with no statistical difference in infection rate.[72]

Nitric Oxide (NO) is a small molecule produced in the body, as a natural immune defense, that acts as a vasodilator, neurotransmitter, and anti-thrombogenic and antimicrobial agent.[74–77] Bacterial infections stimulate macrophages to produce NO, which is a strong oxidizing agent. NO diffuses across the bacteria cell and targets important structures within the cells, including DNA and proteins.[65] NO released from materials is effective against multiple strains of gram-positive and gram-negative bacteria and is not prone to drug resistance.[76] NO-releasing polysaccharide derivative proved effective against *E. coli, Acinetobacter baumannii* (*A. baumannii*), and *S. aureus*, by reducing bacterial growth by an 8-log reduction after 24 hours.[76] To study anti-thrombogenic properties, titania nanotube NO-releasing surfaces have been developed.[75]

Chitosan is a polysaccharide derived from crustaceans and is biocompatible for a range of tissue engineering applications.[3] The chemical structure of chitosan is shown below (**Figure 1.5**). Chitosan has also been used in biomaterials for its anti-microbial properties.[78–80] Chitosan is a positively charged polysaccharide and has thus been used in PEMs to coat surfaces and increase antimicrobial properties.[3,75,80,81]

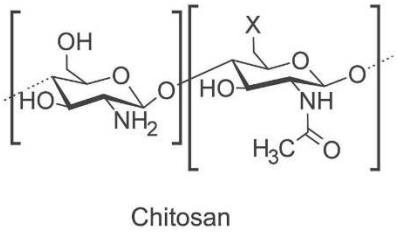

Chitosan

Figure 1.5: The chemical structure of Chitosan

Another surface modification is the ultraviolet (UV) treatment of titanium oxide. When treated with UV light, superoxide and hydroxyl ions form on the surface. These ions cause oxidative damage to the bacterial membranes.[3] Titanium and titanium oxide (TiO_2) pins were inserted into rabbits and then inoculated with methicillin-resistant *S. aureus* (MRSA). Pins were then treated with ultraviolet A (UVA) light for 60 min per day for seven days and the number of colonies formed was measured. The TiO_2 pins had significantly less bacteria *in vivo*.[82] While UVA treatment of pins was successful in rabbits, it can have unsafe side effects. To overcome the concerns of treating with UVA, carbon-containing TiO_2 can also be made photoactive under visible-light and provide bacteria-killing properties against *S. aureus*, *Shigella flexneri*, and *Acinetobacter baumannii*.[83] While both of these techniques show promise, they would be impractical for implants that are not exposed to air and therefore difficult to expose to light (UVA or visible).

1.4.2 Antibiotic Delivery

Antibiotic-delivering matrices and coatings are used to help prevent post-operative infections of complete joint replacement surgeries. By controlling the release of antibiotics directly from the implant, high doses of the drug can be delivered without exceeding the systemic toxicity level of the drug.[65] Antibiotics including, gentamicin, amoxicillin, tobramycin, cefamandole, cephalothin, carbenicillin, and vancomycin, have been included in and released from implants[65,84]

[89]. Some of these coatings have already been demonstrated to actively prevent infections *in vivo* and are used in especially critical conditions.[7] When PMMA cements are used in cemented joint replacements, post-operative infections increase 13%.[20] Therefore, antibiotics have been incorporated into PMMA bone cements to prevent infection.[3,20,88,89] However, with the addition of antibiotics, such as vancomycin, there is a potential for a negative effect on bending and fatigue strength.[88]

Gentamicin is an aminoglycoside and is used to treat various bacterial infections. The chemical structure of gentamicin can be seen below (**Figure 1.6**). All aminoglycosides are poly-cations, and the resulting polarity is responsible for the pharmacokinetic properties shared by all members of the group. Gentamicin irreversibly binds to the 30S component of the ribosome. This binding disrupts the normal ribosomal function, limiting protein synthesis, accumulation of abnormal initiation complex, and misreading of the mRNA template.[90] While gentamicin is mainly used to treat gram-negative bacterial infections, it is effective against gram-positive bacteria such as *Staphylococcus aureus* and *Pseudomonas aeruginosa*.[91]

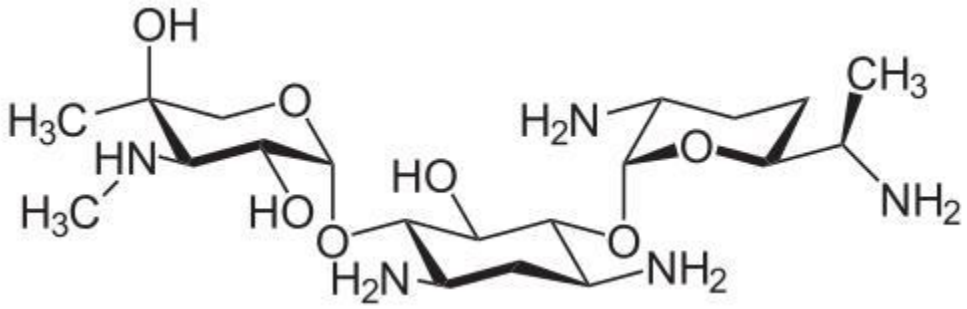

Figure 1.6: The chemical structure of gentamicin.

Because of gentamicin's ability to treat various bacterial infections, it has been incorporated into scaffolds and coatings for medical devices and implants.[20,84,92,93] Gentamicin has been incorporated into bone cement, and when at a concentration lower than 2/60

(gentamicin/cement), there was no significant change in compressive or diametral tensile strength compared to the PMMA control.[20] While including gentamicin in bone cement did not have negative impacts on mechanical properties, there is still worry of the incomplete release of gentamicin from the surface. Therefore either lower concentrations of antibiotics reach the implant site or higher doses of antibiotics are required to be seeded into the scaffold.[65] One strategy to increase and control the release of gentamicin from the surface of the implant is through gentamicin loaded biodegradable polymers.

Biodegradable polymers have been extensively reviewed and provide a reliable way to deliver antibiotics in a controlled manner.[3,65] To accomplish this and polyelectrolyte multilayers (PEMs) are used to deliver tunable amounts of gentamicin, like the delivery of growth factors stated earlier.[94–97] The study by Escobar *et al.* used poly-L-lysine (PLL) and complexes of poly(acrylic acid) (PAA) to absorb gentamicin onto glass surfaces. These surfaces exhibited a burst release of gentamicin and were more effective than glass at preventing the proliferation of *S. aureus*.[96] This is similar to previous studies that found a burst release of gentamicin during the first six hours.[92,96] The burst release of gentamicin in the study by Escobar *et al.* was thought to be due to gentamicin incorporation into the PEMs at a pH 4.5. Gentamicin becomes less protonated at a physiological pH (7.4), weakening the interaction between the antibiotic and the poly(acrylic acid) (PAA).

While gentamicin has proven to be a valuable antibiotic, it is also cytotoxic and inhibits osteogenic cells.[94,98,99] Because of gentamicin's potential cytotoxic effects it is important to develop gentamicin-delivering surfaces intended for orthopedics that do not inhibit cellular attachment and growth.

1.5 Preventing Infection and Implant Loosening

Implant loosening and implant infection are the two main causes of complete joint replacement failure.[5,7] Having an implant that decreases the risk for both causes of failure, could drastically reduce the need for corrective surgery after the initial surgery fails. However, surfaces that promote osteointegration often also promote bacterial adhesion, and those that have great amicrobial properties have poor cell attachment, proliferation, and/or osteogenic properties.[3,10,21,100] Therefore, current research is being conducted on combing the previously mentioned ideas. Work is focused on either increase the cytocompatibility and osseointegration properties of antimicrobial surfaces designed for orthopedic implants, or increasing the antimicrobial properties of osseointegrating surfaces.

1.5.1 Combining Antimicrobial and Osseointegrating Surfaces

Antimicrobial agents have been released from PEMs to increase antimicrobial properties of surfaces because components of the PEM layers do not inhibit the ability for mammalian cell attachment and proliferation.[95,101,102] The study by Moskowitz *et al.* used PEMs to absorb gentamicin on flat titanium surfaces, where a lower infection rate of *S. aureus* was found on coated samples compared to non-coated samples.[95] This is a similar result to the previously mentioned study by Moskowitz *et al.*, which found that the coatings were nontoxic to MC3T3-E1 murine preosteoblast.

As topography modifications have been shown to increase cellular attachment and osteogenic properties of surfaces, nontopographic features and antibiotics have been combined to increase the cytocompatibility of antimicrobial surfaces. Nanotubes loaded with gentamicin may inhibit bacterial adhesion without causing cytotoxicity.[103] The study by Harris *et al.* modified

titania nanotube surfaces with gentamicin and found that this combination was effective against *S. aureus,* while still promoting the attachment of human marrow-derived mesenchymal stem cells (hMSC). The hMSCs were cultured separately from the bacteria and in antibiotic-containing media.[97]

Dual-drug delivery systems have also been studied to increase osteogenesis and antimicrobial properties of surfaces.[92,102,104] In the study by Lee *et al.* gentamicin and BMP-2 were added to flat titanium surfaces with the use of heparin. Heparin was immobilized onto the surfaces using dopamine. Then surfaces were immersed in gentamicin followed by BMP-2 (**Figure 1.7**). The release of gentamicin was observed over multiple days and surfaces proved effective against *S. aureus*. The surfaces also proved to be non-cytotoxic against MG 63 cells.[92]

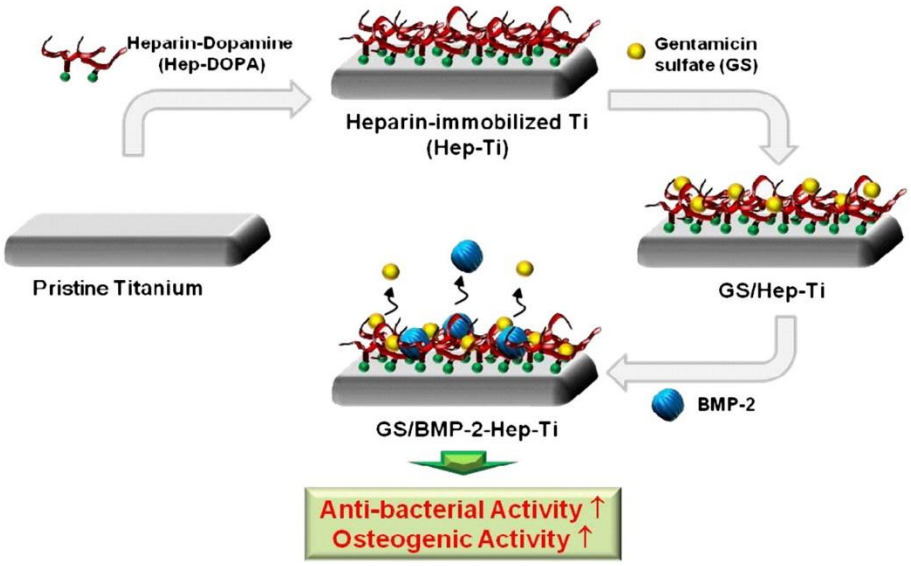

Figure 1.7: Schematic diagram for the immobilization of gentamicin sulfate and bone morphogenic protein-2 (BMP-2) to heparinized-Ti substrate. *Reproduced with permission from* [91] *copyright 2012, International Bone and Mineral Society*

While the studies mentioned in this section proved effective in promoting mammalian cell growth while inhibiting bacterial growth, the bacteria and mammalian cell responses to the surfaces were assessed separately.

1.5.2 Race to the Surface

Infection of a prosthetic implant is thought to be a "race to the surface," in which the probability of infection is determined by which cell type colonizes the surfaces first, bacteria or osteogenic cells.[105] If osteogenic cells colonize the surface first then no infection happens because the bacteria die off; however if bacteria colonize the surface first then infection ensues.[105] Surfaces that promote quick osteointegration and colonization of cells should therefore reduce the number of bacteria that can colonize the surface. However, surfaces that promote osteogenic cell attachment usually promote bacterial attachment as well.[3] Therefore, it is necessary to find surfaces that promote osteogenic cell colonization, while simultaneously inhibiting the attachment of bacteria. Some authors have proposed that co-culture of bacteria with mammalian cells is a better model for infection of orthopedic implants.[100,106,107]

There are few current studies, regarding orthopedic implants, that have tested the surfaces using the "race to the surface" model, by co-culturing bacteria with mammalian cells. The study by Chu *et al.* developed a biofunctional material consisting of polylactide-*co*-glycolide (PLGA), hydroxyapatite (HA), and quarternized chitosan (HACC). The HA promotes osteoblast adhesion and colonization while the HACC exhibited antimicrobial properties. These surfaces were tested by co-culturing osteoblast cells with *S. aureus*. When compared to PLGA, and PLGA plus HA surfaces the surfaces with HA and HACC had less bacterial growth and more osteoblast colonization.[108]

1.5.1 Future Directions and Conclusions

There have been extensive reviews and research conducted on antimicrobial, osteogenic, and osteoconductive surfaces designed for orthopedic implants. Most research in the past aimed at solving orthopedic implant failure has focused on either solving the problem of aseptic loosening or implant failure due to infection. Implant materials, surface topography, surface coatings, and drug delivery have all been widely studied to increase osteogenesis. These same techniques have also been used to increase the antimicrobial properties of similar surfaces to prevent infection of the implant.

Because of the similar strategies used to combat the two most common modes of failure of orthopedic implants, the current trend of research is to combine these technologies to develop surfaces that both promote osteogenesis and prohibit bacterial growth. This has been accomplished through dual drug delivery, surface coatings, antibiotic delivery from osteogenic surface coatings, and antibiotic delivery from surfaces with nanotopography. While these dual-functional surfaces show promise of increased antimicrobial activity without inhibiting cellular attachment, most researchers continue to test two separate hypotheses: 1) surface modification(s) increase cytocompatibility and the osteogenic properties of mammalian bone cells; and 2) surface modification(s) reduce bacterial adhesion, proliferation, and infection rate, without decreasing cytocompatibility.

While testing two separate hypotheses provides useful information on the properties of the surface, it does test the surface under the conditions where both the mammalian cells and bacteria are competing for the same resources as an orthopedic implant would. Therefore, the current direction of the field is starting to test a new hypothesis: surface modification(s) provide a favorable environment in which mammalian cells can beat bacterial cells and colonize the surface

first, thus increasing the osteogenic and antimicrobial properties of the surface. This is done by co-culturing bacteria cells and mammalian cells to test the "race to the surface" theory. It has been suggested that this is a more suitable model for studying infection and osseointegration of orthopedic implants. To better test this new third hypothesis, increased mechanistic co-culture studies for how the mammalian cells and bacteria interact are needed. Dual-functioning antimicrobial surfaces that promote osteogeneses could dramatically reduce implant failure and the need for corrective surgery.

REFERENCES

1. Ethgen, O., Bruyère, O., Richy, F., Dardennes, C. & Reginster, J.-Y. Health-Related Quality of Life in Total Hip and Total Knee Arthroplasty. *J. Bone Jt. Surg.* **86**, 963–974 (2004).

2. Etkin, C. D. & Springer, B. D. The American Joint Replacement Registry the first 5 years. *Arthroplast. Today* **3**, 67–69 (2017).

3. Zhang, B. G. X., Myers, D. E., Wallace, G. G., Brandt, M. & Choong, P. F. M. Bioactive coatings for orthopaedic implants-recent trends in development of implant coatings. *Int. J. Mol. Sci.* **15**, 11878–11921 (2014).

4. Vincent, G. K. & Velkoff, V. A. *THE NEXT FOUR DECADES The Older Population in the United States: 2010 to 2050 Population Estimates and Projections Current Population Reports*. (2010).

5. Raphel, J. *et al.* Engineered protein coatings to improve the osseointegration of dental and orthopaedic implants. *Biomaterials* **83**, 269–282 (2016).

6. Kurtz, S., Ong, K., Edmond, L., Mowat, F. & Halpern, M. Projections of Primary and Revision Hip and Knee Arthroplasty in the United States from 2005 to 2030. *J. Bone Jt. Surg.* **89**, 780 (2007).

7. Campoccia, D., Montanaro, L. & Arciola, C. R. The significance of infection related to orthopedic devices and issues of antibiotic resistance. *Biomaterials* **27**, 2331–2339 (2006).

8. Viceconti, M., Muccini, R., Bernakiewicz, M., Baleani, M. & Cristofolini, L. Large-sliding contact elements accurately predict levels of bone-implant micromotion relevant to osseointegration. *J. Biomech.* **33**, 1611–1618 (2000).

9. Geetha, M., Singh, A. K., Asokamani, R. & Gogia, A. K. Ti based biomaterials, the ultimate choice for orthopaedic implants – A review. *Prog. Mater. Sci.* **54**, 397–425 (2009).

10. Albrektsson, T. & Johansson, C. Osteoinduction, Osteocondiction and Osseointegration. *J. Eur. Spine* **10**, 96–101 (2001).

11. Beck, G. R. Inorganic phosphate as a signaling molecule in osteoblast differentiation. *J. Cell. Biochem.* **90**, 234–243 (2003).

12. Kirsch, T. Annexins—their role in cartilage mineralization. *Front. Biosci.* **10**, 576–581 (2005).

13. Anderson, H. C. Matrix vesicles and calcification. *Curr. Rheumatol. Rep.* **5**, 222–226 (2003).

14. Lotsari, A., Rajasekharan, A. K., Halvarsson, M. & Andersson, M. Transformation of amorphous calcium phosphate to bone-like apatite. *Nat. Commun.* **9**, 1–11 (2018).

15. Lossdörfer, S. *et al.* Microrough implant surface topographies increase osteogenesis by reducing osteoclast formation and activity. *J. Biomed. Mater. Res. - Part A* **70**, 361–369 (2004).

16. Lincks, J. *et al.* Response of MG63 osteoblast-like cells to titanium and titanium alloy is dependent on surface roughness and composition. *Biomater. Silver Jubil. Compend.* **19**, 147–160 (1998).

17. Schwartz, Z. *et al.* Implant surface characteristics modulate differentiation behavior of cells in the osteoblastic lineage. *Adv. Dent. Res.* **13**, 38–48 (1999).

18. Ballo, A., Agheli, H., Lausmaa, J., Thomsen, P. & Petronis, S. Nanostructured model implants for in vivo studies: influence of well-defined nanotopography on de novo bone formation on titanium implants. *Int. J. Nanomedicine* **6**, 3415–3428 (2011).

19. Bjursten, L. M. *et al.* Titanium dioxide nanotubes enhance bone bonding in vivo. *J. Biomed. Mater. Res. Part A* **92**, 1218–1224 (2009).

20. Arora, M., Chan, E. K. S., Gupta, S. & Diwan, A. D. Polymethylmethacrylate bone cements and additives : A review of the literature. *World J. Orthop.* **4**, 67–74 (2013).

21. Wang, C., Yu, B., Fan, Y., Ormsby, R. W. & Mccarthy, H. O. Incorporation of multi-walled carbon nanotubes to PMMA bone cement improves cytocompatibility and osseointegration. *Mater. Sci. Eng. C* **103**, 1–13 (2019).

22. Dalby, M. J. *et al.* The control of human mesenchymal cell differentiation using nanoscale symmetry and disorder. *Nat. Mater.* **6**, 997–100 (2007).

23. Biggs, M. J. P. *et al.* The use of nanoscale topography to modulate the dynamics of adhesion formation in primary osteoblasts and ERK/MAPK signalling in STRO-1+ enriched skeletal stem cells. *Biomaterials* **30**, 5094–5103 (2009).

24. Fiedler, J. *et al.* The effect of substrate surface nanotopography on the behavior of multipotnent mesenchymal stromal cells and osteoblasts. *Biomaterials* **34**, 8851–8859 (2013).

25. Alenezi, A. *et al.* Characteristics of 2 Different Commercially Available Implants with or without Nanotopography. *Int. J. Dent.* **2013**, (2013).

26. Popat, K. C., Leoni, L., Grimes, C. A. & Desai, T. A. Influence of engineered titania nanotubular surfaces on bone cells. *Biomaterials* **28**, 3188–3197 (2007).

27. Bai, J. *et al.* The formation mechanism of titania nanotube arrays in hydrofluoric acid electrolyte. *J. Mater. Sci. Mater. Med.* **43**, 1880–1884 (2008).

28. Luetzner, J., Krummenauer, F., Lengel, A. M., Ziegler, J. & Witzleb, W. C. Serum metal ion exposure after total knee arthroplasty. *Clin. Orthop. Relat. Res.* 136–142 (2007). doi:10.1097/BLO.0b013e31806450ef

29. Shu, R., McMullen, R., Baumann, M. J. & McCabe, L. R. Hydroxyapatite accelerates differentiation and suppresses growth of MC3T3-E1 osteoblasts. *J. Biomed. Mater. Res. - Part A* **67**, 1196–1204 (2003).

30. Smith, I. O., McCabe, L. R. & Baumann, M. J. MC3T3-E1 osteoblast attachment and proliferation on porous hydroxyapatite scaffolds fabricated with nanophase powder. *International Journal of Nanomedicine* **2**, 189–194 (2006).

31. Chang, B. S. *et al.* Osteoconduction at porous hydroxyapatite with various pore configurations. *Biomaterials* **21**, 1291–1298 (2000).

32. Rajaratnam, S. S. *et al.* Long-term results of a hydroxyapatite-coated femoral component in total hip replacement: A 15- to 21-year follow-up study. *J. Bone Jt. Surg. - Ser. B* **90**, 27–30 (2008).

33. Boden, H., Salemyr, M., Skoldenberg, O., Torbjorn, A. & Adolphson, P. Total hip arthroplasty with an uncemented hydroxyapatite-coated tapered titanium stem: results at a minium of 10 years' follow-up in 104 hips. *Orthop. Sci.* **11**, 175–197 (2006).

34. Voigt, J. D. & Mosier, M. Hydroxyapatite (HA) coating appears to be of benefit for implant durability of tibial components in primary total knee arthroplasty. *Acta Orthop.* **82**, 448–459 (2011).

35. Goosen, J. H. M., Kums, A. J., Kollen, B. J. & Verheyen, C. C. P. M. Porous-coated femoral components with or without hydroxyapatite in primar uncemented total hip arthroplasy: a systematic review of randomized controlled trials. *Orthop. Trauma Surg.* **129**, 1165–1169 (2009).

36. Liu, Q., Ding, J., Mante, F. K., Wunder, S. L. & Baran, G. R. The role of surface functional groups in calcium phosphate nucleation on titanium foil: A self-assembled monolayer technique. *Biomaterials* **23**, 3103–3111 (2002).

37. Chen, X. B., Li, Y. C., Plessis, J. Du, Hodgson, P. D. & Wen, C. Influence of calcium ion deposition on apatite-inducing ability of porous titanium for biomedical applications. *Acta Biomater.* **5**, 1808–1820 (2009).

38. Nayab, S. N., Jones, F. H. & Olsen, I. Effects of calcium ion implantation on human bone cell interaction with titanium. *Biomaterials* **26**, 4717–4727 (2005).

39. Cooper, L. F. *et al.* Fluoride modification effects on osteoblast behavior and bone formation at TiO2 grit-blasted c.p. titanium endosseous implants. *Biomaterials* **27**, 926–936 (2006).

40. Zreiqat, H. *et al.* Mechanisms of magnesium-stimulated adhesion of osteoblastic cells to commonly used orthopaedic implants. *J. Biomed. Mater. Res.* **62**, 175–184 (2002).

41. Carragee, E. J., Hurwitz, E. L. & Weiner, B. K. A critical review of recombinant human bone morphogenetic protein-2 trials in spinal surgery: emerging safety concerns and lessons learned. *Spine J.* **11**, 471–491 (2011).

42. Bishop, G. B. & Einhorn, T. A. Current and future clinical applications of bone morphogenetic proteins in orthopaedic trauma surgery. *Int. Orthop.* **31**, 721–727 (2007).

43. Carreira, A. C. *et al.* Bone Morphogenic Proteins: Facts, Challenges, and Future Perspectives. *Crit. Rev. Oral Biol. Med.* **93**, 335–345 (2014).

44. Ong, C. T., Choon, D. S. K., Cabrera, N. P. & Maffulli, N. The treatment of open tibial fractures and of tibial non-union with a novel external fixator. *Injury* **33**, 829–834 (2002).

45. Hustedt, J. W. & Blizzard, D. J. *The Controversy Surrounding Bone Morphogenetic Proteins in the Spine: A Review of Current Research*. *YALE JOURNAL OF BIOLOGY AND MEDICINE* **87**, (2014).

46. Suliman, S. *et al.* Release and bioactivity of bone morphogenetic protein-2 are affected by scaffold binding techniques in vitro and in vivo. *J. Control. Release* **197**, 148–157 (2015).

47. U.S. Food and Drug Administration. *Infuse bone graft Important Medical Information*.

48. Mohammadi, M. *et al.* Fabrication of hybrid scaffold based on hydroxyapatite-biodegradable nanofibers incorporated with liposomal formulation of BMP-2 peptide for bone tissue engineering. *Nanomedicine Nanotechnology, Biol. Med.* **14**, 1987–1997 (2018).

49. Jeon, O., Song, S. J., Kang, S. W., Putnam, A. J. & Kim, B. S. Enhancement of ectopic bone formation by bone morphogenetic protein-2 released from a heparin-conjugated poly(l-lactic-co-glycolic acid) scaffold. *Biomaterials* **28**, 2763–2771 (2007).

50. Yamamoto, M., Takahashi, Y. & Tabata, Y. Controlled release by biodegradable hydrogels enhances the ectopic bone formation of bone morphogenetic protein. *Biomaterials* **24**, 4375–4383 (2003).

51. Shah, N. J. *et al.* Tunable dual growth factor delivery from polyelectrolyte multilayer films. *Biomaterials* **32**, 6183–6193 (2011).

52. Detzel, C. J., Larkin, A. L. & Rajagopalan, P. Polyelectrolyte Multilayers in Tissue Engineering. *Tissue Eng. Part B* **17**, 11–113 (2011).

53. Decher, G. Fuzzy nanoassemblies: Toward layered polymeric multicomposites. *Science (80-.).* **277**, 1232–1237 (1997).

54. Ruppert, R., Hoffmann, E. & Sebald, W. Human bone morphogenetic protein 2 contains a heparin-binding site which modifies its biological activity. *Eur. J. Biochem.* **237**, 295–302 (1996).

55. Zhao, B. *et al.* Heparin Potentiates the in Vivo Ectopic Bone Formation Induced by Bone Morphogenetic Protein-2 *. (2006). doi:10.1074/jbc.M511039200

56. Volpato, F. Z. *et al.* Preservation of FGF-2 bioactivity using heparin-based nanoparticles, and their delivery from electrospun chitosan fibers. *Acta Biomater.* **8**, 1551–1559 (2012).

57. Almodóvar, J., Bacon, S., Gogolski, J., Kisiday, J. D. & Kipper, M. J. Polysaccharide-based polyelectrolyte multilayer surface coatings can enhance mesenchymal stem cell response to adsorbed growth factors. *Biomacromolecules* **11**, 2629–2639 (2010).

58. Place, L. W., Sekyi, M. & Kipper, M. J. Aggrecan-Mimetic, Glycosaminoglycan-Containing Nanoparticles for Growth Factor Stabilization and Delivery. *Biomacromolecules* **15**, 680–689 (2014).

59. Romero, R. *et al.* Combined delivery of FGF-2, TGF-β1, and adipose-derived stem cells from an engineered periosteum to a critical-sized mouse femur defect. *J. Biomed. Mater. Res. - Part A* **105**, 900–911 (2017).

60. Hu, Y. *et al.* Regulation of the differentiation of mesenchymal stem cells in vitro and osteogenesis in vivo by microenvironmental modification of titanium alloy surfaces. *Biomaterials* **33**, 3515–3528 (2012).

61. Lai, M. *et al.* Surface Functionalization of TiO 2 Nanotubes with Bone Morphogenetic Protein 2 and Its Synergistic Effect on the Differentiation of Mesenchymal Stem Cells. *Biomacromolecules* **12**, 1097–1105 (2011).

62. Sanderson, P. J. *Infection in orthopaedic implants*. *Journal of Hospital Infection* **1**, (1991).

63. Kaltsas, D. S. Infection after total hip arthroplasty. *Ann. R. Coll. Surg. Engl.* **86**, 267–271 (2004).

64. Brady, R. A., Calhoun, J. H., Leid, J. G. & Shirtliff*, M. E. Infections of Orthopaedic Implants and Devices. in *Springer Series on Biofilms* 1–41 (Springer Berlin Heidelberg, 2008). doi:10.1007/7142_2008_25

65. Hetrick, E. M. & Schoenfisch, M. H. Reducing implant-related infections: Active release strategies. *Chem. Soc. Rev.* **35**, 780–789 (2006).

66. Vacheethasanee, K. & Marchant, R. E. Surfactant polymers designed to suppress bacterial (Staphylococcus epidermidis) adhesion on biomaterials. *J. Biomed. Mater. Res.* **50**, 302–312 (2000).

67. An, Y. H. *et al.* Prevention of bacterial adherence to implant surfaces with a crosslinked albumin coatingin vitro. *J. Orthop. Res.* **14**, 846–849 (1996).

68. Arciola, C. R., Radin, L., Alvergna, P., Cenni, E. & Pizzoferrato, A. Heparin surface treatment of poly(methylmethacrylate) alters adhesion of a Staphylococcus aureus strain: utility of bacterial fatty acid analysis. *Biomaterials* **14**, 1161–1164 (1993).

69. Feng, Q. L. *et al.* A mechanistic study of the antibacterial effect of silver ions on Escherichia coli and Staphylococcus aureus. *J. Biomed. Mater. Res.* **52**, 662–668 (2000).

70. Chen, W. *et al.* Antibacterial and osteogenic properties of silver-containing hydroxyapatite coatings produced using a sol gel process. *J. Biomed. Mater. Res. Part A* **82**, 899–906 (2006).

71. Gosheger, G. *et al.* Silver-coated megaendoprostheses in a rabbit model - An analysis of the infection rate and toxicological side effects. *Biomaterials* **25**, 5547–5556 (2004).

72. Massè, A. *et al.* Prevention of pin track infection in external fixation with silver coated pins: Clinical and microbiological results. *J. Biomed. Mater. Res.* **53**, 600–604 (2000).

73. Coester, L. M., Nepola, J. V., Allen, J. & Marsh, J. L. The effects of silver coated external fixation pins. *Iowa Orthop.* **26**, 48–53 (2006).

74. De Groote, M. A. & Fang, F. C. NO Inhibitions : Antimicrobial Properties of Nitric Oxide. *Oxford Univ. Press* **21**, S162–S165 (1995).

75. Simon-Walker, R. *et al.* Glycocalyx-inspired nitric oxide-releasing surfaces reduce platelet adhesion and activation on titanium. *ACS Biomater. Sci. Eng.* **3**, 68–77 (2017).

76. Pegalajar-Jurado, A. *et al.* Reprint of: Nitric oxide-releasing polysaccharide derivative exhibits 8-log reduction against Escherichia coli, Acinetobacter baumannii and Staphylococcus aureus. *J. Control. Release* **220**, 617–623 (2015).

77. Damodaran, V. B. *et al.* Antithrombogenic properties of a nitric oxide-releasing dextran derivative: Evaluation of platelet activation and whole blood clotting kinetics. *RSC Adv.* **3**, 24406–24414 (2013).

78. Tavaria, F. K. *et al.* Chitosan: antimicrobial action upon staphylococci after impregnation onto cotton fabric. *J. Appl. Microbiol.* **112**, 1034–1041 (2012).

79. Mansilla, A. Y. *et al.* Evidence on antimicrobial properties and mode of action of a chitosan obtained from crustacean exoskeletons on Pseudomonas syringae pv. tomato DC3000. *Appl. Microb. Cell Physiol.* **97**, 6957–6966 (2013).

80. Martins, A. F. *et al.* Chitosan/iota-carrageenan and chitosan/pectin polyelectrolyte multilayer scaffolds with antiadhesive and bactericidal properties. *Appl. Surf. Sci.* **502**, 144282 (2020).

81. Wigmosta, T. B., Popat, K. C. & Kipper, M. J. BMP -2 Delivery from Polyelectrolyte Multilayers EnhancesOsteogenic Activityon Nanostructured Titania . *J. Biomed. Mater. Res. Part A* 1–10 (2020). doi:10.1002/jbm.a.37109

82. Oka, Y. *et al.* Efficacy of Titanium Dioxide Photocatalyst for Inhibition of Bacterial Colonization on Percutaneous Implants. *J. Biomed. Mater. Res. Part B Appl. Biomater.* **86**, 530–540 (2008).

83. Cheng, C. *et al.* The effects of the bacterial interaction with visible-light responsive titania photocatalyst on the bactericidal performance. *J. Biomed. Sci.* **16**, 1–10 (2009).

84. Stigter, M., Bezemer, J., De Groot, K. & Layrolle, P. Incorporation of different antibiotics into carbonated hydroxyapatite coatings on titanium implants, release and antibiotic efficacy. *J. Control. Release* **99**, 127–137 (2004).

85. Radin, J. S., Campbellt, J. T., Ducheyne, P. & Cuckler+, J. M. Calcium phosphate ceramic coatings as carriers of vancomvcin. *Biomoteriols* **18**, 777–782 (1997).

86. Lin, T. L. *et al.* Antimicrobial coatings: a remedy for medical device-related infections. *Artic. Med. device Technol.* (2001).

87. Stigter, M., De Groot, K. & Layrolle, P. Incorporation of tobramycin into biomimetic hydroxyapatite coating on titanium. *Biomaterials* **23**, 4143–4153 (2002).

88. Persson, C. *et al.* Mechanical effects of the use of vancomycin and meropenem in acrylic bone cement. *Acta Orthop.* **77**, 617–621 (2009).

89. Deboer, D. & Christie, M. The Use of Vancomycin and Tobramycin in Acrylic Bone Cement Biomechanical Effects and Elution Kinetics for Use in Joint Arthroplasty. *J. Arthroplasty* **14**, 339–346 (1999).

90. Mohan, M., Shetty, D., Shetty, T. & Banerjee, S. *Gentamicin: Myths and Truths*.

91. Tam, V. H., Kabbara, S., Vo, G., Schilling, A. N. & Coyle, E. A. Comparative Pharmacodynamics of Gentamicin against Staphylococcus aureus and Pseudomonas aeruginosa. *Antimicrob. Agents Chemother.* **50**, 2626–2631 (2006).

92. Lee, D. W., Yun, Y. P., Park, K. & Kim, S. E. Gentamicin and bone morphogenic protein-2 (BMP-2)-delivering heparinized-titanium implant with enhanced antibacterial activity and osteointegration. *Bone* **50**, 974–982 (2012).

93. Campos, M. G. N. *et al.* In vitro gentamicin sustained and controlled release from chitosan cross-linked films. *J. Mater. Sci. Mater. Med.* **20**, 537–543 (2009).

94. Ince, A., Schütze, N., Karl, N., Löhr, J. F. & Eulert, J. Gentamicin negatively influenced osteogenic function in vitro. *Int. Orthop.* **31**, 223–228 (2007).

95. Moskowitz, J. S. *et al.* Biomaterials The effectiveness of the controlled release of gentamicin from polyelectrolyte multilayers in the treatment of Staphylococcus aureus infection in a rabbit bone model. *Biomaterials* **31**, 6019–6030 (2010).

96. Escobar, A. *et al.* Antibacterial Layer-by-Layer Films of Poly(acrylic acid)–Gentamicin Complexes with a Combined Burst and Sustainable Release of Gentamicin. *Adv. Mater. Interfaces* **6**, 1–9 (2019).

97. Harris, L. G., Tosatti, S., Wieland, M., Textor, M. & Richards, R. G. Staphylococcus aureus adhesion to titanium oxide surfaces coated with non-functionalized and peptide-functionalized poly(L-lysine)-grafted- poly(ethylene glycol) copolymers. *Biomaterials* **25**, 4135–4148 (2004).

98. Isefuku, S., Joyner, C. J. & Simpson, A. H. R. W. Gentamicin may have an adverse effect on osteogenesis. *J. Orthop. Trauma* **17**, 212–216 (2003).

99. Duewelhenke, N., Krut, O. & Eysel, P. Influence on mitochondria and cytotoxicity of different antibiotics administered in high concentrations on primary human osteoblasts and cell lines. *Antimicrob. Agents Chemother.* **51**, 54–63 (2007).

100. Martínez-Pérez, M. *et al.* The "Race for the Surface" experimentally studied: In vitro assessment of Staphylococcus spp. adhesion and preosteoblastic cells integration to doped Ti-6Al-4V alloys. *Colloids Surfaces B Biointerfaces* **173**, 876–883 (2019).

101. Rodríguez, A. D. L. *et al.* Preventing S . aureus biofilm formation on titanium surfaces by the release of antimicrobial b -peptides from polyelectrolyte multilayers q. *Acta Biomater.* **93**, 50–62 (2019).

102. Wong, S. Y. *et al.* Dual Functional Polyelectrolyte Multilayer Coatings for Implants : Permanent Microbicidal Base with Controlled Release of Therapeutic Agents. *J. Am. Chem. Soc.* **132**, 17840–17848 (2010).

103. Lin, W. *et al.* Inhibited bacterial biofilm formation and improved osteogenic activity on gentamicin-loaded titania nanotubes with various diameters. *Int. J. Nanomedicine* **9**, 1215–1230 (2014).

104. Johnson, C. T. *et al.* Lysostaphin and BMP-2 co-delivery reduces S . aureus infection and regenerates critical-sized segmental bone defects. *Sci. Adv.* **17**, (2019).

105. Gristina, A. G. Biomaterial-Centered Infection : Microbial Adhesion Versus Tissue Integration. *Science (80-.).* **237**, 1588–1595 (1987).

106. Martinez-Perez, M. *et al.* Evaluation of bacterial adherence of clinical isolates of Staphylococcus sp. using a competitive model: An in vitro approach to the 'race for the surface' theory. *Bone Jt. Res.* **6**, 315–322 (2017).

107. Foss, B. L., Ghimire, N., Tang, R., Sun, Y. & Deng, Y. Bacteria and osteoblast adhesion to chitosan immobilized titanium surface: A race for the surface. *Colloids Surfaces B Biointerfaces* **134**, 370–376 (2015).

108. Chu, L. *et al.* Preferential colonization of osteoblasts over co-cultured bacteria on a bifunctional biomaterial surface. *Frontiers in Microbiology* **9**, (2018).

CHAPTER 2: BMP-2 DELIVERY FROM POLYELECTROLYTE MULTILAYERS ENHANCES OSTEOGENIC ACTIVITY ON NANOSTRUCTURED TITANIA[1]

Overview

Incomplete osseointegration is primary cause of failure for orthopedic implants. New biomaterials that present stable signals promoting osteogenesis could reduce failure rates of orthopedic implants. In this study bone morphogenetic protein 2 (BMP-2) was delivered from titania nanotubes (Nt) modified with chitosan/heparin polyelectrolyte multilayers (PEMs). The surfaces were characterized by scanning electron microscopy (SEM) and X-ray photoelectron spectroscopy (XPS). BMP-2 release from the surfaces was measured *in vitro* for up to 28 days. After an initial burst release of BMP-2 during the first two days, most of the BMP-2 remained on the surface. To determine the osteogenic properties of these surfaces, they were seeded with rat bone marrow cells; alkaline phosphatase (ALP) activity, total protein, calcium deposition and osteocalcin were measured up to four weeks *in vitro*. When compared to Nt surfaces, the surfaces with BMP-2 induce greater osteocalcin and calcium deposition. PEMs provide sustained presentation of BMP-2, from a biomimetic surface. This enhances the osteogenic properties of the surface without requiring supraphysiologic growth factor dose. This growth factor delivery strategy could be used to improve bone healing outcomes and reduce complications for recipients of orthopedic implants.

---

[1] Portions of this chapter are reproduced from: T.B. Wigmosta, K.C. Popat, and M.J. Kipper, "Bone morphogenetic protein-2 delivery from polyelectrolyte multilayers enhances osteogenic activity on nanostructured titania," *Journal of Biomedical Materials Research* (2020), DOI:10.1002/jbm.a.37109.

2.1 Introduction

Complete joint replacement is a widely used and effective treatment for patients with injured or diseased joints. Total joint replacement causes a substantial improvement in physical health, including a reduction in chronic pain and improved physical functioning.[1] There are currently over 1 million total knee and hip implants performed annually in the United States.[2] Elderly patients suffering from joint deterioration due to osteoarthritis or rheumatoid arthritis make up the majority of these surgeries.[3] It is projected that the population of people aged 65 years or older in the US will more than double from 40.2 million in 2010 to 88.5 million by 2050.[4] As a result, the number of complete joint replacement surgeries is expected to increase to over 4 million by 2030.[5]

While most complete joint replacement surgeries are successful, over 60,000 revision surgeries due to implant failure are performed annually.[6] Revision surgeries are costly and expose patients to risks associated with infection and anesthesia. Patients that undergo a revision surgery also experience significant decreases in physical functioning compared to those that have only a primary surgery.[1] It is imperative that a solution to secure implants and decrease the number of revision surgeries is found. The most common cause of orthopedic implant failure is aseptic loosening of the implant from the surrounding bone tissue, followed by failure of the implant due to infection.[5,7] These failure modes could be addressed by implant surfaces that enhance osseointegration and infection to avoid the increased cost and decreased health associated with revision surgery.

Successful orthopedic implant surfaces allow for bone-forming cells to attach to the surface and synthesize new bone. Nanotopographical structures can enhance bone formation both in vitro and in vivo.[8–13] A study by Ballo et al. histologically evaluated bone growth on implants

after 7 and 28 d. Surfaces with 60 nm features had significantly higher bone-implant contact compared to 120 nm and 220 nm surfaces.[8] Our group has fabricated novel nanotubular titania surfaces using an anodization process. This process uniformly modifies titanium surfaces with titania nanotubes.[14] These titania nanotube surfaces provide a favorable template for bone cell growth and differentiation.[8,14] Nanotube surfaces support higher cell adhesion, proliferation and viability for up to seven days in culture compared to titanium surfaces.[14] Cells cultured on nanotube surfaces demonstrate higher alkaline phosphatase (ALP) activity, and improved calcium and phosphorus accumulation.[14] This suggests that osteoblast activity can be significantly enhanced using controlled nanotopographies, such as nanotubes.

A second strategy for improving bone growth around orthopedic implants is the delivery of growth factors from scaffolds for bone tissue engineering. Bone morphogenetic proteins (BMPs) have been extensively researched because of their ability to induce bone and cartilage development.[15] The first BMP was isolated in the 1980s, with the crystal structures of human BMP-2 and BMP-7 published in the 1990s.[16] Bone morphogenetic protein 2 (BMP-2) improves healing of critical-sized bone defects.[15] The use of BMP-2 for the treatment of tibial fractures was investigated by the Surgery for Tibial Trauma (BESTT-ALL) trial.[17] At 12 months post-surgery, the treatment group receiving the largest does of rhBMP-2 had a 44% reduction in the risk of failure, significantly fewer invasive interventions, and significantly faster fracture true-healing, compared with control patients.[17] Because of BMP-2's success in bone healing, it has been approved by the Food and Drug Administration (FDA) and used in spinal fusions since 2002.[18] There are currently two BMP products available for clinical applications: recombinant human BMP-2 (rhBMP-2, (INFUSE); Medtronic Sofamor Danek, Memphis, TN) and rhBMP-7 (osteogenic protein 1 (OP-1), Stryker Biotech, Hopkinton, MA).[15]

However, these techniques use super-physiological amounts of growth factors to compensate for the short half-life in vivo (1-4 hours).19 The INFUSE product, for example, uses a very high dose of BMP-2 (1.5 mg/ml).[20] The use of large amounts of growth factor can result in nonspecific delivery and overgrowth of the tissue with the potential for unsafe side effects.[21] In June 2008 the FDA issued a Public Health Notification of life-threating complications associated with rhBMP-2 use.[21]

Surfaces that stabilize BMP-2 and control its delivery could reduce the need for and risks associated with supraphysiologic doses.[22–31] One solution is to use polyelectrolyte multilayers (PEMs) to provide tunable growth factor concentration and release.[25,32,33] Our group has shown that chitosan-heparin polyelectrolyte multilayers (PEMs) and polyelectrolyte complexes can bind and stabilize growth factors, preserving growth factor activity for weeks in physiological pH and temperature, and enabling their presentation to cells in a context that enhances growth factor activity.[34–36] BMP-2 has a binding site for heparin that modulates its bioactivity; in the presence of heparin, degradation of BMP-2 is blocked and the half-life in culture media is prolonged by nearly 20-fold.[37,38] Our group has also successfully absorbed PEMs onto nanotubes.[39] The stabilization of growth factors provided by the PEMs enables the use of biologically relevant amounts of heparin-binding growth factors, such as FGF-2 and TGF-β1.[40]

In this study, we designed surfaces to promote osteogenic differentiation of rat bone marrow cells. This is accomplished using a combination of nanotopography and coatings for growth factor delivery. BMP-2, is delivered from nanotube surfaces, because it has been shown to promote bone formation and is currently used in commercial products.[15,17,18,20] Chitosan/heparin polyelectrolyte multilayers (PEMs) are used to deliver BMP-2 from the titania nanotube surfaces. While previous studies have incorporated a combination of PEMs, BMP-2,

heparin, and/or nanostructured topography onto titanium surfaces to increase bone formation, no studies have combined all of them to increase bone formation.[22–26,41] It is the goal of the this study to combine nanotopography with growth factor release, to increase the osteogenic properties of cells without requiring costly and potentially dangerous superphysiologic growth factor doses.

2.2 Materials and Methods

2.2.1 Surface Characterization and BMP-2 Release

2.2.1a Titania Nanotube Fabrication

Titania nanotube surfaces were created using an anodization process.[14] Flat titanium foil (0.25 mm thickness and 99.8% purity) was cut into identical circles 8 mm in diameter, using water jet cutting. Electrolyte solution consisted of 2 vol% hydrofluoric acid, 95 vol% diethylene glycol (DEG, basic, 99% reagent Sigma-Aldrich, St. Louis, MO) and 3 vol% DI water. A platinum electrode served as a cathode. Anodization was performed at a constant voltage of 55 V for 22 h. Nanotubes were then annealed in an oven at 530 °C for 3 h. The resulting samples are referred to as Nt.

2.2.1b Construction of Polyelectrolyte Multilayers (PEMs)

Chitosan was purchased from Heppe Medical Chitosan (Halle, Germany). Heparin sodium from porcine intestinal mucosa (12.5% sulfur) was purchased from Celsus Laboratories, (Cincinnati, OH). Glacial acetic acid and ethanol (99.5+ %, 200 proof) was purchased from Acros Organics (Geel, Belgium). Sodium acetate was purchased from Fisher Scientific (Pittsburgh, PA). A Millipore Synthesis water purification unit was used to obtain 18.2 MΩ cm water, and this was used for making all aqueous solutions (Millipore, Billerica, MA).

Polyelectrolyte multilayers were prepared by the layer-by-layer deposition of alternating layers of chitosan and heparin. Chitosan (1 mg/ml) and heparin (3 mg/ml) solutions were prepared in acetate buffer (0.2 M, pH 5). All solutions were filtered through 0.22 µm poly vinylidene fluoride (PVDF) syringe filters. Titania nanotube substrates were first washed for five minutes in acidified water rinse (pH 4.0, acidified with acetic acid). Construction of PEMs was performed by alternating 5-min absorption steps of the polyelectrolytes (starting with chitosan) with 4-min acidified water rinses between absorption steps.[42] Heparin-terminated PEMs were constructed with 18 layers. The resulting samples are referred to as Nt + PEM.

2.2.1c Surface Characterization with X-Ray Photoelectron Spectroscopy (XPS) and Scanning Electron Microscopy (SEM)

The surface chemistry of samples was characterized using Phi Electronics 5800 Spectrometer (Chanhassen, MN). Spectra were obtained with a monochromatic A1 Kα X-ray source ($h\nu$ = 1486.6 eV), a hemispherical analyzer, and a multichannel detector. High-resolution spectra were obtained using a 23.5 eV analyzer pass energy with 0.1 eV steps and an X-ray spot for 800 µm. All spectra were obtained with a 45° photoelectron take-off angle. Spectra curve fitting was done in OriginLab (OriginPro, 2019b, OriginLab Corporation, Northampton, MA, USA). All spectra curve fitting used a Shirley background. Spectra were shifted by locating the aliphatic C1s peak at 284.8 eV. Gaussian peaks were fit according to expected functional groups.[43]

Nanotubes (Nt) and PEM-modified nanotubes (Nt + PEM) were visually observed using SEM. Samples were sputter-coated with palladium-gold alloy (Polaron SC 7620 Sputter Coater, Quorum Technologies, Newhaven, UK) at a thickness of 10 nm (10-15 mA, under a vacuum of 130 mTorr). The SEM (JSM-6500F, field emissions scanning electron microscope, JEOL, Japan)

was operated at an accelerating voltage of 15 kV, and three areas at two different magnifications (2500×, and 250×) on each sample were imaged.

2.2.1d Absorption and release of BMP-2 on Titania Nanotubes + PEM

Ten 8-mm diameter disks of titania nanotube samples were constructed and 18-layer PEMs, terminated with heparin were adsorbed onto the surfaces as previously described, to prepare Nt + PEM samples. Samples were dried overnight and then sterilized by incubating in 70% ethanol for 30 min. To ensure no ethanol remained on the samples, samples were rinsed three times with sterile phosphate buffered saline (PBS), pH 7.2 without calcium chloride or magnesium chloride, (Fisher Scientific, Waltham, MA) for five min each wash. To determine the adsorption and release of BMP-2 from samples, two concentrations of BMP-2 (355-BM-010, R&D Systems, Minneapolis, MN) were adsorbed onto Nt + PEM. The release of BMP-2 was measured over 28 d.

Two concentrations (100 ng/ml and 500 ng/ml) of BMP-2 were aseptically prepared in PBS. Under aseptic conditions, 250 µl of BMP-2 solution (n = 5) were added to sterile 48-well plates with Nt + PEM samples and placed on a shaker at 150 rpm for 1 h at room temperature. The solution was then removed and stored at -20 °C until further analysis. To determine the amount of BMP-2 adsorbed onto the samples, the amount of BMP-2 in the 1-hour post BMP-2 addition was subtracted from the total amount of BMP-2 added to the sample. Next, 250 µl of fibronectin (10 µg/ml; FisherScientific, Waltham, MA) in PBS was incubated on the samples for 1 h at 150 rpm at room temperature, then the fibronectin solution was removed. The BMP-2-modified samples after fibronectin addition are referred to as Nt + PEM + BMP-2.

Nt + PEM + BMP-2 samples were kept in 48-well plates with 200 µl of PBS at 37 °C throughout the rest of the experiment. At 6, 12 and 24 h, as well as 2, 4, 7, 14, 21 and 28 d, 450 µl of solution was removed and replaced with fresh PBS. The removed samples were stored -20 °C.

The concentration of BMP-2 in solution was measured using an enzyme-linked immunosorbent assay (ELISA) (R&D Systems DY355-05). Total BMP-2 released from the sample was calculated and plotted versus time.

2.2.2 Cellular Response to BMP-2-Modified Surfaces

2.2.2a Harvest of Bone Marrow from Rats

Rats were obtained from the Laboratory Animal Resource Center (LARC) at Colorado State University, Fort Collins, Colorado. Rats were euthanized according to an IACUC-approved protocol. The femurs and humeri were removed from the limbs and placed in sterile PBS on ice. Bones were dissected from the remaining soft tissue in a sterile tissue-culture hood. Metaphyseal ends of the bones were removed to allow access to the marrow cavity. Marrow from the cavity was flushed out using a 12-gauge needle attached to a 10-ml syringe filled with culture medium, which consisted of alpha modified minimum essential medium (α-MEM; ThermoFisher, Waltham, MA) supplemented with 10% fetal bovine serum (FBS; ThermoFisher, Waltham, MA) and 1% penicillin/streptomycin (pen/strep; ThermoFisher, Waltham, MA). The syringe was refilled with the same medium and the cavity was re-flushed with an 18-gauge needle. The flushed cell suspension was then filtered through a 70-µm nylon strainer into a fresh conical tube (15-mL or 50-mL centrifuge tube). Cells were then counted by diluting the cell solution 1:1 in 0.4% Trypan Blue (ThermoFisher, Waltham, MA) and counting on a hemocytometer.[14]

2.2.2b Sample Preparation and Bone Marrow Seeding

Nt, Nt + PEM, and Nt + PEM + BMP-2 samples (prepared using 500 ng/ml BMP-2) were prepared as described above. Rat bone marrow cells were seeded onto samples at a density of 10^6 cells/ml in maintenance media. Samples were incubated at 37 °C and 5% CO_2 for the remainder

of the experiment. Half of the media was removed and replaced with fresh cell culture media on day 4. On day 7 all the media was removed and replaced with complete media. Complete media consisted of αMEM supplemented with 10% FBS, 1% pen/strep, ascorbic acid (50 μg/ml) (255564, Sigma), and β-glycerol phosphate (8 mM) (G-6251, Sigma). As a positive control for BMP-2 delivery, some Nt samples also had BMP-2 added to the complete media (Nt + BMP-2 in media). For samples Nt + BMP-2 in media samples, BMP-2 was added to complete media at a final concentration of 100 ng/ml at each media change. For all samples, the media was changed every other day for the remainder of the experiments. Table 1 summarizes the sample groups.

TABLE 1 Summary of media used for each sample type

Surface type	First 7 days[a]	After 7 days[b]
Nt + BMP-2 (in media)	Maintenance media	Complete media + BMP-2
Nt	Maintenance media	Complete media
Nt + PEM	Maintenance media	Complete media
Nt + PEM + BMP-2	Maintenance media	Complete media

Abbreviations: BMP-2, bone morphogenetic proteins-2; Nt, nanotube; PEMs, polyelectrolyte multilayers.
[a]Maintenance media: α-MEM + 10% FBS + 1% pen-strep.
[b]Complete media: maintenance media + β-glycerol phosphate (8 mM) + ascorbic acid (50 μg/ml).

2.2.3 Alkaline Phosphatase (ALP) Activity, Total Protein, and Calcium

Alkaline phosphatase activity, total protein, and calcium were assessed at 14, 21, and 28 d post cell seeding. Five samples per group and per time point were prepared. The media was removed from wells and samples were washed with PBS. Samples were then moved to new wells

and incubated in 0.2% Triton-X100 in DI water at room temperature on a shaker at 150 rpm. The solution was removed and stored at -20 °C until total protein and ALP analysis. Samples were then rinsed in DI water, allowed to air dry, and stored in a desiccator for later calcium analysis.

ALP activity was measured using a commercially available kit (QuantiChrom, Alkaline Phosphatase Assay Kit DALP-250). Total protein was determined using another commercially available kit (ThermoScientific, Micro BCA Protein Assay Kit 23235). Calcium was determined using a kit from Abcam (Calcium Assay Kit (Colorimetric)). Dried and stored samples were incubated in 6 N HCL for 2 h. Calcium reagent (1 ml) was added to each well, and then 100 µl of the solution was added to a 96-well plate. Absorbance was read at 570 nm and compared to a calcium standard. Calcium and ALP activity was normalized to total protein.

2.2.4 Cell Counts and Osteocalcin Production

Samples were fixed in 3.7% formaldehyde in PBS on days 14 and 28. Samples were stored in PBS at room temperature until the fluorescent staining. The samples were stained with 4′,6-diamidino-2-phenylindole (DAPI, Invitrogen), rhodamine phalloidin (actin), and osteocalcin (P-18 purified goat polyclonal antibody of mouse origin, Santa Cruz Biotechnology). The osteocalcin antibody was diluted 1:100 in 1% BSA in PBS and incubated on the samples for 1 h at room temperature. A FITC-conjugated secondary antibody for osteocalcin (donkey antigoat IgG, Santa Cruz Biotechnology) was then diluted 1:200 in 1% BSA in PBS and incubated on samples for 45 min. Rhodamine phalloidin at a concentration of 14 µM in PBS was added to wells and incubated for 25 min at room temperature. Samples were stored in PBS until fluorescence imaging.

Each sample was imaged at 10× in three locations using a Zeiss Axiovision fluorescence microscope. Cell nuclei were counted using ImageJ software (NIH). Percent area of osteocalcin was also determined in ImageJ and normalized to the number of cell nuclei.

2.2.5 Scanning Electron Microscopy (SEM)

Samples (three per group and time point) were fixed at 14 and 28 days for SEM. Samples were placed in primary fixative (3% glutaraldehyde with 0.1 M sucrose and 0.1 M sodium cacodylate in deionized water) for 45 min, followed by a rinse in buffer solution (primary fixative without glutaraldehyde) for 10 min. Then samples were dehydrated in increasing concentrations of ethanol (30%, 50%, 70%, 90%, and 100%) for 10 min each at room temperature. Finally, samples were incubated in hexamethyldisilazane for 10 min and air-dried for imaging. Samples were then imaged using SEM (the same as for determining PEM absorption) to determine morphology.

2.3 Statistical Analysis

One representative experiment was conducted, and all results were analyzed using a one-way Analysis of Variance (ANOVA) comparing experimental group means. Statistical significance was considered at $p < 0.05$ (JMP®, Version *15.0.0*. SAS Institute Inc., Cary, NC, 1989-2019).

2.4 Results

2.4.1 Surface Characterization

The SEM images show uniform vertical nanotubes on the surfaces, and coating with 18-layer PEM maintains the nanotube morphology (**Figure 2.1a**). XPS survey scans for Nt surfaces indicate oxygen (O1s), carbon (C1s), and titanium (Ti2p) elements on the surface with no visible nitrogen (N1s) or sulfur (S2p) elements present. However, survey scans for Nt + PEM indicate the presence of O1s, C1s, N1s, S2p elements with no discernable Ti2p (**Figure 2.1b**). High-resolution nitrogen spectra show ammonium, amine and amide peaks, consistent with the polysaccharide

PEM composition. High-resolution C1s spectra indicate alcohol, ether and amine groups contributing to the overall C1s peak (**Figure 2.2b**).

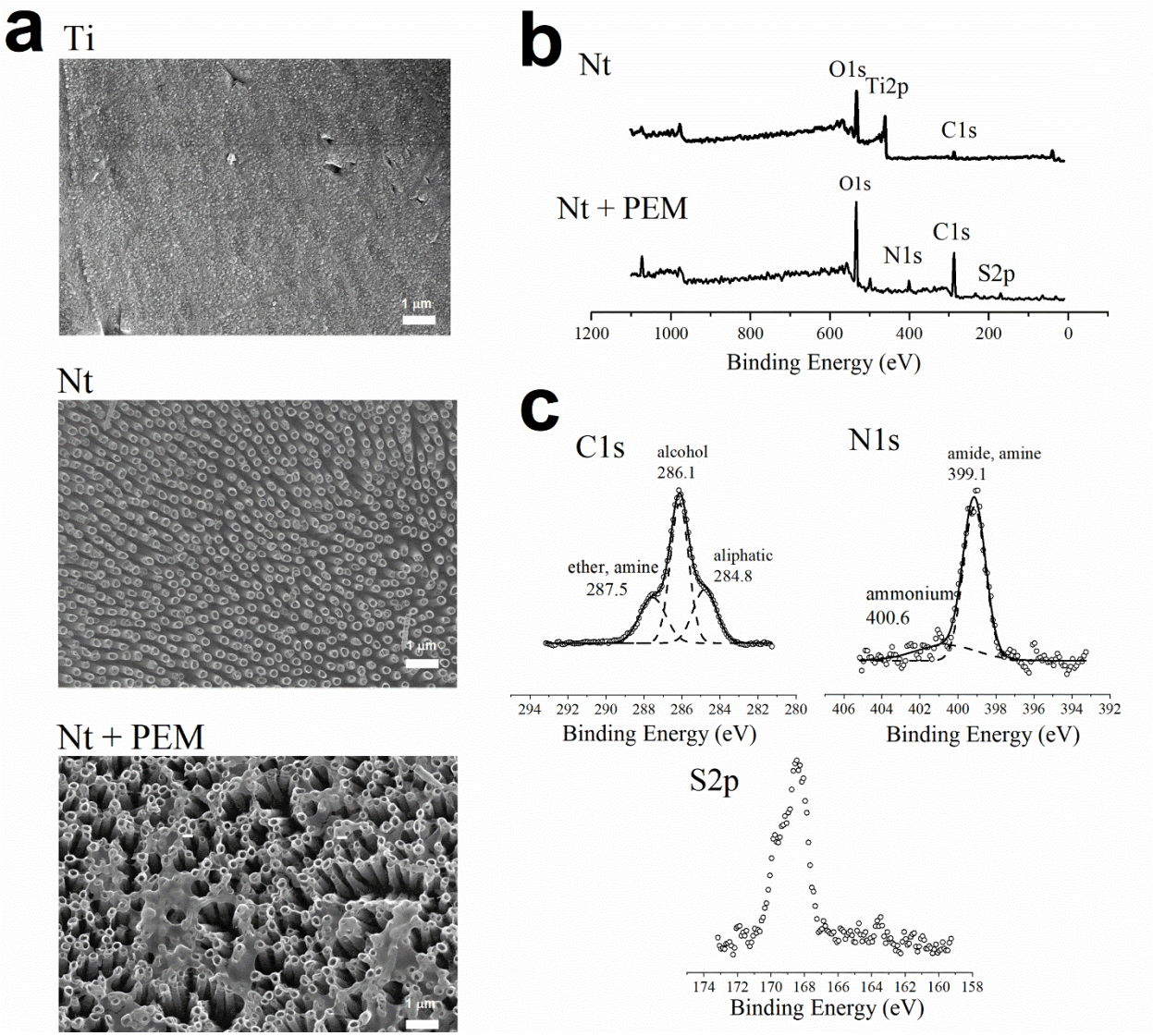

Figure 2.1 (a) Representative SEM images of surfaces. The Ti image is a representative image of the flat titanium surface, before anodization. The Nt image is a representative image of the titanium surface after anodization and the addition of nanotubes on the surface. The Nt + PEM image shows a nanotube surface after the addition of PEMs. Nanotube morphology is maintained after addition of PEMs. (b) Full XPS survey spectra of Nt and Nt + PEM surfaces. O1s, $Ti2p_{3/2}$, C1s, N1s, and S2p peaks are labeled. (c). High-resolution XPS spectra of C1s, N1s, and S2p for Nt + PEM surfaces.

2.4.2 BMP-2 Adsorption and Release from Surfaces

BMP-2 adsorbed onto Nt + PEM + PEM surfaces was measured using an ELISA. The average (± standard deviation) amount of BMP-2 loaded onto the Nt samples from 100 ng/ml and 500 ng/ml was 23.18 ± 0.11 ng (92.7 ± 0.4% of total BMP-2 added) and 92.5 ± 5.5 ng (74 ± 4.4% of total BMP-2 added) respectively. Nt + PEM samples loaded with 500 ng/ml have a lower percentage of growth factor adsorbed than those loaded with 100 ng/ml, but a higher total amount of growth factor adsorbed.

The cumulative release of BMP-2 was measured over 28 d. After 2 d the amount of BMP-2 released is below the threshold of the ELISA and considered zero (data not shown). The largest amount of BMP-2 is released from the surface during the first six hours and starts to level off after 24 h (**Figure 2.2**). Only 1.2 to 1.5% of the adsorbed growth factor is released and detectable in solution, suggesting that a large fraction of the BMP-2 remains surface-bound.

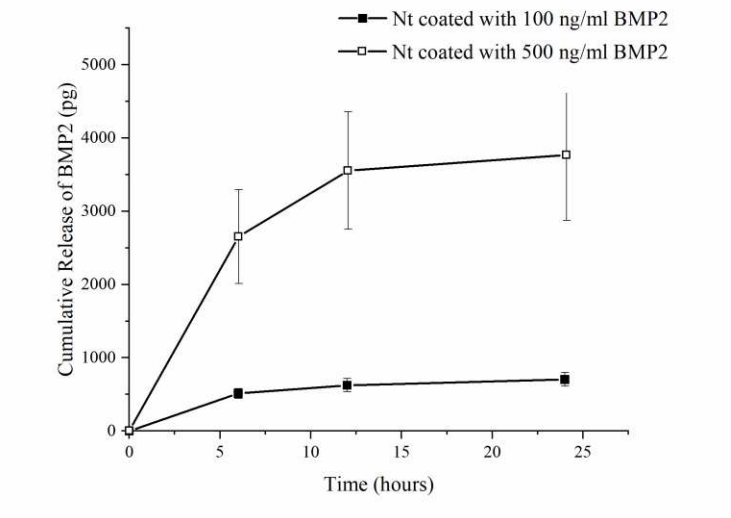

Figure 2.2 Cumulative Release of BMP-2 in vitro from Nt + PEM + BMP-2 surfaces (average ± *SE).*

2.4.3 ALP Activity and Calcium Deposition

ALP activity was measured at up to 28 d in culture (**Figure 2.3a**) and was normalized to total protein content. For all ALP, calcium and total protein results, "week 1" represents one week after switching to complete media (14 days after the initial cell seeding). There are no significant differences between the groups after 1 week and 2 weeks in complete media. After three weeks in complete media Nt samples with BMP-2 in the media have a significantly higher ALP activity when compared to the other three samples.

Calcium content (normalized to total protein content) was measured on surfaces up to 28 d (**Figure** 2.**3b**). After 1 week in complete media, Nt + PEM samples have significantly more calcium than Nt and Nt + BMP-2 in media samples. There is no significant difference between the samples at week two. At week three Nt + PEM +BMP-2 samples have significantly more calcium than Nt surfaces.

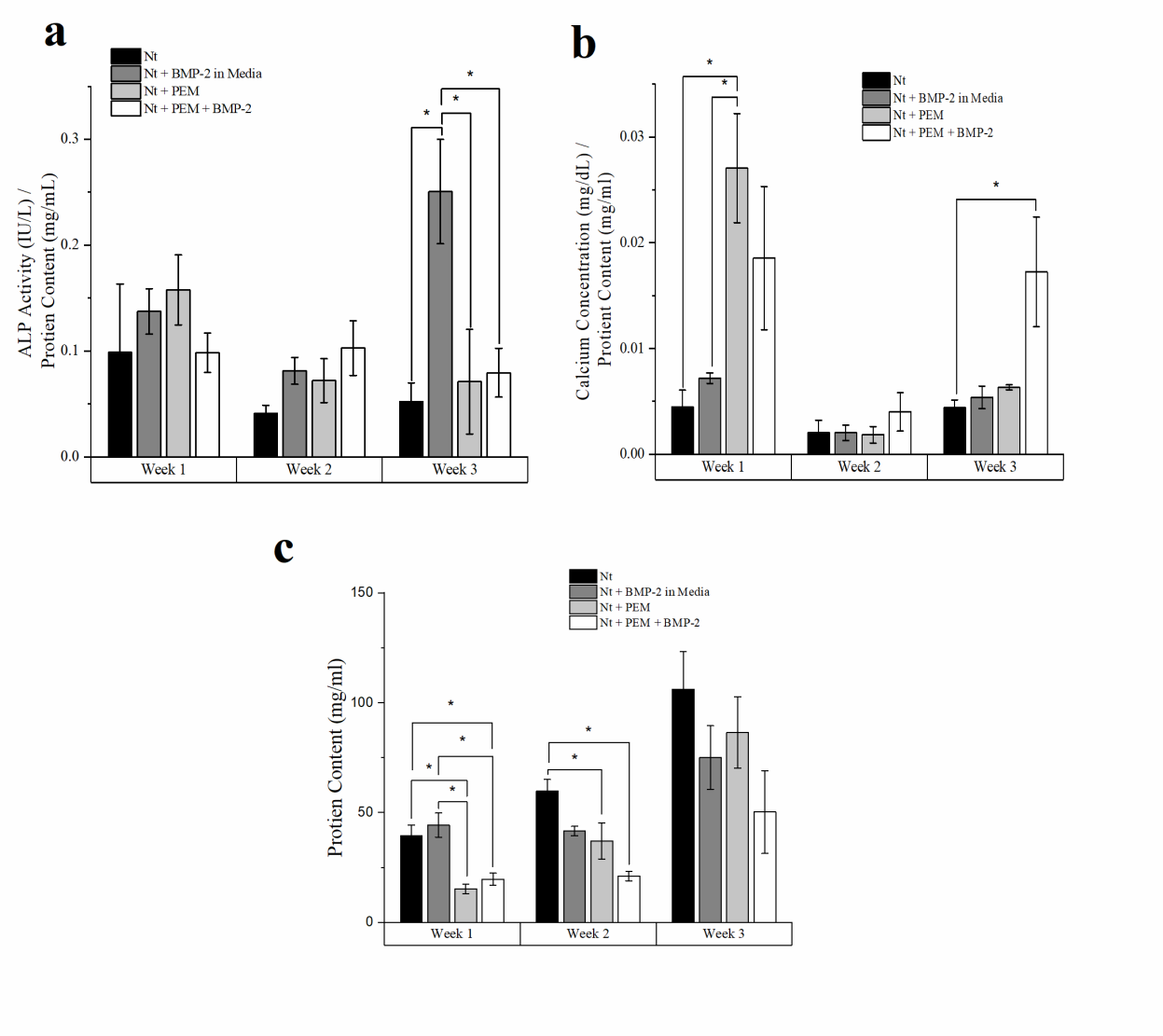

Figure 3.2 (a) ALP activity of rat bone marrow cells on surfaces at 1, 2, and 3 weeks post change to complete media. (b) Calcium concentration on surfaces 1, 2, and 3 weeks post change to complete media. (c) Total protein concentration on surfaces at 1, 2, and 3 weeks post change to complete media. (* indicates $p < .05$).

2.4.4 Cell Counts and Osteocalcin

Samples were stained for osteocalcin one and three weeks after switching to complete media. (**Figure 2.4a**). The total number of cells (nuclei) was determined (**Figure 2.4b**), and the percent area of osteocalcin (normalized to number of nuclei) was measured (**Figure 2.4c**). As with the ALP activity, calcium, and total protein, "week 1" represents 1 week after switching to

complete media or 14 days since initial cell seeding. For both week 1 and 3, Nt + PEM + BMP-2 samples have significantly more % area of osteocalcin compared to the other three samples. At week 1 Nt surfaces have a greater number of cells than both the Nt + PEM samples and the Nt + PEM + BMP-2 samples. At week 3 Nt + BMP-2 in media samples have a greater number of cells than Nt + PEM samples. By week 3 fluorescence images show clusters of cells and actin fibers on all samples, other than Nt samples. On Nt samples the cells were aligned so the actin fibers of all the cells remained parallel.

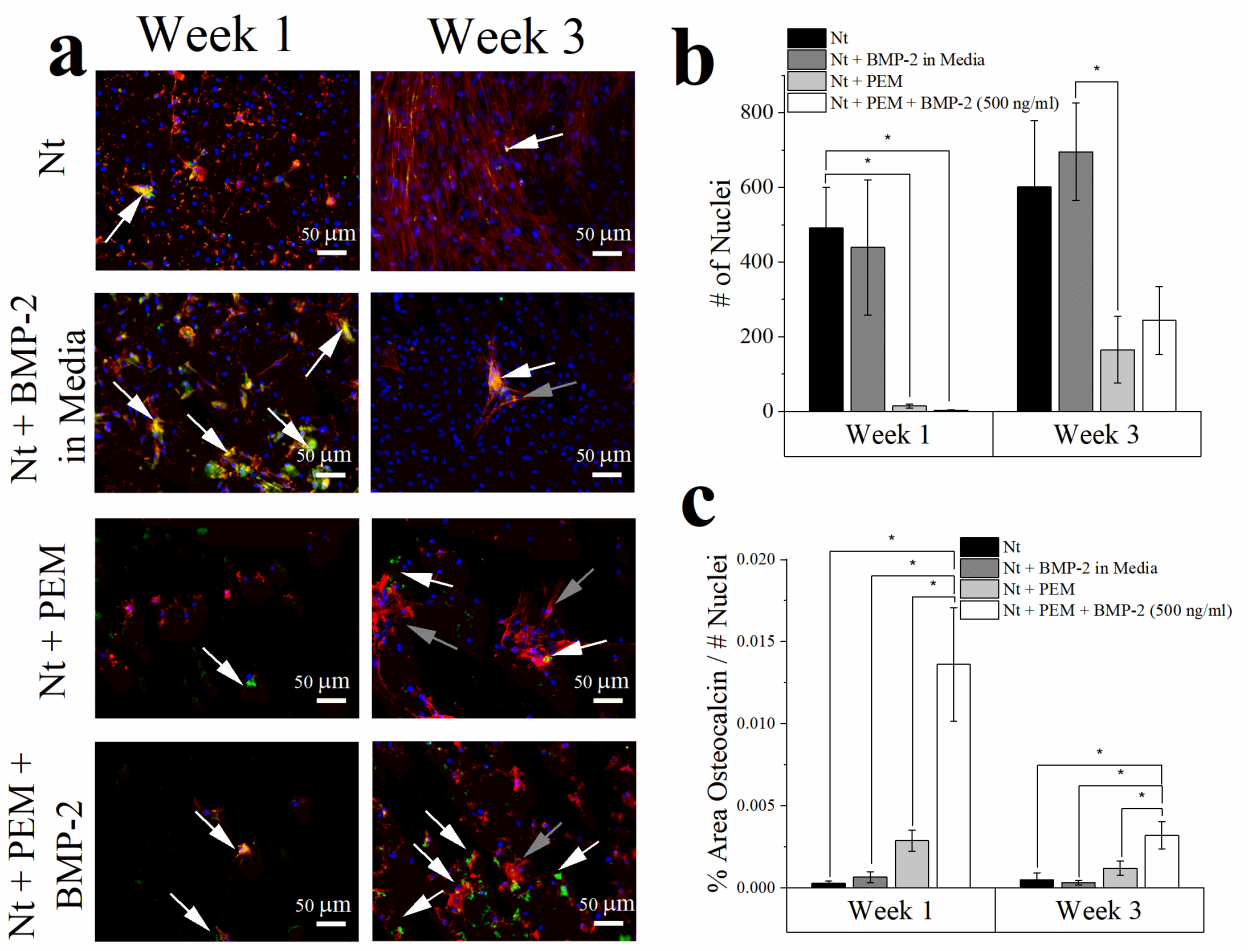

Figure 2.4 (a) Fluorescent images (20×) of stromal cells on Nt surfaces. Osteocalcin (green), nuclei (blue) and Actin (red). White arrows point to examples of osteocalcin staining. Gray arrows point to examples of nonparallel Actin fibers. (b) Number of nuclei on samples at week 1 and 3 (calculated using 10× images). (c) % area of osteocalcin/nuclei at week 1 and 3 (calculated using 10× images). (* indicates $p < .05$).

2.4.5 Cell Morphology SEM

All surfaces show cell attachment by week 1 and cell spreading by week 3 (**Figure 2.5**). At week 1, Nt and Nt + BPM-2 in media surfaces show the beginning of cell spreading and cells interacting with the nanotubes. At week 1, Nt + PEM and Nt + PEM + BMP-2 samples show cells with less spreading and interaction with surfaces, but the addition of protein-like structures that are not present by week 3. By week 3, cells on Nt + BMP-2 in the media samples have started to form clusters and are covering most of the surface. Cells have started to cover the surface of Nt + PEM + BMP-2 surfaces, but there are not cell clusters on the surface.

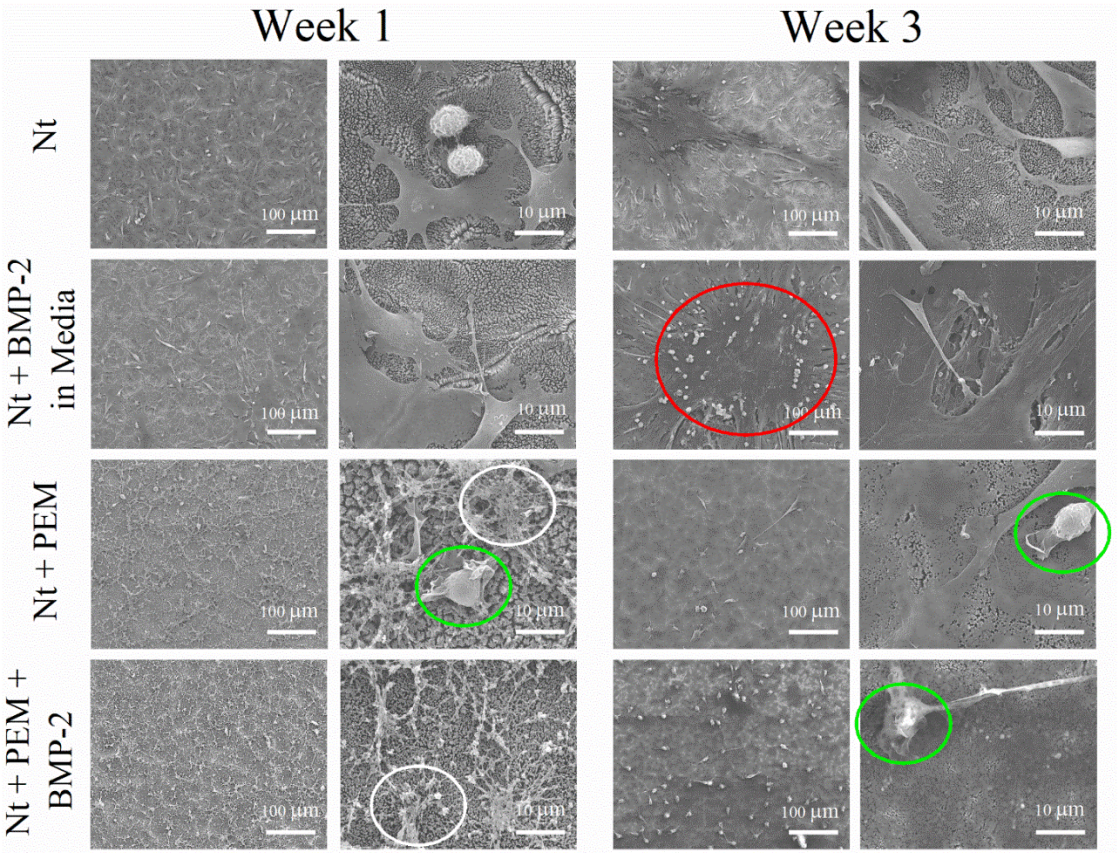

Figure 2.5 Representative SEM images of each sample at week 1 and week 3. The images under each week were taken at 250× (left) and at 2500× (right). Examples of cells are circled in greed and the white circles represent protein-like structures observed only on the PEM coated samples. Cell clusters are circled in red.

2.5 Discussion

The combination of nanotopography and growth factor presentation increases the osteogenic properties of surfaces. These new surfaces combine nanotopography introduced via titania nanotubes, and glycosaminoglycan coatings that conformally coat the nanotubes while retaining some nanoscale features. The glycosaminoglycan-based coatings bind and stabilize BMP-2, with less than 2% of the BMP-2 released over the first 48 hours. The samples coated with a higher dose of BMP-2 show a lower percentage of BMP-2 binding to the surfaces. This could be because the surfaces' capacity to bind BMP-2 is approaching saturation. These results differ from similar studies that investigated release of BMP-2 from titanium surfaces over 30 days *in vitro*.[29,30] The study by Lee *et al.* bound a similar amount (50 ng) of BMP-2 with heparin onto flat titanium surfaces.[29] The study by Yang *et al.* bound 50 ng BMP-2 with the addition of heparin and human growth and differentiation factor 5 onto flat titanium.[30] Both studies bound heparin directly to the surfaces and observed a burst release of BMP-2 in the first day followed by sustained release over 30 days.[29,30] In our study the majority of the BMP-2 is retained on the surfaces. The main differences between the two studies and ours is the surface topography of the samples and the way the heparin was absorbed onto the samples.

The cells responsible for new bone formation are osteoblasts. Phase one of mineralization takes place in matrix vesicles released from osteoblasts. ALP is responsible for the generation of inorganic phosphate and internal transport into the vesical.[44-46] Therefore ALP is one of the first markers of osteogeneses. The only difference in ALP activity was found at week three, where there was significantly more ALP activity on the Nt + BMP-2 in media samples compared to the other three groups (**Figure 2.3a**). ALP activity varies during differentiation and mineralization and can reflect the distributions of cells throughout the cell cycle.[47] Because of this, it is possible that the

time points chosen missed the peak in ALP activity for the other samples. The high ALP activity at week three for the Nt + BMP-2 in media sample, indicate that the cells have an osteogenic response to BMP-2.

During osteogenesis, after ALP activity peaks, calcium and inorganic phosphate are internalized into the vesical. In the vesical they form non-crystalline amorphous CaP that is then converted into octa CaP crystals, and then eventually into insoluble hydroxyapatite crystals.[48] During phase two of mineralization hydroxyapatite is released from the vesicle and extra-vesicular Ca^{2+} and P_i increases. Differences in calcium content were only found at week one and week three (**Figure 2.3b**). It was unexpected that Nt + PEM samples have greater calcium compared to other samples at week 1. All samples are normalized to total protein. Nt + PEM and Nt + PEM + BMP-2 have a significantly lower total protein content at week 1 than samples without PEMs. Because of this, the large calcium content observed on the Nt + PEM samples could be due to the low total protein content at week one (**Figure 2.3c**). By week 2 total protein on the Nt + PEM samples is no longer significantly less than total protein on the Nt + BMP-2 in media samples. This could explain the observed decrease in calcium content observed in week 2 on the Nt + PEM samples (**Figure 2.3b**). While not statistically significant, there is more calcium on the Nt + PEM + BMP-2 samples. By week 3 there is significantly more calcium on the Nt + PEM + BMP-2 samples compared to the Nt samples. At this time point there was no significant difference in total protein between the samples. The greater amount of calcium on the Nt + PEM + BMP-2 surfaces at week three shows that the way BMP-2 is presented on the surface increases the cells' calcium production compared to Nt surfaces alone.

With the increase of extra-vesicular Ca^{2+} and P_i, binding proteins including osteocalcin regulate the continued nucleation of hydroxyapatite crystals.[46] Osteocalcin can be visualized using

immunohistochemistry (IHC) staining (**Figure 2.4**). At both week 1 and week 3 there is significantly more osteocalcin per nucleus on the Nt + PEM + BMP-2 samples compared to the other three samples. This corresponds to the calcium results, confirming that the cells have a favorable osteogenic response to how BMP-2 is presented on Nt surfaces.

Undifferentiated mesenchymal stem cells MSCs and osteoblasts have different actin cytoskeletal structures. Upon differentiation into osteoblasts MSCs go from fibroblast like spindle shape with long, thin stress fibers running parallel in orientation with the cell, to thicker crisscrossed pattern of actin fibers.[49] At week 3 there is a clear visual difference on how the actin fibers are oriented on the samples (**Figure 2.4a**). At week three actin fibers on the Nt samples are thin and run parallel to each other, similar to the presentation of fibroblasts and undifferentiated MSCs. The other three samples show thicker actin fibers presented in a crisscross pattern. Whole bone marrow, which contains MSCs, was used in this experiment. The morphology observed here is consistent with expected changes in actin organization as MSCs differentiate into osteoblasts.

At the start of differentiation of MSCs there is a notable change in morphology. Cells go from a fibroblast-like phenotype to a nearly spherical form.[50] Cell roundness has been highly correlated with expression of osteogenic markers.[51] When MSCs are exposed to differentiation factors *in vitro*, cells that form nodular aggregates with visible bare spots have greater mineral deposition.[52] This is consistent with the morphology seen in the SEM images of the samples (**Figure 2.5**). Nodules and cell clustering can be seen on the cells with the Nt, while this is not visible on the Nt + PEM samples. While samples with PEMs do not have these features, there is some covering of the surface and cells starting to form clusters, seen in the Nt + PEM + BMP-2 samples. This could suggest that these samples are delayed in cluster formation or the cells need to be seeded at a higher density to initiate clustering.

These results are consistent with pervious similar studies. One study incorporated BMP-2 into PEMs on titanium foil to increase osteogenesis.[25] Chitosan/gelatin with 2 μg/ml of rhBMP-2 multilayers were constructed on Ti6Al4V surfaces, and showed an increase in ALP activity and mineralization *in vitro* and increased bone density and bone formation *in vivo* when implanted in rabbits.[25] Another study conjugated BMP-2 onto titania nanotube surfaces using dopamine.[61] Surfaces with conjugated BMP-2 increased ALP and mineralization after 7 and 14 days. The total concentration of BMP-2 on the surfaces was not reported, and samples were incubated in 50 ml of 80 ng/ml rhBMP-2.[26] The innovation introduced in our work is the combination of BMP-2 delivery with the nanotopographical features of the Nt, and the binding of BMP-2 in PEMs to stabilize the presentation of small, physiologically relevant doses of BMP-2 from the surfaces.

2.6 Conclusion

Improving surfaces for orthopedic implants by creating surfaces that promote bone growth is still a major problem. In this study, BMP-2 was successfully absorbed onto Nt surfaces via PEMs. The BMP-2 remained on the surfaces for up to 28 d in PBS. Our results show that Nt surfaces modified with BMP-2 can increase osteogenic markers in bone marrow cells including osteocalcin and calcium content by 28 d in culture. When compared to Nt surfaces, BMP-2 surfaces induce greater osteocalcin and calcium deposition. This agrees with other studies that BMP-2 bound to surfaces increase the osteogenic response of cells. Heparin increases the half-life of BMP-2 *in vitro* and its use in the PEMs allow for a lower concentration of BMP-2 to be applied to the surfaces. Previous studies using BMP-2 use high concentrations of BMP-2 or lower concentrations on flat titanium or non-organized topographies, and those studies with BMP-2 and heparin show a constant release of BMP-2 over 30 days *in vitro*. Our study combines organized nontopographic surfaces with BMP-2 and heparin. This unique presentation of BMP-2 on surfaces

provides an increase in osteogenic properties of bone marrow cells. This provides a promising approach to enhance bone healing and improve orthopedic implants.

REFERENCES

1. Ethgen, O., Bruyère, O., Richy, F., Dardennes, C. & Reginster, J.-Y. Health-Related Quality of Life in Total Hip and Total Knee Arthroplasty. *J. Bone Jt. Surg*. 86, 963–974 (2004).

2. Etkin, C. D. & Springer, B. D. The American Joint Replacement Registry the first 5 years. *Arthroplast. Today* 3, 67–69 (2017).

3. Zhang, B. G. X., Myers, D. E., Wallace, G. G., Brandt, M. & Choong, P. F. M. Bioactive coatings for orthopaedic implants-recent trends in development of implant coatings. *Int. J. Mol. Sci.* 15, 11878–11921 (2014).

4. Vincent, G. K. & Velkoff, V. A. THE NEXT FOUR DECADES The Older Population in the United States: 2010 to 2050 Population Estimates and Projections Current Population Reports. (2010).

5. Raphel, J. *et al.* Engineered protein coatings to improve the osseointegration of dental and orthopaedic implants. *Biomaterials* 83, 269–282 (2016).

6. Kurtz, S., Ong, K., Edmond, L., Mowat, F. & Halpern, M. Projections of Primary and Revision Hip and Knee Arthroplasty in the United States from 2005 to 2030. J. *Bone Jt. Surg*. 89, 780 (2007).

7. Campoccia, D., Montanaro, L. & Arciola, C. R. The significance of infection related to orthopedic devices and issues of antibiotic resistance. *Biomaterials* 27, 2331–2339 (2006).

8. Ballo, A., Agheli, H., Lausmaa, J., Thomsen, P. & Petronis, S. Nanostructured model implants for in vivo studies: influence of well-defined nanotopography on de novo bone formation on titanium implants. *Int. J. Nanomedicine* 6, 3415–3428 (2011).

9. Bjursten, L. M. *et al.* Titanium dioxide nanotubes enhance bone bonding in vivo. *J. Biomed. Mater. Res. Part A* 92, 1218–1224 (2009).

10. Dalby, M. J. *et al.* The control of human mesenchymal cell differentiation using nanoscale symmetry and disorder. *Nat. Mater*. 6, 997–100 (2007).

11. Biggs, M. J. P. *et al.* The use of nanoscale topography to modulate the dynamics of adhesion formation in primary osteoblasts and ERK/MAPK signalling in STRO-1+ enriched skeletal stem cells. *Biomaterials* 30, 5094–5103 (2009).

12. Fiedler, J. *et al.* The effect of substrate surface nanotopography on the behavior of multipotnent mesenchymal stromal cells and osteoblasts. *Biomaterials* 34, 8851–8859 (2013).

13. Alenezi, A. *et al.* Characteristics of 2 Different Commercially Available Implants with or without Nanotopography. *Int. J. Dent.* 2013, (2013).

14. Popat, K. C., Leoni, L., Grimes, C. A. & Desai, T. A. Influence of engineered titania nanotubular surfaces on bone cells. *Biomaterials* 28, 3188–3197 (2007).

15. Bishop, G. B. & Einhorn, T. A. Current and future clinical applications of bone morphogenetic proteins in orthopaedic trauma surgery. *Int. Orthop.* 31, 721–727 (2007).

16. Carreira, A. C. *et al.* Bone Morphogenic Proteins: Facts, Challenges, and Future Perspectives. *Crit. Rev. Oral Biol. Med.* 93, 335–345 (2014).

17. Ong, C. T., Choon, D. S. K., Cabrera, N. P. & Maffulli, N. The treatment of open tibial fractures and of tibial non-union with a novel external fixator. *Injury* 33, 829–834 (2002).

18. Hustedt, J. W. & Blizzard, D. J. The Controversy Surrounding Bone Morphogenetic Proteins in the Spine: A Review of Current Research. *Yale of J of Bio and Med.* 87, (2014).

19. Suliman, S. *et al.* Release and bioactivity of bone morphogenetic protein-2 are affected by scaffold binding techniques in vitro and in vivo. *J. Control. Release* 197, 148–157 (2015).

20. U.S. Food and Drug Administration. Infuse bone graft Important Medical Information.

21. Carragee, E. J., Hurwitz, E. L. & Weiner, B. K. A critical review of recombinant human bone morphogenetic protein-2 trials in spinal surgery: emerging safety concerns and lessons learned. *Spine J.* 11, 471–491 (2011).

22. Mohammadi, M. *et al.* Fabrication of hybrid scaffold based on hydroxyapatite-biodegradable nanofibers incorporated with liposomal formulation of BMP-2 peptide for bone tissue engineering. *Nanomedicine Nanotechnology, Biol. Med.* 14, 1987–1997 (2018).

23. Jeon, O., Song, S. J., Kang, S. W., Putnam, A. J. & Kim, B. S. Enhancement of ectopic bone formation by bone morphogenetic protein-2 released from a heparin-conjugated poly(l-lactic-co-glycolic acid) scaffold. *Biomaterials* 28, 2763–2771 (2007).

24. Yamamoto, M., Takahashi, Y. & Tabata, Y. Controlled release by biodegradable hydrogels enhances the ectopic bone formation of bone morphogenetic protein. *Biomaterials* 24, 4375–4383 (2003).

25. Hu, Y. *et al.* Regulation of the differentiation of mesenchymal stem cells in vitro and osteogenesis in vivo by microenvironmental modification of titanium alloy surfaces. *Biomaterials* 33, 3515–3528 (2012).

26. Lai, M. *et al.* Surface Functionalization of TiO 2 Nanotubes with Bone Morphogenetic Protein 2 and Its Synergistic Effect on the Differentiation of Mesenchymal Stem Cells. *Biomacromolecules* 12, 1097–1105 (2011).

27. Simmons, C. A., Alsberg, E., Hsiong, S., Kim, W. J. & Mooney, D. J. Dual growth factor delivery and controlled scaffold degradation enhance in vivo bone formation by transplanted bone marrow stromal cells. *Bone* 35, 562–569 (2004).

28. Li, Y., Song, Y., Ma, A. & Li, C. Surface immobilization of TiO 2 nanotubes with bone morphogenetic protein-2 synergistically enhances initial preosteoblast adhesion and osseointegration. *Biomed Res. Int.* 2019, (2019).

29. Lee, S. *et al.* The effect of titanium with heparin / BMP-2 complex for improving osteoblast activity. *Carbohydr. Polym.* 98, 546–554 (2013).

30. Yang, D. H., Moon, S. W. & Lee, D. Surface Modification of Titanium with BMP-2 / GDF-5 by a Heparin Linker and Its Efficacy as a Dental Implant. *Int. J. Mol. Sci.* 18, 1–16 (2017).

31. Shi, Z., Neoh, K. G., Kang, E. T., Poh, C. K. & Wang, W. Surface Functionalization of Titanium with Carboxymethyl Chitosan and Immobilized Bone Morphogenetic Protein-2 for Enhanced Osseointegration. *Biomacromolecules* 10, 1603–1611 (2009).

32. Shah, N. J. *et al.* Tunable dual growth factor delivery from polyelectrolyte multilayer films. *Biomaterials* 32, 6183–6193 (2011).

33. Detzel, C. J., Larkin, A. L. & Rajagopalan, P. Polyelectrolyte Multilayers in Tissue Engineering. *Tissue Eng. Part B* 17, 11–113 (2011).

34. Volpato, F. Z. *et al.* Preservation of FGF-2 bioactivity using heparin-based nanoparticles, and their delivery from electrospun chitosan fibers. *Acta Biomater.* 8, 1551–1559 (2012).

35. Almodóvar, J., Bacon, S., Gogolski, J., Kisiday, J. D. & Kipper, M. J. Polysaccharide-based polyelectrolyte multilayer surface coatings can enhance mesenchymal stem cell response to adsorbed growth factors. *Biomacromolecules* 11, 2629–2639 (2010).

36. Place, L. W., Sekyi, M. & Kipper, M. J. Aggrecan-Mimetic, Glycosaminoglycan-Containing Nanoparticles for Growth Factor Stabilization and Delivery. *Biomacromolecules* 15, 680–689 (2014).

37. Ruppert, R., Hoffmann, E. & Sebald, W. Human bone morphogenetic protein 2 contains a heparin-binding site which modifies its biological activity. *Eur. J. Biochem.* 237, 295–302 (1996).

38. Zhao, B. *et al.* Heparin Potentiates the in Vivo Ectopic Bone Formation Induced by Bone Morphogenetic Protein-2

39. Simon-Walker, R. *et al.* Glycocalyx-inspired nitric oxide-releasing surfaces reduce platelet adhesion and activation on titanium. *ACS Biomater. Sci. Eng.* 3, 68–77 (2017).

40. Romero, R. *et al.* Combined delivery of FGF-2, TGF-β1, and adipose-derived stem cells from an engineered periosteum to a critical-sized mouse femur defect. *J. Biomed. Mater. Res. - Part A* 105, 900–911 (2017).

41. Lee, D. W., Yun, Y. P., Park, K. & Kim, S. E. Gentamicin and bone morphogenic protein-2 (BMP-2)-delivering heparinized-titanium implant with enhanced antibacterial activity and osteointegration. *Bone* 50, 974–982 (2012).

42. Almodóvar, J., Bacon, S., Gogolski, J., Kisiday, J. D. & Kipper, M. J. Polysaccharide-Based Polyelectrolyte Multilayer Surface Coatings can Enhance Mesenchymal Stem Cell Response to Adsorbed Growth Factors. *Biomacromolecules* 10, 2629–2639 (2010).

43. Martins, J. G., Camargo, S. E. A., Bishop, T. T., Popat, K. C. & Kipper, M. J. Pectin-chitosan membrane scaffold imparts controlled stem cell adhesion and proliferation. *Carbohydr. Polym.* 197, 47–56 (2018).

44. Beck, G. R. Inorganic phosphate as a signaling molecule in osteoblast differentiation. *J. Cell. Biochem.* 90, 234–243 (2003).

45. Kirsch, T. Annexins—their role in cartilage mineralization. Front. Biosci. 10, 576–581 (2005).

46. Anderson, H. C. Matrix vesicles and calcification. *Curr. Rheumatol. Rep*. 5, 222–226 (2003).

47. Fedarko, N. S., Bianco, P., Vetter, U. & Robey, P. G. Human bone cell enzyme expression and cellular heterogeneity: Correlation of alkaline phosphatase enzyme activity with cell cycle. *J. Cell. Physiol.* 144, 115–121 (1990).

48. Lotsari, A., Rajasekharan, A. K., Halvarsson, M. & Andersson, M. Transformation of amorphous calcium phosphate to bone-like apatite. *Nat. Commun*. 9, 1–11 (2018).

49. Yourek, G., Hussain, M. A. & Mao, J. J. Cytoskeletal Changes of Mesenchymal Stem Cells During Differentiation. ASAIO J (American Soc. Artif. Intern. Organs 1992) 53, 219–228 (2007).

50. Rodriguez, P., Gonzalez, M., Rios, S. & Cambiazo, V. Cytoskeletal Organization of Human Mesenchymal Stem Cells (MSC) Changes During Their Osteogenic Differentiation. *J. Cell. Biochem.* 731, 721–731 (2004).

51. Chen, L., Tredget, E. E., Wu, P. Y. G. & Wu, Y. Paracrine Factors of Mesenchymal Stem Cells Recruit Macrophages and Endothelial Lineage Cells and Enhance Wound Healing. *Public Libr. Sci. 3*, (2008).

52. Cho, H. *et al*. Effective Immobilization of BMP-2 Mediated by Polydopamine Coating on Biodegradable Nanofibers for Enhanced in Vivo Bone Formation BK21 Plus Future Biopharmaceutical Human Resources Training and Research Team. ACS *Appl. Mater. Interfaces* 6, 11225–11235 (2014).

CHAPTER 3: CHITOSAN/*IOTA*-CARRAGEENAN AND CHITOSAN/PECTIN POLYELECTROLYTE MULTILAYER SCAFFOLDS WITH ANTIADHESIVE AND BACTERICIDAL PROPERTIES[2]

Overview

It has been a challenge to develop durable and cytocompatible antibacterial coatings with antiadhesive and antimicrobial activities. To overcome the problems caused by bacteria contamination on biomedical devices, we are proposing layer-by-layer films based on iota-carrageenan/chitosan, and pectin/chitosan polyelectrolyte multilayers (PEMs) assembled in an acetic acid/acetate buffer solution at pH 5.0. PEMs with 5 and 15 layers are established with chitosan-terminated layers. As compared to pectin, the *iota*-carrageenan promotes a PEM with a more wettable surface (water contact angle of 25°) and a low roughness. The PEMs have strong antiadhesive and bactericidal activities against *Pseudomonas aeruginosa* (*P. aeruginosa*) and *Staphylococcus aureus* (S. aureus). For *P. aeruginosa*, the effect is seen after 6 h and for S. aureus the effect is seen after 24 h. The antibacterial test *in vitro* indicates that PEMs can kill and avoid the attachment of bacteria effectively. To confirm the biomedical potential of these PEMs to act as coatings for tissue scaffolds and implants, adhesion and proliferation of bone marrow-derived stem cells (BMSCs) is demonstrated after 4 and 7 days of incubation. The iota-

[2] Portions of this chapter are reproduced from: Martins, A. F., Vlcek, J., Wigmosta, T., Hedayati, M., Reynolds, M. M., Popat, K. C., & Kipper, M. J. (2020). Chitosan/iota-carrageenan and chitosan/pectin polyelectrolyte multilayer scaffolds with antiadhesive and bactericidal properties. *Applied Surface Science*, *502*, 144282.

carrageenan/chitosan PEM supports the BMSCs adhesion, proliferation and spreading, inhibits the attachment and growth of bacteria and promotes cytocompatibility of surfaces.

3.1 Introduction

Polyelectrolyte multilayers (PEMs) can easily be prepared on suitable substrates by the layer-by-layer (LbL) approach.[1] PEMs are built up by deposition/adsorption of alternating cationic and anionic layers of polyelectrolytes on a solid substrate.[2] The resulting thin films can be interpenetrated assemblies principally stabilized by the electrostatic interactions between polycation-polyanion pairs. The LbL method has been used to create surfaces with tunable biological functions for use in biomedical devices.[3] Several studies have reported using the LbL technique to modify the surfaces of poly(ethylene terephthalate), polystyrene (PS), polyurethane-coated decellularized scaffold , gold, and other substrates with PEMs composed of chitosan (CS), chitosan derivatives and glycosaminoglycans (heparin, hyaluronic acid and chondroitin sulfate).[2,4-9]

PEMs have been constructed to deliver a growth factor (bone morphogenetic protein 2) for bone regeneration, prevent bacteria adhesion and proliferation, as well as to prolong blood coagulation time, enhance resistance to platelet adhesion, and prevent fibrin network formation.[1,3,5,7,9] The biological responses to PEMs can be controlled by modulating the processing conditions and surface features used during the LbL assembly. Important parameters include the surface wettability, roughness, pH of the polyelectrolyte solutions, and the polyelectrolytes from which the PEMs are assembled.[7] In complex protein solutions, such as blood, serum, and dairy products, cell and bacteria adhesion are thought to be mediated by a layer surface adsorbed proteins.[10,11] Direct contact of bacteria with surfaces and the adsorption of planktonic bacteria directly to the surface in protein deficient environments (e.g. water, urine, saliva) are also

important routes for bacterial colonization.[10] Therefore, surfaces that prevent bacterial contamination may need to both be antiadhesive toward bacteria (to prevent direct adsorption), and possess antimicrobial activity, to kill bacteria which attach through protein- mediated mechanisms. Polysaccharide-based coatings may have both antimicrobial and antiadhesive properties.[12-14] For example CS/glycosaminoglycan-based multilayers have antiadhesive and bactericidal actions against *Escherichia coli* (*E. coli*) when the PEMs were assembled at pH 3.0.[5,7] However, these papers reported only the antimicrobial activity of the PEMs toward *E. coli*.[4,5,7]

Pseudomonas aeruginosa (*P. aeruginosa*) is a Gram-negative bacterium associated with potentially fatal infections, including pneumonia, perianal/genital infections, urinary infections, and sepsis in patients at care units. Also, *P. aeruginosa* and *Staphylococcus aureus* (*S. aureus*, a Gram-positive bacterium) impart infections on skin and soft tissues.[15-17] A surface coating for medical implants and tissue scaffolds should be durable in aqueous and biological fluid media, prevent the adhesion and growth of bacteria, and mimic other extracellular matrix (ECM) functions to promote tissue healing.[18-20] Fibrillar, adhesive proteins, glycosaminoglycans, and proteoglycans are the major ECM components.[21] PEMs prepared from natural and semi-synthetic polysaccharides (CS/heparin, CS/dextran sulfate, CS/ carboxymethyl cellulose, and others) may provide a microenvironment to support cell adhesion and proliferation because they present similar chemistries and biochemical functions as other ECM components.[22,23] Furthermore, PEMs can be designed to perform important ECM functions that can control so-called "cell fate decisions" by promotion of cell-cell interactions, provision of cell-matrix anchorage sites, and stabilization and presentation of signals that control cell proliferation and differentiation.[19,24-29]

CS and its N-quaternized derivatives have well-known antimicrobial and antifungal activities and because of these traits, published papers about CS-based PEMs often focus on the

antimicrobial and antifungal properties.[4,5,7,22,30] CS/heparin/silver nanoparticle PEMs demonstrated antimicrobial activity attributed to the release of silver ions.[22] However, depending on the purpose, the silver ion concentration released can be toxic to living cells.[31] Carrageenan (*iota*-carrageenan, CA) and pectin (PC) are plant-derived, polyanionic polysaccharides that have favorable processing characteristics and can be combined with CS to form durable, biologically active PEMs. There are few reports describing CS/CA PEMs. Existing publications focus on their nanoscale properties, production of nanocoatings on poly(ε-caprolactone) films and biomineralization of calcium phosphate and calcium carbonate within CS/CA PEMs. CS/PC PEMs have been proposed as candidate materials for biocompatible coatings for food matrix and drug delivery devices.[32.33.35-37] Here, we purpose for the first time that durable CS/CA and CS/PC PEMs assembled in a weakly acidified condition (pH 5.0) can support strong antiadhesive and antimicrobial properties to prevent the attachment and growth of bacteria, and can be used to coat biomaterials to promote healing in applications that demand protection against the proliferation of bacteria.

This study describes the development of durable PEMs by assembling CS with CA and CS with PC on oxidized glass surfaces. CP Kelco produces commercial CA and PC for food industry applications.[38-41] PEMs are assembled from polyelectrolytes solutions obtained in an aqueous acetic acid/acetate buffer solution (pH 5.0). After PEM preparation, they are washed and maintained in ultrapure water until sterilization to perform the biological assays (antiadhesive, antimicrobial, and cell culture assays). By tuning the PEM surface properties, we develop durable and cytocompatible surfaces with potent antiadhesive and antimicrobial activities against both *P. aeruginosa* and *S. aureus.*

3.2.1 Materials and Methods

3.2.2 Materials

Chitosan (CS) composed of randomly distributed β(1 → 4)-D-glucosamine (85%) and N-acetyl-D-glucosamine (15%) units, with average molar weight of 87×10^3 g mol^{-1} was purchased from Golden-Shell Biochemical (China). GENU® pectin (PC) with an O-methylation degree of 56% and molar weight of 190×10^3 g mol^{-1}, as well as GENUVISCO® *iota*-carrageenan (CA, 277 × 103 g mol−1) formed from alternating α-(1 → 3)-D-galactose-4-sulfate and β-(1 → 4)-3,6-anhydro-D-galactose units, were kindly supplied by CP Kelco (Brazil). All the polysaccharides used in this study are previously well-characterized.[39,42,43]

3.2.3 Preparing the Polyelectrolyte Multilayer Assemblies

The glass substrates (disks of 10 mm diameter and 0.2 mm thickness) were placed in the wells of sterile Nuclon Δ TCPS 24-well plates, Nunc ALS (Roskilde, Denmark) and oxidized at 200 V in 10 cm^3 min^{-1} oxygen gas plasma for 10 min for promoting polycation deposition. The CS, CA, and PC solutions (1.0 mg mL^{-1}) were individually prepared in 0.2 mol L^{-1} acetate buffer solution (pH 5.0, prepared from 0.1 M sodium acetate and acetic acid solutions); an aqueous acetic acid solution (pH 4.0) was also prepared for rinsing. All solutions were filtered (0.22 μm polyvinylidene fluoride syringe filters, Fisher Scientific); the oxidized glass surfaces were rinsed with 1.0 mL rinse solution under shaking (100 rpm) for 6.0 min. The LbL depositions were carried out on the oxidized glass surfaces. The rinse solution was aspirated, and 1.0 mL CS solution (polycation) was added to the oxidized glass surfaces under shaking (100 rpm). After 6.0 min, the CS polycation solution was aspirated and the surface was rinsed under shaking for 6 min. Then, the rinse solution was aspirated and CA or PC solutions (polyanions, 1.0 mL) were deposited onto the oxidized glass surfaces containing one layer of CS (polycation). After assembling the second

layer (polyanion), the process of deposition was repeated to achieve 5- and 15-layer PEMs with a CS polycation-terminated layer. After deposition of the 5- or 15- layers, the PEMs were rinsed (6.0 min), and the rinse solution was aspirated to wash the PEMs with ultrapure water for 30 s. The PEMs were kept in phosphate buffer solution (PBS, pH 7.4) in a 48-well plate for 12 h before the biological assays and atomic force microscopy (AFM) characterization. The PEMs prepared from iota-carrageenan/chitosan, and pectin/chitosan are called (CA-CS)5, (CA-CS)15, (PC-CS)5 and (PCCS)15, respectively, where, the numbers 5 and 15 represent the number of layers deposited on the oxidized glass substrate.

3.2.4 Characterization

Surface chemistry of the PEMs was investigated using a Phi Electronics 5800 Spectrometer (Chanhassen, MN). The X-ray photoelectron spectroscopy (XPS) was performed with a monochromatic Al Kα X-ray source (hν = 1486.6 eV), a hemispherical analyzer, and a multichannel detector.[42] Before XPS, the as-obtained PEMs (washed surfaces) were dried with $N_{2(g)}$. Then, high-resolution spectra were obtained using a 23.5 eV analyzer pass energy with 0.10 eV steps and an X-ray spot of 800 μm. All spectra were obtained with a photoelectron take-off angle of 45°. A low-energy electron gun was used for charge neutralization. Spectra curve fitting was done using Origin version 8.5. Curve fitting of all spectra used a Shirley background. Gaussian peaks were fit according to expected functional groups. The height of each peak was fit first while keeping each peaks' position, full-width half max (fwhm) and percent Gaussian fixed. Then the fwhm, percent Gaussian, and finally position was fit while minimizing the chi-squared value.

3.2.5 Antimicrobial and Antiadhesive Tests

Bacterial studies were performed as previously described.[47] Briefly, *P. aeruginosa* (ATCC 15442) and *S aureus* (ATCC 29213) were thawed at room temperature after being frozen in a 1:1

glycerol solution. Cultures were then centrifuged at 4700 rpm for 10 min. After centrifugation, the supernatant was disposed of and the pellet was re suspended in warm LB broth. The bacterial cultures were incubated in liquid culture at 37 °C at 100 rpm. After at least 24 h of incubation, optical density measurements were taken and bacterium samples were seeded (500 μL) on the PEMs in a 48-well plate at optical density (OD_{600nm}) of 0.35 (concentration of approximately 2.8 × 10^8 cells mL^{-1}). At this density bacteria are all in the logarithmic growth phase. After 6 and 24 h samples were removed from the 48-well plate and fixed for scanning electron microscopy (SEM; JEOL JSM6500F) analysis. The samples were fixed in the primary fixative [3% glutaraldehyde (Sigma), 0.10 mol L^{-1} sodium cacodylate (Sigma), and 0.10 mol L^{-1} sucrose (Sigma)] for 45 min at room temperature. The samples were then washed with a buffer [0.10 mol L^{-1} sodium cacodylate, and 0.10 mol L^{-1} sucrose] for 10 min. The samples were then dried with increasing concentrations of ethanol solutions (35, 50, 75, and 100%) for 10 min each. To prepare samples for imaging, they were sputter-coated with palladium-gold alloy (Polaron SC 7620 Sputter Coater, Quorum Technologies, Newhaven, UK) at a thickness of 10 nm (10–15 mA, under a vacuum of 130 mTorr) and were grounded with copper tape. Samples were imaged using a scanning electron microscope (JSM-6500F, field emission scanning electron microscope, JEOL, Japan) with an accelerating voltage of 5 kV at 1000× for counting (five images per sample) and 3500× for cell morphology (one image per sample). We considered three samples (n = 3) for each PEM surface at each time point. Percent area of bacteria was found per sample using ImageJ software.

3.2.6 Cell Adhesion and Proliferation Assays

Bone marrow-derived stem cells (BMSCs) were isolated from male Wistar rats (Rattus norvegicus) according to the procedure reported by our research group.[48] Culture media [α-minimum essential medium (α-MEM) with 10% fetal bovine serum (FBS, Sigma) and 1%

penicillin/ streptomycin (pen/strep, Sigma)] containing 0.5 million cells was added to each well (0.5 million well^{-1}). The BMSC responses to the PEMs were investigated after 4 and 7 days of culture at 37 °C and 5% CO_2, in growth media. Cell adhesion and proliferation assays were carried out by staining the cells with rhodamine-phalloidin to visualize the cytoskeleton, while the cell nuclei were visualized by staining the cells with 4′,6-diamidino-2-phenylindole (DAPI), using a fluorescence microscope (Zeiss). Before staining, the media was aspirated, and the substrates were rinsed once in PBS before being transferred to a new 48- well plate, where the cells were fixed at 3.7% vol/vol formaldehyde solution for 15 min at room temperature. The fixative was aspirated, and the substrates were rinsed thrice with PBS for 5.0 min before being transferred to a new 48-well plate. The cells were permeabilized at 1.0% vol/vol triton-X solution for 3.0 min at room temperature. The permeant was aspirated, and the substrates were rinsed and transferred to a new 48-well plate where they were incubated at 37 °C in 5% CO_2 in a 5.0 μL mL^{-1} rhodamine-phalloidin solution for 25 min at 25 °C. Next, 1.0 μL mL^{-1} DAPI was added to the system, and the samples incubated for additional 5.0 min at room temperature. The solution was aspirated, substrates were rinsed twice with PBS, and kept in a light-resistant container at 4 °C until imaging. Fluorescence images were analyzed and processed with ImageJ software. The number of cells on the PEM surfaces was summed over five non-overlapping fields of view of the microscope (at 20×) for each sample; three samples are used for each condition, at each time point.[19]

3.2.7 Stability of the PEMs in PBS

To be applied as a coating for biomedical materials or scaffold for tissue engineering, a biomaterial needs to be durable and stable in aqueous systems, especially when the physiological condition is required (pH 7.4). To evaluate durability, the sterilized PEMs were kept in PBS (pH 7.4) for 7 days to mimic the experimental conditions used in the cell culture assay. Then, the PEMs

were submitted to the same experimental protocol used in the cell culture and proliferation test (Section 3.2.6); however, without the presence of BMSCs. The PEMs were then removed from the PBS and dried with $N_{2(g)}$ before the acquisition of XPS spectra. These conditions mimic the aqueous and thermal conditions of the cell culture assay, which could degrade the PEMs, by dissolution or degradation.

3.2.8 Statistical Analysis

The results were statistically analyzed using ANOVA and Tukey tests at a 5.0% significance level (GraphPad Prism 6.0).

3.3 Results and Discussion

3.3.1 X-ray Photoelectron Spectroscopy (XPS)

XPS is used to quantify the atomic composition of the PEMs surfaces and to evaluate whether the PEMs are covering the glass surface completely. Survey XPS spectra for the PEMs constructed from 15 layers are presented in **Figure 3.1a**, while the high-resolution XPS for carbon (C1s) and nitrogen (N1s) envelopes are shown in **Figure 3.1b**. The survey XPS spectra show the presence of characteristic atoms found in CA (sulfur, S2s, and S2p), and CS (nitrogen N1s). The N1s peak occurs in both XPS spectra, indicating that CS comprises the PEM surfaces. The (PC-CS)15 does not contain sulfur peaks because the polyanion used to prepare this material is based on PC (**Figure 3.2**). The survey XPS spectra of the 5-layer PEMs are shown in **Figure A1** (Appendix A). The 5-layer PEMs do not completely cover the oxidized glass surface, as both the (CA-CS)5 and (PC-CS)5 XPS spectra show silicon from the underlying glass substrate (**Figure A1b**). To ensure complete surface coverage, we have chosen the PEMs constructed from 15 layers for further studies.

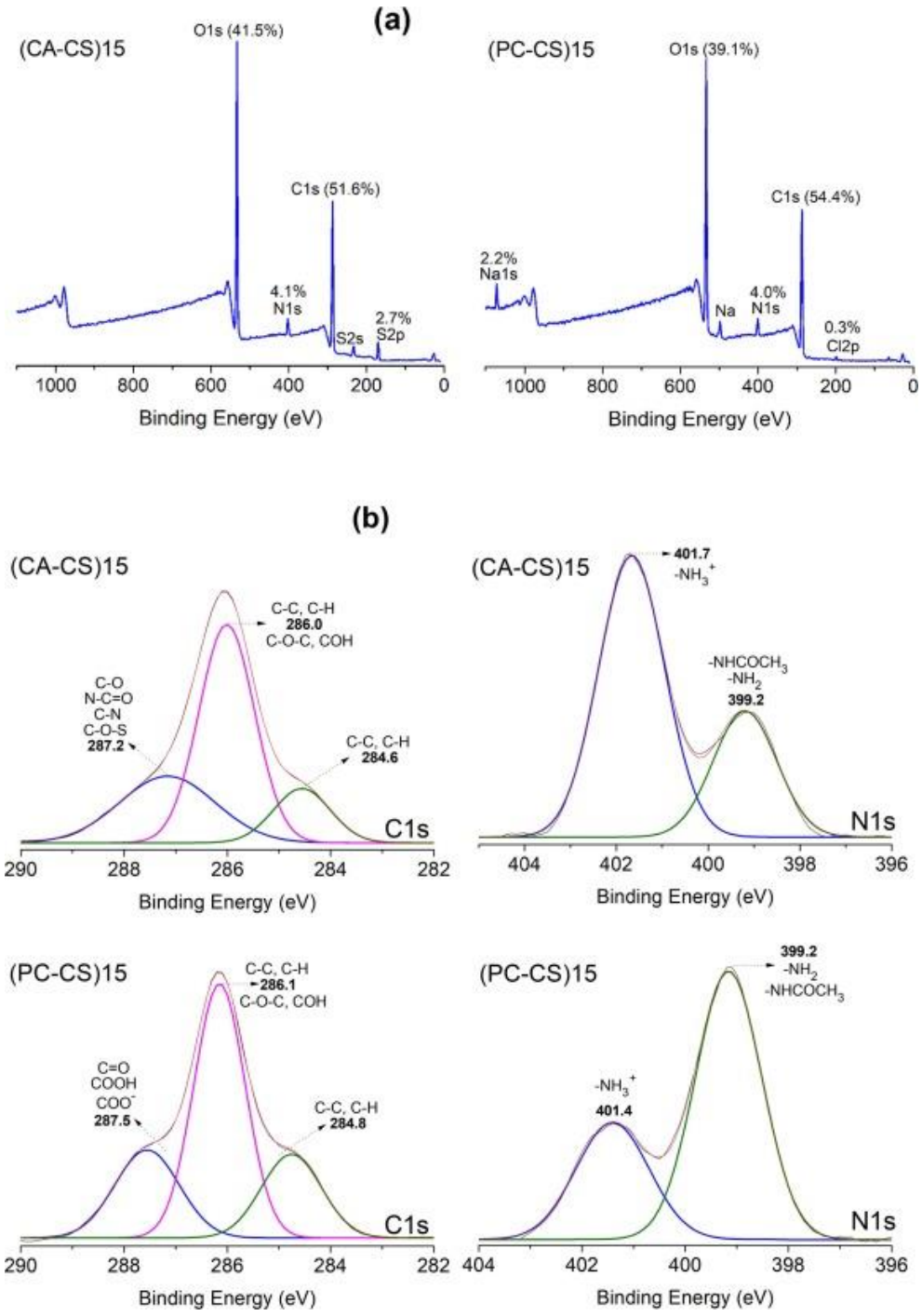

Figure 3.1 XPS spectra (survey) of the PEM surfaces (a). High-resolution XPS spectra for C 1s and N 1s envelopes (b).

The chemical groups of the CS, PC, and CA, such as $-NH_3^+$, $-NH_2$, $-COO^-$, $-COOH$, $-C-O-S$, and others respectively, are identified in the C1s and N1s envelopes (**Figure 3.1b**). All

PEMs are prepared in an acetic acid/acetate buffer solution (pH 5.0) and then washed in ultrapure water before XPS characterization. The weak acid condition (pH 5.0) is chosen to obtain PEMs because it imparts ionized polysaccharides (CS, CA and PC) in solution and because the normal pH of the skin in humans is approximately 4.7–5.5.[49] Based on the functional groups observed in the XPS, the CS-PC PEMs are stabilized by the electrostatic interactions between $-COO^-$ (pKa ≈ 3.6–4.1) [50] and $-NH_3^+$ ($pK_a \approx 6.5$) groups.[51] In an aqueous solution of pH 5.0, CA ($pK_a \approx 2.2$) is ionized as well. Therefore, the aqueous polysaccharide solutions promote conditions to produce the PEMs, mainly due to the establishment of electrostatic interactions between $-NH_3^+$ (401–402 eV) and $-OSO_3^-$ (168–169 eV, **Figure A2**, Appendix A) sites in the CA-CS assemblies and $-NH_3^+$ and $-COO^-$ (287.5 eV) interactions in the PC-CS multilayers. The electrostatic interactions comprise long-range forces in the washed PEMs. The presence of non-ionized chemical sites (−OH, −NH2, and −COOH) on the PEMs surfaces may enable the formation of some short-range forces (H bonds) between the polymer chains. Therefore, washed PEMs likely contain both Coulombic and H-bond forces between the polysaccharide chains.

There are significant differences in the relative $-NH_3^+$ and $-NH_2$ peak intensities (**Figure 3.1b**) between the (CA-CS)15 and (PC-CS)15 samples. The $-NH_3^+$ peak intensity on (CA-CS)15 surface is higher than $-NH_3^+$ peak intensity on (PC-CS)15, compared to the respective $-NH_2$ peak intensities (**Figure 3.1b**). This occurs because the ion-pairing between $-COO^-$ and Na^+ (counterion provided from the acetate/acetic acid buffer solution) are more effective when compared to the $-OSO_3^-$ and Na^+ ion-pairing. This is inferred by the presence of sodium atoms (Na1s = 2.2%) in the (PC-CS)15 XPS spectrum (**Figure 3.1a**). The presence of the Na^+ counterions reduces the relative amount of $-COO^-$ evaluable to interact with $-NH_3^+$. So, the washing step

should deprotonate free $-NH_3^+$ sites on CS, and thereby reduce the ratio of $-NH_3^+$ to $-NH_2$ groups on the (PC-CS)15 surface (**Figure 3.1b**).

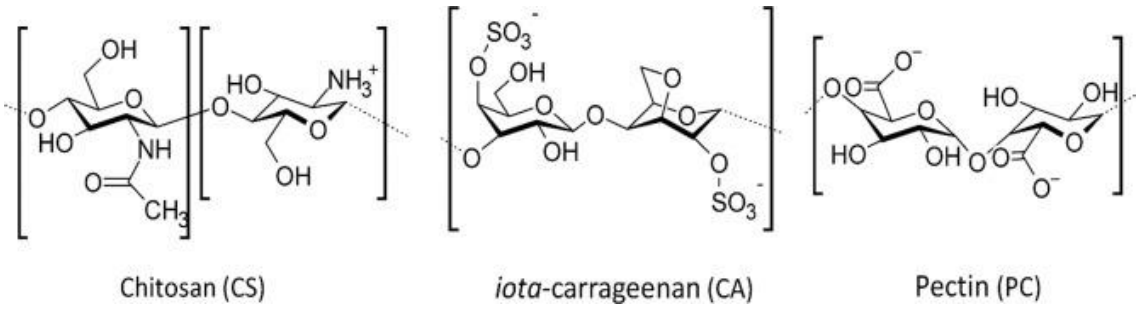

Figure 3.2 The major chemical structures of the polysaccharides.

3.3.2 Initial Bacteria Adhesion and Antimicrobial Activity

To help prevent implant associated infections, biomaterials surfaces should be designed to prevent the adhesion and proliferation of bacteria, as well as kill the adhered bacteria. *P. aeruginosa* (Gram-negative) and *S. aureus* (Gram-positive) have received attention because they are associated with potentially fatal infections.[54] Therefore, we determined the antiadhesive and antimicrobial activities of the PEMs toward both *P. aeruginosa* and *S. aureus* bacteria. These properties are influenced by the surface wettability, surface topography, and composition, as well as the experimental conditions used for the LbL assembly.[7,55]

We evaluate the number of bacterium cells adhered to the PEMs and polystyrene (PS, negative control), considering those cells with normal integrity, i.e., coccus (spherical form) for *S. aureus* and bacillus (rod form) for *P. aeruginosa*. Polystyrene (PS) was chosen as a negative control because it does not have antimicrobial and antiadhesive activities and it is used in food packaging and biomedical applications.[5,56,57] The number of cells per cm^2 adhered on the PEMs and PS was estimated in triplicate by counting the cells in SEM images (at 1000×) on each sample (**Figure 3.3**). After 6 h, the number of *P. aeruginosa* on the (CA-CS)15 and (PC-CS)15 surfaces

were 23 per cm^{-2} and 11 per cm^{-2}, respectively, compared to 974 per cm^{-2} for the PS control. After 24 h, the number of bacteria adhered was only 11 per cm^{-2} and 47 per cm^{-2}, respectively compared to 2515 per cm^{-2} on the PS control (**Figure 3.3a**). After 6 h for *S. aureus*, the number of bacteria adhered achieved 51 per cm^{-2} on (CA-CS)15 and 23 per cm^{-2} on (PC-CS)15, compared to 86 per cm^{-2} on the PS control, and 40 and 18 (after 24 h), respectively, compared to 446 per cm^{-2} onto PS (**Figure 3.3b**). The polysaccharide-based PEM coatings dramatically reduce both *P. aeruginosa* and *S. Aureus* adhesion compared to the PS control (**Figure 3.3**).

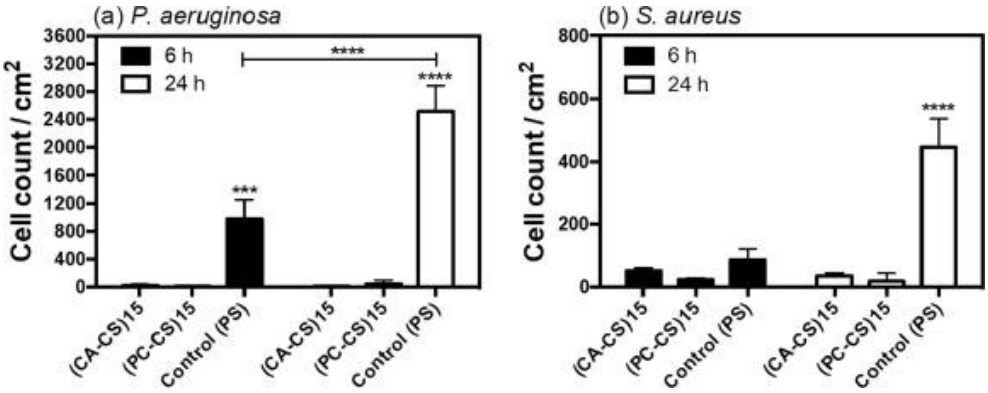

Figure 3.4 Quantification of bacteria cells adhered on the PEMs and native Polystyrene (PS) after 6 and 24 h of incubation. Significant differences were observed between the results (*** and **** indicate $p \leq 0.001$ and $p \leq 0.0001$, respectively. (CA = iota-carrageenan, PC = pectin, CS = chitosan, control (PS) = tissue culture polystyrene).

Representative SEM images from which the cell counts were conducted are shown in **Figure 3.4** for *P. aeruginosa* after 6 and 24 h of incubation. There is a low content of bacterium cells with normal integrity adhered onto the PEMs as compared to the PS (**Figure 3.4a-b**). The result suggests that PEMs present great antiadhesive property over this Gram-negative bacterium. Compared to the PS, the assemblies also promote bactericidal activity, because many *P. aeruginosa* cells adhered on the PEMs are found with irregular and damaged shape (**Figure 3.4**).

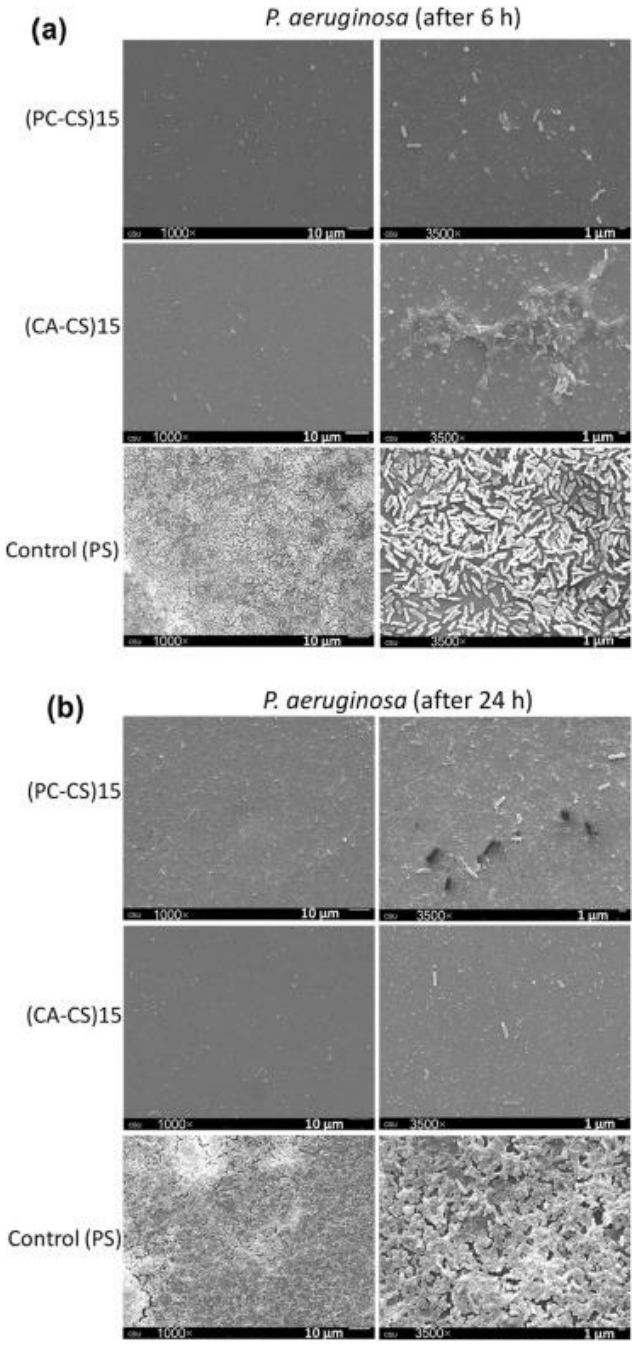

Figure 3.4 SEM images of the PEMs and PS incubated with *P. aeruginosa* after 6 h (a) and 24 h (b).

Figure 3.5 shows SEM images of *S. aureus* incubated on the PEMs and PS after 6 and 24 h. After 6 h, the different surfaces do not have significantly different cell densities. Furthermore, there is no evidence that the PEMs have bactericidal action toward *S. aureus* after 6 h because,

there are no damaged *S. aureus* cells on the PEM surfaces (**Figure 3.5a**). However, after 24 h the PEMs impart bactericidal activity; the number of cells adhered with regular integrity does not significantly increase on the PEMs as compared to the findings reported in 6 h (**Figure 3.5b**). However, after 24 h, the number of cells on PS significantly increases compared to the number of cells adhered to the PEMs (**Figure 3.5**).

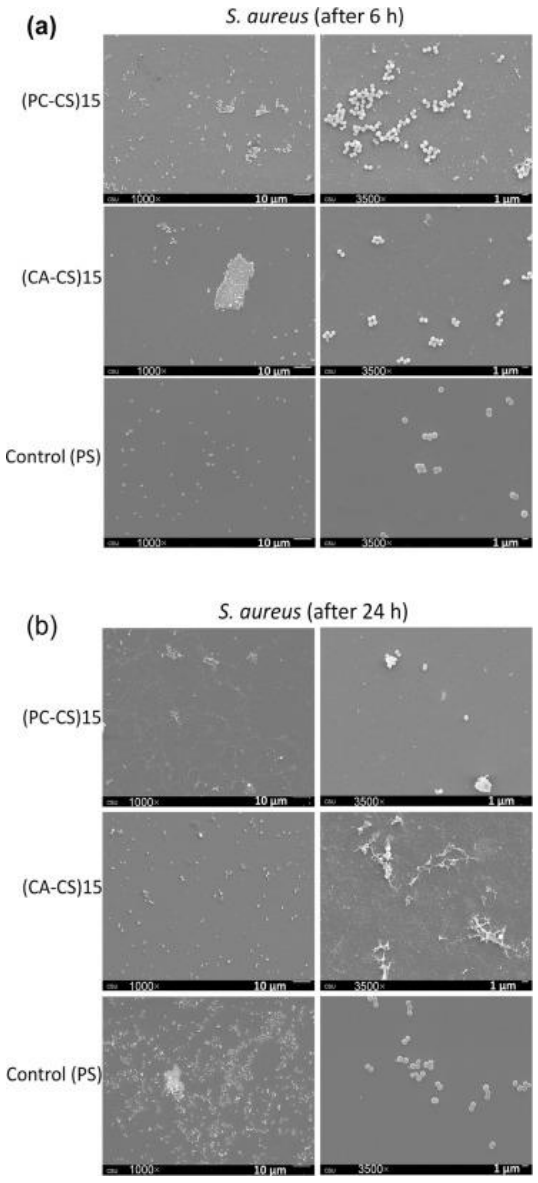

Figure 3.5: SEM images of the PEMs and PS incubated with *S. aureus* after 6 h (a) and 24 h (b).

The antiadhesive capacity should occur due to the negative charge density imparted by the chemical groups $-OSO_3^-$ and $-COO^-$ found on the PEMs as indicated in XPS and because of the higher wettability of the PEMs surfaces [(CA-CS)15 = 25° and (PC-CS)15 = 51°] as compared to the native PS control (82°).[5] Follmann *et al.* reported that microbial adhesion (*E. coli*) onto N,N,N-trimethyl chitosan/heparin PEMs was significantly influenced by the surface hydrophobicity.[5] Gram-negative bacterial cell walls have a thin layer of glycoproteins covered by a thick layer formed mainly by lipoproteins and lipids, while Gram-positive cell walls are mostly composed of 15–40 interconnected layers of peptidoglycans.[58] A hydrophobic surface should produce favorable interactions with the bacterium cell walls to provide microbial adhesion.[5] So, the PEM surface should be hydrophilic and durable to avoid the attachment, as well as to prevent the growth of bacteria.

The bactericidal action of the PEMs can be ascribed to the CS presence, which imparts cationic sites ($-NH_3^+$) to the PEMs. Cationic moieties, including aminoglycosides, can electrostatically interact with the anionic phospholipid dipalmitoyl phosphatidylglycerol, which is a major component of both Gram-negative and Gram-positive bacteria.[59] The effective interactions between PEMs and bacteria increase the membrane permeability of cell walls, promoting leakage of intracellular materials (lactate dehydrogenase, nucleic acid, and glucose) and suppressing the nutrient transport to the microbial cells.[60] These events can cause the death of bacteria.[60]

The pH condition at which the PEMs are assembled can influence the antimicrobial activity. The acetic acid/acetate buffer solution (pH 5.0) used to prepare the polysaccharide solutions can provide residual H_3O^+ ions, which may also be released during the antimicrobial assay and thereby promote the death of bacteria. However, before antimicrobial tests, the PEMs were washed in ultrapure water, kept in PBS (12 h), and sterilized in PBS for 30 min under UV

irradiation. These steps should reduce the free H_3O^+ content in the assemblies. Fu *et al.* coated the aminolyzed poly(ethylene terephthalate) with multilayer films based on CS-heparin LbL assemblies by using polyelectrolyte solutions prepared at different pHs (2.9, 3.8, and 6.0) [7]. The number of bacterium (*E. coli*) cells adhered on the PEMs was significantly reduced by decreasing the pH of the CS and heparin polyelectrolyte solutions. The pH of the polyelectrolyte solutions had a remarkable effect on the antimicrobial activity because the number of viable bacteria on PEMs assembled at pH 3.8, and 6.0 decreased from 68 to 46% after 24 h, respectively.[7] However, Fu and coworkers did not carry out cell culture assays to show that CS/heparin-based PEMs could have cytocompatibility toward mammalian cells. Almodóvar *et al.* studied PEMs of CS and heparin or N,N,N-trimethyl chitosan and heparin applied to the surfaces of cortical bone allografts.[12] They showed that both polycation-terminated and polyanion-terminated PEMs on the surfaces of bone allografts were bactericidal towards both *E. coli* and *S. aureus*, but enabled attachment of BMSCs. For biomedical applications, suitable biomaterials must be durable, prevent the attachment of bacteria, promote bactericidal action and support mammalian cell cytocompatibility.

3.3.3 Bone Marrow-Derived Stem Cells Adhesion and Proliferation

Survey XPS spectra indicate that the PEMs remained on the oxidized glass surface even after 7 days in PBS and incubated at 37 °C, and after all steps of washing performed in the cell culture assay (**Figure A3**, Appendix A). Table 3 shows the C/O ratios found on the PEM surfaces determined by XPS before and after the stability assay. The C/O ratio increased after PBS contact, showing that the washing steps performed in the cell culture test influenced the PEM surface composition. At pH 5.0, CS mainly interacts with CA and PC by electrostatic interactions; however, in PBS (pH 7.4) the amine groups on CS should be deprotonated, altering the chemical

composition and hydrophilicity of the PEM surfaces, because they were prepared with CS polycation-terminated layer at pH 5.0. At pH 5.0, protonated amine interacts better with water molecules, increasing the content of O1s on the PEM surfaces. On the other hand, after deprotonation at pH 7.4, the content of water molecules adsorbed to PEMs should decrease. We see no evidence that partial dissolution of the PEMs occurs in PBS; XPS indicates that the glass is entirely covered by the PEMs (**Figure A3**), and CS is generally insoluble at neutral pH. AFM images of the PEMs imaged in PBS after the stability assay confirmed that the PEMs remain on the glass surface as well (Appendix A, **Figure A4**)

Table 3
Relative atomic content (C/O ratio) determined from the peak areas in each XPS spectrum (survey) acquired before (**Figure 3.1a**) and after (**Figure A3**) the stability assay in PBS for 7 days

Surface	C/O ratio (before)*	C/O ratio (after)
(CA-CS)15	1.2	2.7
(PC-CS)15	1.4	2.1

* Results found on the as-obtained surfaces

To determine the capacity of the PEMs to support mammalian cells, surfaces were seeded with BMSCs for 4 and 7 days. The cell adhesion and proliferation on the PEMs were investigated by cell counting (**Figure 3.6**), using fluorescence images (**Figure 3.7**).

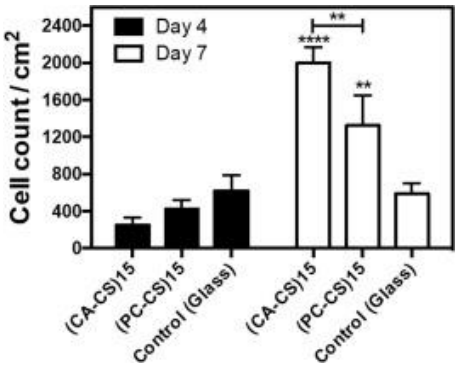

Figure 3.6 Quantification of BMSCs proliferation on the PEMs and native glass surfaces after 4 and 7 days of culture. Significant results were observed (** and **** indicate $p \leq 0.01$ and $p \leq 0.0001$, respectively.

After day 4, the number of BMSCs adhered on the PEMs was similar to the number of cells on the unmodified glass ($p > 0.05$, **Figure 3.6 and 3.7**). The cell counting subsequent to 4 days, indicated 249 cells cm^{-2} on (CA-CS)15, 424 cells cm^{-2} on (PC-CS)15 and 621 cells cm^{-2} on the glass control (**Figure 3.6 and 3.7**). The number of cells on the glass did not increase, and the cells did not spread on the glass after 7 days. As compared to the PEMs, the native glass has a high WCA (62°). Mesenchymal stem cells can interact and spread better on hydrophilic surfaces.[53,61,62] However, surfaces that are too hydrophilic can prevent protein adsorption and may completely resist adhesion of mammalian cells.[11]

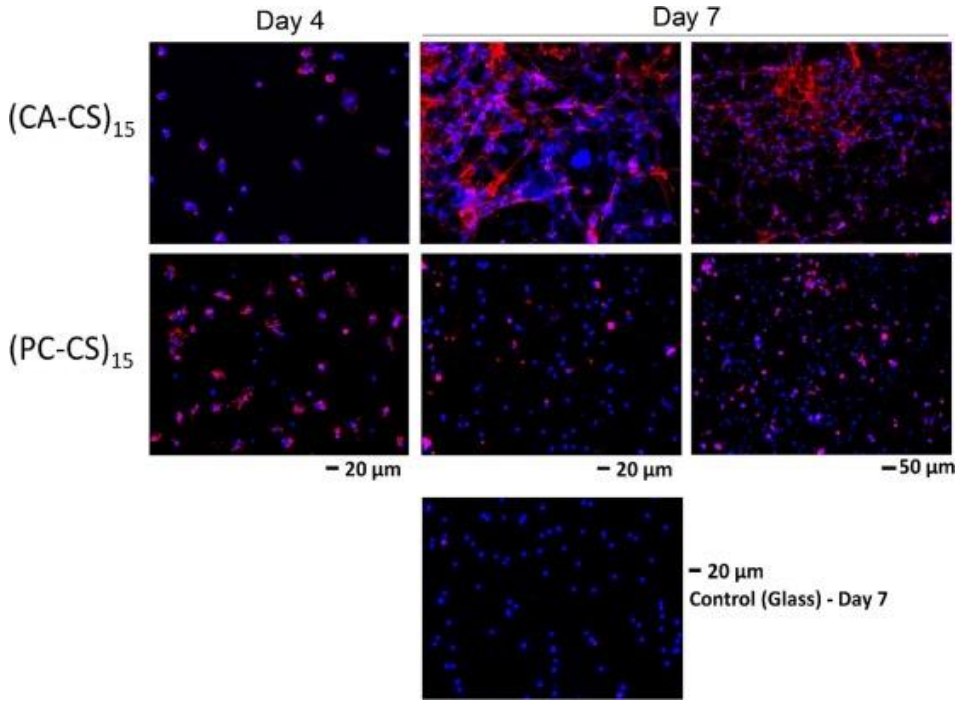

Figure 3.7 Representative fluorescent images of BMSCs cells on the PEMs (CA-CS)15 and (PC-CA)15 after 4 and 7 days and on unmodified glass surface (control) after 7 days.

The (CA-CS)15 surface significantly promoted the attachment, proliferation, and spreading of BMSCs cells after 7 days (**Figures 3.6 and 3.7**). The number of cells on (CA-CS)15 increased from 249 cells cm^{-2} (day 4) to approximately 2000 cells cm^{-2} at day 7 (**Figure 3.6**). In

the same period but on (PC-CS)15, the number of BMSCs significantly increased from 424 to 1324 cells cm^{-2} (**Figures 3.6 and 3.7**). As compared to the control (glass), PEMs supported the proliferation of BMSCs. However, the (CACS)15 had a superior capacity to provide attachment and proliferation of BMSCs. The (CA-CS)15 assembly had the lowest WCA (25°) and R_q (2.6 nm). Therefore, (CA-CS)15 has a greater potential to act as a coating for implants and tissue scaffolds that support BMSCs, as well as prevent the attachment and growth of Gram-negative and Gram-positive bacteria.

The ECM components such as glycosaminoglycans and proteins should intimately interact with the PEMs after day 7, enabling attachment and growth of BMSCs. The surface wettability and topography of LbL assemblies play essential roles in the biological responses to biomaterials.[63] PEMs based on polystyrene sulfonate and polyallylamine hydrochloride were constructed on activated polyetheretherketone. As compared to the native polyetheretherketone (WCA = 39.7°), a PEM (WCA = 21.7°) of 20-layers containing polymeric clusters in its surface supported the adhesion and proliferation of BMSCs, and induced higher cell growth rate.[63] In orthopedic materials, preventing the initial attachment of bacteria, bactericidal activity, and promoting the growth of healthy tissue in the short term, are essential to the long-term success of implant placement. The subsequent apposition of healthy tissue at an implant surface is essential for preventing later long-term failure modes. Recent research has also focused on the development of strategies that can present bactericidal properties over the long term, for example by covalent attachment of bactericidal moieties.[64] The polysaccharide-based coatings proposed here may be further optimized for specific applications by long-term stability and activity studies, to demonstrate that they impart long-term inherent bactericidal activity to surfaces, while promoting tissue healing.

3.4 Conclusion

New polyelectrolyte multilayers based on commercial *iota*-carrageenan (CA) and pectin (PC) were prepared. Their antimicrobial properties toward Gram positive and Gram negative bacteria were demonstrated. Furthermore, both surfaces are shown to support mammalian cell attachment and growth over 7 days. Both polyanions were assembled to chitosan (CS) in an acetic acid/acetate buffer solution at pH 5.0. Imparting suitable microenvironments to support the bone marrow stem cells (BMSCs) adhesion, proliferation and spreading after 7 days of cell culture. This work shows for the first time that commercial CA and PC could be associated with CS in a weak acid condition (pH 5.0) to produce PEMs with antimicrobial and antiadhesive activities and desirable properties to act as coatings for biomedical materials and tissue engineering scaffolds. PEM composed of CA and CS could prevent deposition and growth of *S. aureus* and *P. aeruginosa* and could also provide efficient cell culture with a high cell growth rate. This biomaterial can be applied as a coating to support healing around orthopedic implants, especially as a scaffold for skeletal tissue engineering, particularly in applications that demand protection against the proliferation of bacteria.

REFERENCES

1. X. Zhu, X. Jun Loh, Layer-by-layer assemblies for antibacterial applications, *Biomater*. Sci. 3 (2015) 1505–1518

2. M. Hedayati, M.J. Kipper, Atomic force microscopy of adsorbed proteoglycan mimetic nanoparticles: toward new glycocalyx-mimetic model surfaces, *Carbohydr. Polym*. 190 (2018) 346–355,

3. M. Hedayati, M.M. Reynolds, D. Krapf, M.J. Kipper, Nanostructured surfaces that mimic the vascular endothelial glycocalyx reduce blood protein adsorption and prevent fibrin network formation, *ACS Appl. Mater. Interfaces* 10 (2018) 31892–31902,

4. S. del Hoyo-Gallego, L. Pérez-Álvarez, F. Gómez-Galván, E. Lizundia, I. Kuritka, V. Sedlarik, J.M. Laza, J.L. Vila-Vilela, Construction of antibacterial poly (ethylene terephthalate) films via layer by layer assembly of chitosan and hyaluronic acid, *Carbohyd. Polym*. 143 (2016) 35–43.

5. H.D.M. Follmann, A.F. Martins, A.P. Gerola, T.A.L. Burgo, C.V. Nakamura, A.F. Rubira, E.C. Muniz, Antiadhesive and antibacterial multilayer films via layerby-layer assembly of TMC/heparin complexes, *Biomacromolecules* 13 (2012) 3711–3722

6. J. Zhang, D. Wang, X. Jiang, L. He, L. Fu, Y. Zhao, Y. Wang, H. Mo, J. Shen, Multistructured vascular patches constructed via layer-by-layer self-assembly of heparin and chitosan for vascular tissue engineering applications, *Chem. Eng*. J. 370 (2019) 1057–1067

7. J. Fu, J.Ã. Ji, W. Yuan, J. Shen, Construction of anti-adhesive and antibacterial multilayer films via layer-by-layer assembly of heparin and chitosan*, Biomaterials* 26 (2005) 6684–6692,

8. H.D.M. Follmann, A.F. Naves, A.F. Martins, O. Félix, G. Decher, E.C. Muniz, R. Silva, Advanced fibroblast proliferation inhibition for biocompatible coating by electrostatic layer-by-layer assemblies of heparin and chitosan derivatives*, J. Colloid Interface Sci.* 474 (2016) 9–17

9. R. Anouz, A. Repanas, E. Schwarz, T. Groth, Novel surface coatings using oxidized glycosaminoglycans as delivery systems of bone morphogenetic protein 2 (BMP-2) for bone regeneration, *Macromol. Biosci*. 18 (2018) 1800283

10. D. Campoccia, L. Montanaro, C.R. Arciola, A review of the biomaterials technologies for infection-resistant surfaces*, Biomaterials* 34 (2013) 8533–8554

11. M. Hedayati, M.J. Neufeld, M.M. Reynolds, M.J. Kipper, The quest for bloodcompatible materials: recent advances and future technologies, *Mater. Sci. Eng. R Rep.* 138 (2019) 118–152

12. J. Almodóvar, J. Mower, A. Banerjee, A.K. Sarkar, N.P. Ehrhart, M.J. Kipper, Chitosan-heparin polyelectrolyte multilayers on cortical bone: periosteum-mimetic, cytophilic, antibacterial coatings, *Biotechnol. Bioeng.* 110 (2013) 609–618

13. M.R. Ruggieri, P.M. Hanno, R.M. Levin, Reduction of bacterial adherence to catheter surface with heparin, *J. Urol.* 138 (1987) 423–426

14. C.R. Arciola, R. Caramazza, A. Pizzoferrato, In vitro adhesion of Staphylococcus epidermidis on heparin-surface-modified intraocular lenses, *J. Cataract Refract. Surg.* 20 (1994) 158–161

15. E. Persyn, M. Sassi, M. Aubry, M. Broly, S. Delanou, K. Asehnoune, N. Caroff, L. Crémet, Rapid genetic and phenotypic changes in Pseudomonas aeruginosa clinical strains during ventilator-associated pneumonia, *Sci. Rep.* 9 (2019) 4720

16. G. Rodríguez-Macías, M. Machado, M. Kwon, N. Alba, J.L. Díez Martín, E. Chamorro-de-Vega, P. Muñoz, M.A. Semiglia-Chong, E. Cercenado, A. FernándezCruz, L. Pérez-Lago, B.D. Padilla, García de Viedma, A case-control study of real-life experience with ceftolozane-tazobactam in patients with hematologic malignancy and pseudomonas aeruginosa infection, *Antimicrob. Agents Chemother.* 63 (2018) e02340-18

17. K.D. Triplett, S. Pokhrel, M.J. Castleman, S.M. Daly, B.O. Elmore, J.A. Joyner, G. Sharma, G. Herbert, M.J. Campen, H.J. Hathaway, E.R. Prossnitz, P.R. Hall, GPER activation protects against epithelial barrier disruption by Staphylococcus aureus α-toxin, *Sci. Rep.* 9 (2019) 1343

18. S.K. Jaganathan, M.P. Mani, P. Prabhakaran, E. Supriyanto, A.F. Ismail, Production, blood compatibility and cytotoxicity evaluation of a single stage non-woven multicomponent electrospun scaffold mixed with sesame oil, honey and propolis for skin tissue engineering, *Int. J. Polym. Anal. Charact.* 24 (2019) 457–474

19. J.G. Martins, S.E.A. Camargo, T.T. Bishop, K.C. Popat, M.J. Kipper, A.F. Martins, Pectin-chitosan membrane scaffold imparts controlled stem cell adhesion and proliferation, *Carbohydr. Polym.* 197 (2018) 47–56

20. B. Machado, S. Roberto, E. Bonafé, S. Camargo, C. Camargo, K. Popat, M. Kipper, A. Martins, Chitosan imparts better biological properties for poly(ε-caprolactone) electrospun membranes than dexamethasone, *J. Braz. Chem. Soc.* 00 (2019) 1–10

21. R. Davies, N. Kuiper, Regenerative medicine: a review of the evolution of autologous chondrocyte implantation (ACI) therapy, *Bioengineering* 6 (2019) 22

22. W. Li, Y. Yang, H. Zhang, Z. Xu, L. Zhao, J. Wang, Y. Qiu, B. Liu, Improvements on biological and antimicrobial properties of titanium modified by AgNPs-loaded chitosan-heparin polyelectrolyte multilayers, *J. Mater. Sci. Mater. Med.* 30 (2019) 52

23. V.I. Kulikouskaya, S.V. Pinchuk, K.S. Hileuskaya, A.N. Kraskouski, I.B. Vasilevich, K.A. Matievski, V.E. Agabekov, I.D. Volotovski, Layer-by-layer buildup of polysaccharide-containing films: physico-chemical properties and mesenchymal stem cells adhesion, *J. Biomed. Mater. Res. – Part A.* 106 (2018) 2093–2104

24. F. Zomer Volpato, J. Almodóvar, K. Erickson, K.C. Popat, C. Migliaresi, M.J. Kipper, Preservation of FGF-2 bioactivity using heparin-based nanoparticles, and their delivery from electrospun chitosan fibers, *Acta Biomater.* 8 (2012) 1551–1559

25. J. Almodovar, S. Bacon, J. Gogolski, J.D. Kisiday, M.J. Kipper, Polysaccharidebased polyelectrolyte multilayer surface coatings can enhance mesenchymal stem cell response to adsorbed growth factors, *Biomacromolecules* (2010) 2629–2639.

26. R. Romero, L. Chubb, J.K. Travers, T.R. Gonzales, N.P. Ehrhart, M.J. Kipper, Coating cortical bone allografts with periosteum-mimetic scaffolds made of chitosan, trimethyl chitosan, and heparin, *Carbohydr. Polym.* 122 (2015) 144–151

27. R. Simon-Walker, R. Romero, J.M. Staver, Y. Zang, M.M. Reynolds, K.C. Popat, M.J. Kipper, Glycocalyx-inspired nitric oxide-releasing surfaces reduce platelet adhesion and activation on titanium, *ACS Biomater. Sci. Eng*. 3 (2017) 68–77

28. R. Romero, J.K. Travers, E. Asbury, A. Pennybaker, L. Chubb, R. Rose, N.P. Ehrhart, M.J. Kipper, Combined delivery of FGF-2, TGF-β1, and adipose-derived stem cells from an engineered periosteum to a critical-sized mouse femur defect*, J. Biomed. Mater. Res. – Part A* 105 (2017) 900–911

29. C. Lin, R. Romero, L.V. Sorokina, K.R. Ballinger, L.W. Place, M.J. Kipper, S.R. Khetani, A polyelectrolyte multilayer platform for investigating growth factor delivery modes in human liver cultures*, J. Biomed. Mater. Res. Part A* 106 (2018) 971–984

30. J. Jung, L. Li, C.-K. Yeh, X. Ren, Y. Sun, Amphiphilic quaternary ammonium chitosan/sodium alginate multilayer coatings kill fungal cells and inhibit fungal biofilm on dental biomaterials, *Mater. Sci. Eng. C.* 104 (2019) 109961

31. A.F. Martins, H.D.M. Follmann, J.P. Monteiro, E.G. Bonafé, S. Nocchi, C.T.P. Silva, C.V. Nakamura, E.M. Girotto, A.F. Rubira, E.C. Muniz, Polyelectrolyte complex containing silver nanoparticles with antitumor property on Caco-2 colon cancer cells, *Int. J. Biol. Macromol.* 79 (2015) 748–755

32. Z. Gezgin, T.C. Lee, Q. Huang, Nanoscale properties of biopolymer multilayers, *Food Hydrocoll.* 63 (2017) 209–218

33. S.M. Oliveira, T.H. Silva, R.L. Reis, J.F. Mano, Nanocoatings containing sulfated polysaccharides prepared by layer-by-layer assembly as models to studycell–material interactions, *J. Mater. Chem. B* 1 (2013) 4406

34. R. Shahlori, D.R. McDougall, G.I.N. Waterhouse, F. Yao, J.P. Mata, A.R.J. Nelson, D.J. McGillivray, Biomineralization of calcium phosphate and calcium carbonate within iridescent chitosan/iota-carrageenan multilayered films, Langmuir 34 (2018) 8994–9003

35. F. Wei, F. Ye, S. Li, L. Wang, J. Li, G. Zhao, Layer-by-layer coating of chitosan/ pectin effectively improves the hydration capacity, water suspendibility and tofu gel compatibility of okara powder, Food *Hydrocoll.* 77 (2018) 465–473

36. K. Kamburova, K. Mitarova, T. Radeva, Polysaccharide-based nanocapsules for controlled release of indomethacin, *Colloids Surf. A Physicochem. Eng. Asp*. 519 (2017) 199–204

37. M. Fathi, M. Mirlohi, J. Varshosaz, G. Madani, Novel caffeic acid nanocarrier: production, characterization, and release modeling, *J. Nanomater*. 2013 (2013) 1–9

38. Kappa Carrageenan, CP Kelco, n.d. https://www.cpkelco.com/products/ carrageenan/.

39. B.B.S. Ramin, K.B. Rufato, R.M. Sabino, K.C. Popat, M.J. Kipper, A.F. Martins, E.C. Muniz, Chitosan/iota-carrageenan/curcumin-based materials performed by precipitating miscible solutions prepared in ionic liquid, *J. Mol. Liq*. 111199 (2019)

40. J.G. Martins, A.C. de Oliveira, P.S. Garcia, M.J. Kipper, A.F. Martins, Durable pectin/chitosan membranes with self-assembling, water resistance and enhanced mechanical properties, *Carbohydr. Polym*. 188 (2018) 136–142

41. M.M. Bomgardner, Call in the food fixers: Ingredient suppliers provide alternatives to fat, sugar, and gluten in food products, *Chem. Eng. News.* 89 (2011)

42. A.C. de Oliveira, B.H. Vilsinski, E.G. Bonafé, J.P. Monteiro, M.J. Kipper, A.F. Martins, Chitosan content modulates durability and structural homogeneity of chitosan-gellan gum assemblies, *Int. J. Biol. Macromol.* 128 (2019) 114–123

43. D.P. Facchi, A.L. Cazetta, E.A. Canesin, V.C. Almeida, E.G. Bonafé, M.J. Kipper, A.F. Martins, New magnetic chitosan/alginate/Fe3O4@SiO2hydrogel composites applied for removal of Pb(II) ions from aqueous systems, *Chem. Eng. J.* 337 (2018) 595–608

44. J. Almodóvar, L.W. Place, J. Gogolski, K. Erickson, M.J. Kipper, Layer-by-layer assembly of polysaccharide-based polyelectrolyte multilayers: a spectroscopic study of hydrophilicity, composition, and ion pairing, *Biomacromolecules* 12 (2011) 2755–2765

45. S. Boddohi, C.E. Killingsworth, M.J. Kipper, Polyelectrolyte multilayer assembly as a function of pH and ionic strength using the polysaccharides chitosan and heparin, *Biomacromolecules* 9 (2008) 2021–2028.

46. A.F. Martins, S.P. Facchi, P.C.F. Da Câmara, S.E.A. Camargo, C.H.R. Camargo, K.C. Popat, M.J. Kipper, Novel poly(e-caprolactone)/amino-functionalized tannin electrospun membranes as scaffolds for tissue engineering, *J. Colloid Interface Sci.* 525 (2018) 21–30
47. A. Pegalajar-Jurado, K.A. Wold, J.M. Joslin, B.H. Neufeld, K.A. Arabea, L.A. Suazo, S.L. McDaniel, R.A. Bowen, M.M. Reynolds, Reprint of: nitric oxide-releasing polysaccharide derivative exhibits 8-log reduction against Escherichia coli, Acinetobacter baumannii and Staphylococcus aureus, *J. Control. Release.* 220 (2015) 617–623

48. T.T. Ruckh, K. Kumar, M.J. Kipper, K.C. Popat, Osteogenic differentiation of bone marrow stromal cells on poly(ε-caprolactone) nanofiber scaffolds, *Acta Biomater.* 6 (2010) 2949–2959

49. T. Wang, M. Turhan, S. Gunasekaran, Selected properties of pH-sensitive , biodegradable chitosan – poly(vinyl alcohol)hydrogel, *Polym. Int.* 918 (2004) 911–918

50. K. Ofori-Kwakye, J.T. Fell, Biphasic drug release: the permeability of films containing pectin, chitosan and HPMC, *Int. J. Pharm.* 226 (2001) 139–145

51. S.P. Facchi, D.B. Scariot, P.V.A. Bueno, P.R. Souza, L.C. Figueiredo, H.D.M. Follmann, C.S. Nunes, J.P. Monteiro, E.G. Bonafé, C.V. Nakamura, E.C. Muniz, A.F. Martins, Preparation and cytotoxicity of N-modified chitosan nanoparticles applied in curcumin delivery, *Int. J. Biol. Macromol.* 87 (2016) 237–245

52. A.T. Shah, S. Zahid, F. Ikram, M. Maqbool, A.A. Chaudhry, M.I. Rahim, F. Schmidt, O. Goerke, A.S. Khan, I. Ur Rehman, Tri-layered functionally graded membrane for potential application in periodontal regeneration, *Mater. Sci. Eng.* C 103 (2019)

53. E.A. Chudinova, M.A. Surmeneva, A.S. Timin, T.E. Karpov, A. Wittmar, M. Ulbricht, A. Ivanova, K. Loza, O. Prymak, A. Koptyug, M. Epple, R.A. Surmenev, Adhesion, proliferation, and osteogenic differentiation of human mesenchymal stem cells on additively manufactured Ti6Al4V alloy scaffolds modified with calcium phosphate nanoparticles, *Colloids Surf. B Biointerfaces* 176 (2019) 130–139

54. A.K. Bhardwaj, K. Vinothkumar, N. Rajpara, Bacterial quorum sensing inhibitors: attractive alternatives for control of infectious pathogens showing multiple drug resistance, *Recent Pat. Antiinfect. Drug Discov.* 8 (2013) 68–83

55. Y. Pei, Y. Hu, K. Cai, B. Tao, Y. He, Q. Ran, J. Liu, Z. Yuan, X. Shen, T. Shen, Nhalamine-based multilayers on titanium substrates for antibacterial application, Colloids Surf. B *Biointerfaces* 170 (2018) 382–392

56. Y. Cha, B. Son, S. Ryu, Effective removal of staphylococcal biofilms on various food contact surfaces by Staphylococcus aureus phage endolysin LysCSA13, *Food Microbiol.* 84 (2019) 103245

57. C. Milho, M. Andrade, D. Vilas Boas, D. Alves, S. Sillankorva, Antimicrobial assessment of phage therapy using a porcine model of biofilm infection, *Int. J. Pharm*. 557 (2019) 112–123,

58. A.F. Martins, S.P. Facchi, H.D.M. Follmann, A.G.B. Pereira, A.F. Rubira, E.C. Muniz, Antimicrobial activity of chitosan derivatives containing N-quaternized moieties in its backbone: a review, *Int. J. Mol. Sci*. 15 (2014) 20800–20832

59. M.M. Fernandes, A. Francesko, J. Torrent-Burgués, T. Tzanov, Effect of thiol-functionalisation on chitosan antibacterial activity: interaction with a bacterial membrane model, *React. Funct. Polym*. 73 (2013) 1384–1390

60. A. Muñoz-Bonilla, M. Fernández-García, Polymeric materials with antimicrobial activity, *Prog. Polym. Sci.* 37 (2012) 281–339

61. M. Wang, Y. Zhou, D. Shi, R. Chang, J. Zhang, M. Keidar, T.J. Webster, Cold atmospheric plasma (CAP)-modified and bioactive protein-loaded core–shell nanofibers for bone tissue engineering applications, *Biomater. Sci.* 7 (2019) 2430–2439

62. A.Z. Kharazi, M. Atari, E. Vatankhah, S.H. Javanmard, A nanofibrous bilayered scaffold for tissue engineering of small-diameter blood vessels, *Polym. Adv. Technol*. 29 (2018) 3151–3158

63. X. Liu, F. Han, P. Zhao, C. Lin, X. Wen, X. Ye, Layer-by-layer self-assembled multilayers on PEEK implants improve osseointegration in an osteoporosis rabbit model, *Nanomed. Nanotechnol. Biol. Med.* 13 (2017) 1423–1433

64. J. Raphel, M. Holodniy, S.B. Goodman, S.C. Heilshorn, Multifunctional coatings to simultaneously promote osseointegration and prevent infection of orthopaedic implants, *Biomaterials* 84 (2016) 301–314

CHAPTER 4: GENTAMICIN-RELEASING TITANIA NANOTUBE SURFACES INHIBIT BACTERIA AND SUPPORT ADIPOSE-DERIVED STEM CELL GROWTH IN CO-CULTURES[3]

Overview: Infection is the second leading cause of failure for orthopedic implants, following incomplete osseointegration. New materials that increase the antimicrobial properties of surfaces while maintaining the ability for bone cells to attach and proliferate could reduce the failure rates of orthopedic implants. In this study gentamicin was delivered from titania nanotubes (Nt) modified with chitosan/heparin polyelectrolyte multilayers (PEMs), and the antimicrobial activity of the surfaces was tested in a novel way of co-culturing bacteria with mammalian cells. After an initial burst release of gentamicin during the first day, over 60% of gentamicin remained on the surface. To determine the antimicrobial activity of these surfaces, they were exposed to gram-negative *Escherichia coli* (*E. coli*) and gram-positive *Staphylococcus aureus* (*S. aureus*) for up to 24 h. Gentamicin surfaces had less live *E. coli* and *S. aureus* by 6 hours, and less *E. coli* by 24 hours compared to Nt surfaces. *S. aureus* and human adipose derived stem cells (hADSCs) were co-cultured on surfaces for up to 7 days to characterize the so-called "race to the surface" between bacteria and mammalian cells, which is hypothesized to ultimately determine the outcome of orthopedic implants. By day seven there was no significant difference in bacteria on surfaces between surfaces with gentamicin adsorbed on the surface and surfaces with gentamicin in solution. However, there was significantly less hADSC nuclei when gentamicin was delivered in solution versus on the surface by day 7. PEMs provide a sustained presentation of gentamicin from

[3] Portions of this chapter are reproduced from: T. Wigmosta, K.C. Popat, and Matt J. Kipper, "Gentamicin-releasing titania nanotube surfaces inhibit bacteria and support adipose-derived stem cell growth in co-cultures." Submitted to *ACS Applied Bio Materials*, 2020.

a surface. This enhances the antimicrobial properties of the surfaces without inhibiting cell attachment and cell growth. Delivering gentamicin from the surfaces is therefore superior to delivering gentamicin in solution, and represents a strategy that could improve the antimicrobial activity of orthopedic implants and reduce risk of failure due to infection, without reducing mammalian cell attachment.

4.1 Introduction

Total joint replacement causes a substantial improvement in physical health, including a reduction in chronic pain and improved physical functioning for patients with injured or diseased joints.[1] There are currently over one million total knee and hip implants performed annually in the United States, and this number is expected to increase to over four million by 2030.[2,3] While most complete joint replacement surgeries are successful, over 60,000 revision surgeries due to implant failure are performed annually.[4] Patients that undergo a revision surgery also experience significant decreases in physical functioning compared to those that have only a primary surgery.[1] The most common cause of orthopedic implant failure is aseptic loosening of the implant from the surrounding bone tissue, followed by failure of the implant due to infection.[2,5] Failure due to infection could be addressed by antimicrobial surfaces that do not inhibit cell growth, to avoid the increase in cost and decrease in health associated with implant failure.[6]

The most common pathogens in orthopedic implant-associated infections are *Staphylococcus epidermidis* (*S. epidermidis*) (32%) and *Staphylococcus aureus* (*S. aureus*) (34%).[5] Antimicrobial surface coatings, including using surfactants, proteins such as albumin, and the polysaccharides heparin and chitosan, have been studied to prevent infections.[5,7-11] The antibiotics, gentamicin, amoxicillin, tobramycin, and vancomycin, have been adsorbed on and

released from various surface coatings.[12-15] These coatings have already demonstrated to actively prevent infections *in vivo* and are used in especially critical conditions.[5] Because of gentamicin's ability to treat various bacterial infections, it has been incorporated into scaffolds and coatings for medical devices and implants.[12,16,17] Gentamicin is mainly used to treat gram-negative bacterial infections, including *Escherichia coli* (*E. coli*) and *Pseudomonas aeruginosa* (*P. aeruginosa*).[18-20] It has also been shown to be effective against gram-positive bacteria such as *S. aureus*.[18] While gentamicin has proven to be a valuable antibiotic, it is also cytotoxic and inhibits osteogenic cells.[21-23] Because of gentamicin's potential cytotoxic effects it is important to develop gentamicin-delivering surfaces intended for orthopedics that do not inhibit cellular attachment and growth.

Nanotopographical structures can increase cellular attachment and enhance bone formation both in vitro and in vivo.[24-29] Our group has fabricated novel nanotubular titania surfaces using an anodization process.[6,30] Nanotube surfaces support higher cell adhesion, proliferation and viability for up to seven days in culture compared to titanium surfaces.[30] This suggests that cellular activity can be enhanced using controlled nanotopographies, such as nanotubes. One solution to increase the antimicrobial properties of surfaces without effecting cellular growth is to deliver a controlled dose of antibiotics from a nanotube surface. Nanotubes loaded with gentamicin may inhibit bacterial adhesion without causing cytoxicity.[31] One way to deliver tunable amounts of gentamicin is with polyelectrolyte multilayers (PEMs).[23,32-34] Our group has shown PEMs can be successfully adsorbed onto nanotubes.[6,35]

In this study, we designed antimicrobial surfaces that allow for cellular attachment. Surfaces were tested against for antimicrobial activity and cellular attachment, by co-culturing human adipose derived stem cells (hADSCs) and *S. aureus* bacteria. This is accomplished using a combination of nanotopgraphy and coatings for the antibiotic delivery. Chitosan/heparin

polyelectrolyte multilayers (PEMs) were adsorbed onto nanotubes, because heparin and chitosan have antimicrobial properties and heparin has been used to bind gentamicin to surfaces.[5,7-11,16,23,32,36] While previous studies have tested antimicrobial properties of surfaces and cellular attachment very few have co-cultured mammalian cells with bacteria to determine whether surfaces can simultaneously inhibit bacteria and promote mammalian cell attachment.[5,7-11,16,23,32,36-39] Infection of a prosthetic implant is described as a "race to the surface," in which the chance of infection is determined by which colonizes the surfaces first, bacteria or osteogenic cells. If osteogenic cells colonize the surface first, then no infection happens because the bacteria dies off; however, if bacteria colonize the surface first then infection ensues.[40] To determine if the samples have increased antimicrobial properties without inhibiting cell attachment, the surfaces were tested in a novel way by co-culturing bacteria with mammalian cells. Some authors have proposed that co-culture of bacteria with mammalian cells is a better model for infection of orthopedic implants.[37-39] It is the goal of this study to combine nanotopography with antibiotic delivery to influence the "race to the surface" in favor of mammalian cells.

4.2.1 Materials and Methods

4.2.2 Titania Nanotube Fabrication

Titania nanotube surfaces were created from flat titanium foil using an anodization process.[6,30] Titanium foil (0.25 mm thickness and 99.8% purity) was cut into identical 8 mm diameter circles, using water jet cutting. Electrolyte solution consisted of 2 vol% hydrofluoric acid, 95 vol% diethylene glycol (DEG, basic, 99% reagent Sigma-Aldrich, St Lous, MO) and 3 vol% DI water. A platinum electrode served as a cathode. Anodization was performed at a constant voltage of 55V for 22h. Nanotubes were then annealed in an oven at 530 °C for 3 h.[6] The resulting titania nanotube-modified samples are referred to as Nt.

4.2.3 Construction of Polyelectrolyte Multilayers (PEMs)

Polyelectrolyte multilayers were prepared by the layer-by-layer deposition of alternating layers of chitosan and heparin as previously done by this group.[81] Chitosan (1 mg/ml; Heppe Medical Chitosan, Halle, Germany) and heparin sodium from porcine intestinal mucosa (3 mg/ml; 12.5% sulfur, Celsus Laboratories, Cincinnati, OH) solutions were prepared in acetate buffer (0.2 M, pH 5, Acros Organics, Geel, Belgium). A Millipore Synthesis water purification unit was used to obtain 18.2 MΩ cm water, and this was used for making all aqueous solutions (Millipore, Billerica, MA). All solutions were filtered through 0.22 µm polyvinylidene fluoride (PVDF) syringe filters. Titania nanotube substrates were first washed for five minutes in acidified water rinse (pH 4.0, acidified with acetic acid). Construction of PEMs was performed by alternating 5-min absorption steps of the polyelectrolytes (starting with chitosan) with 4-min acidified water rinses between absorption steps.[6,41] Heparin-terminated PEMs were constructed with 18 layers. The resulting PEM-modified titania nanotube samples are referred to as Nt + PEM. These surfaces were previously characterized and reported by this group using X-ray photoelectron spectroscopy (XPS) and scanning electron microscopy (SEM).[6]

4.2.4 Absorption and Release of Gentamicin on Titania Nanotubes + PEM

Eight 8 mm-diameter titania nanotube disks were constructed and 18-layer PEMs were adsorbed onto the surfaces as described above, to prepare Nt + PEM samples. Samples were dried overnight and then sterilized by incubating in 70% ethanol (200 proof, Heppe Medical Chitosan, Halle, Germany) for 30 min. To ensure no ethanol remained on the samples, samples were rinsed three times with sterile phosphate buffered saline (PBS), pH 7.2 without calcium chloride or magnesium chloride, (Fisher Scientific, Waltham, MA) for five min each wash.[81] To determine the release of gentamicin from the samples, two concentrations of gentamicin (NC0363642, Fisher

Scientific, Waltham, MA) were adsorbed onto Nt + PEM (n = 4 for each group). The release of gentamicin was measured over 7 days.

Two concentrations of gentamicin (50 mg/ml and 5 mg/ml) were aseptically prepared in PBS. Under aseptic conditions, 250 µl of gentamicin solution (n = 4) were added to sterile 48-well plates with Nt + PEM samples and placed on a shaker at 150 rpm for 1 h at room temperature. The solution was then removed and stored at −20 °C until further analysis. To determine the amount of gentamicin adsorbed onto the samples, the amount of gentamicin in the 1-hour post gentamicin addition was subtracted from the total amount of gentamicin added to the sample. Next, 250 µl of fibronectin (10 µg/ml; Fisher Scientific, Waltham, MA) in PBS was incubated on the samples for 1 h at 150 rpm at room temperature, then the fibronectin solution was removed. The gentamicin-modified samples after fibronectin addition are referred to as Nt + PEM + $G_{adsorbed}$.

Nt + PEM + $G_{adsorbed}$ samples were kept in 48-well plates with 500 µl of PBS at 37 °C throughout the rest of the experiment. At 6, 12 and 24 h, as well as 2 and 7 d, 500 µl of solution was removed and replaced with fresh PBS. The removed samples were stored −20 °C. The concentration of gentamicin in solution was measured using a previously described colorometric assay.[42] Briefly, 30 µL of 1.25% (w/v) ninhydrin (Fisher Scientific, Waltham, MA) was added to 100 µL of the gentamicin solution. Then samples were heated at 95 °C for 15 min in a water bath. Samples were then cooled on ice for 10 min and 100 µL was transferred to a 96-well plate and the absorbance was measured at 400 nm. Concentration was calculated by comparing to a standard curve of gentamicin. Total gentamicin released from the sample was calculated and plotted versus time.

4.2.5 Antimicrobial Activity of Gentamicin-Modified Surfaces

Nt, Nt + PEM, and Nt + PEM + $G_{adsorbed}$ samples (prepared using 5 mg/ml gentamicin) were prepared as described above. Antimicrobial activity of the surfaces was tested using gram-negative *E. coli* and gram-positive *S. aureus*. Both *E. coli* and *S. aureus* were resuspended in 30 g/L tryptic soy broth (TSB) (Sigma-Aldrich, St. Louis, MO) from frozen pellets and incubated at 37 °C for 12 h prior to seeding samples. Bacteria solutions were diluted to a concentration of 10^6 CFU/mL. Samples were seeded with 500 µL of the bacteria solution and incubated at 37 °C for 6 and 24 h.

Live and dead bacteria adhered to the surfaces was counted at 6 and 24 h (n = 5 for each time point and bacteria type). The bacteria solution was removed, and the surfaces were washed with PBS three times. Then the surfaces were incubated in stain solution (3 µL of propidium iodide and SYTO 9 stain 1:1 in PBS; Live/Dead BacLight Bacteria Viability, Invitrogen, Carlsbad, CA) for 20 min in the dark at room temperature. Samples were then rinsed with PBS and fixed in 3.7% formaldehyde (Fisher Scientific, Waltham, MA) in PBS.[43] Samples were then immediately imaged using a Zeiss Axiovision fluorescence microscope. Each sample was imaged at 50× in three locations, and ImageJ software (NIH) was used to calculate the percent of live and dead bacteria on the surfaces.

Bacteria morphology was assessed using SEM at 6 and 24 h (n = 5 for each time point and bacteria type). Samples were placed in primary fixative (3% glutaraldehyde with 0.1 M sucrose and 0.1 M sodium cacodylate in deionized water) for 45 min, followed by a rinse in buffer solution (primary fixative without glutaraldehyde) for 10 min. Then samples were dehydrated in increasing concentrations of ethanol (30%, 50%, 70%, 90%, and 100%) for 10 min each at room temperature. Finally, samples were incubated in hexamethyldisilazane for 10 min and air-dried for imaging.

Samples were sputter-coated with palladium-gold alloy (Polaron SC 7620 Sputter Coater, Quorum Technologies, Newhaven, UK) at a thickness of 10 nm (10-15 mA, under a vacuum of 130 mTorr). The SEM (JSM-6500F, field emissions scanning electron microscope, JEOL, Japan) was operated at an accelerating voltage of 15 kV, at two different magnifications (5000× and 1000×) on each sample were imaged.[6]

4.2.6 Co-culture of Bacteria and Mammalian Cells on Gentamicin Modified Surfaces

Nt, Nt + PEM, and Nt + PEM + $G_{adsorbed}$ samples (prepared using 5 mg/mL gentamicin) were prepared as described above. Human adipose-derived stem cells (hADSC) were obtained at passage three from Dr. Kimberly Cox-York's lab at Colorado State University. hADSCs were grown in culture medium, which consisted of alpha modified minimum essential medium (α-MEM; ThermoFisher, Waltham, MA) supplemented with 10% fetal bovine serum (FBS; ThermoFisher, Waltham, MA). No antibiotics were included in the culture medium. *S. aureus* bacteria was grown as described above in TBS. Sterile samples were placed in sterile 48-well plates under aseptic conditions. 450 µL of hADSCs in culture medium at a final concentration of 5,000 cells/mL were added to each well. Then 50 µL of *S. aureus* at a final concentration of 10^6 CFU/mL was added to each well. As a positive control for gentamicin delivery, some Nt samples also had gentamicin added to the growth media at a final concentration of 5 mg/mL, these samples are referred to as Nt + $G_{solution}$. Samples were incubated at 37 °C and 5% CO_2 for 1, 4 and 7 d.

Some samples were fixed in 3.7% formaldehyde in PBS on days 1, 4 and 7 ($n = 5$ per time point). Samples were stored in PBS at room temperature until the fluorescent staining. The samples were stained with 4′,6-diamidino-2-phenylindole (DAPI, Invitrogen) and rhodamine phalloidin (actin). Rhodamine phalloidin at a concentration of 14 µM in PBS was added to wells and incubated for 25 min at room temperature. DAPI was added to the well at a final concentration of

300 nM and incubated at room temperature for 5 min. Samples were then rinsed once in PBS and then stored in PBS until fluorescence imaging. Each sample was imaged at 10× in three locations using a Zeiss Axiovision fluorescence microscope. Area of total area stained by the DAPI includes the hADSC nuclei and the bacterial cells. The area of hADSC nuclei was determined and subtracted from the total DAPI-stained area to determine the area of bacteria. This is further explained in Appendix B. Area of nuclei was calculated using ImageJ software (NIH).

The remaining samples were fixed for SEM and imaged as described above under the heading Antimicrobial Response to Gentamicin Modified Surfaces.

4.2.7 Statistical Analysis

One representative experiment was conducted, and all results were analyzed using a one-way analysis of variance (ANOVA) with a Tukey post-hoc test comparing experimental group means at each time point. Statistical significance was considered at $p < 0.05$ (Origin(Pro), Version 2020. OriginLab Corporation, Northampton, MA, USA.)

4.3.1 Results and Discussion

4.3.2 Surface Characterization and Gentamicin Release

The Nt and Nt + PEM surfaces were characterized in our previous paper, and the results are shown in Figure 1 a,b,c.[81] As shown in the SEM images, uniform vertical nanotubes are seen on the both the Nt and Nt + PEM surfaces (**Figure 4.1a**). This shows that the PEMs do not change the morphology of the surface. The XPS survey scans for Nt + PEM samples show additional nitrogen (N1s) and sulfur (S2p) peaks compared to the Nt survey scan; additionally, there is no discernable titanium (Ti2p) peak on the Nt + PEM surfaces (**Figure 4.1b**), confirming complete surface coverage of the surfaces with the PEMs. High-resolution nitrogen spectra show

ammonium, amine and amide peaks, which is consistent with the PEM composition. High-resolution C1s spectra indicate alcohol, ether and amine groups (**Figure 4.1c**).[6]

Gentamicin adsorbed onto the surfaces was measured by the previously described colorimetric assay. The average (±SD) amount of gentamicin loaded onto the Nt + PEM samples from 5 and 50 mg/ml was 1.23 ± 0.002 mg (98.39 ± 0.16 % of total gentamicin added) and 8.14 mg ± 1.76 mg (65.10 ± 14.08 % of total gentamicin added) respectively. There was more of the total gentamicin adsorbed onto the 5 mg/mL sample than the 50 mg/mL sample. This could be due to the surface reaching capacity for gentamicin absorption. The cumulative release of gentamicin was measured over 7 days (Figure 1d). After two days the amount of gentamicin released was below the threshold of the assay and was considered zero (data not shown). There was a burst release with most of the gentamicin being released during the first six hours. Of the adsorbed gentamicin the average (±SD) percent of gentamicin released from the 5 mg/mL and 50 mg/mL samples was 18.73 ± 1.87 % and 30.87 ± 3.78 % respectively. The remaining gentamicin remained on the surfaces. This is similar to previous studies that found a burst release of gentamicin during the first six hours.[16,33] The main difference in results between the our study and that of Escobar *et al.* is that they saw a slow release of gentamicin over the next 35 days from a poly(acrylic acid) (PAA) coating. This was attributed to how the gentamicin was added to the surfaces. The gentamicin in the study by Escobar *et al.* gentamicin was incorporated into the PEMs at a pH 4.5, and gentamicin becomes less protonated at a physiological pH (7.4), weakening the interaction between the antibiotic and the PAA. This weakened interaction is thought to be the cause of the sustained release of gentamicin. The gentamicin in this study was added at physiological pH (7.4), so there is no change in protonation of the antibiotic that would contribute to a sustained release.

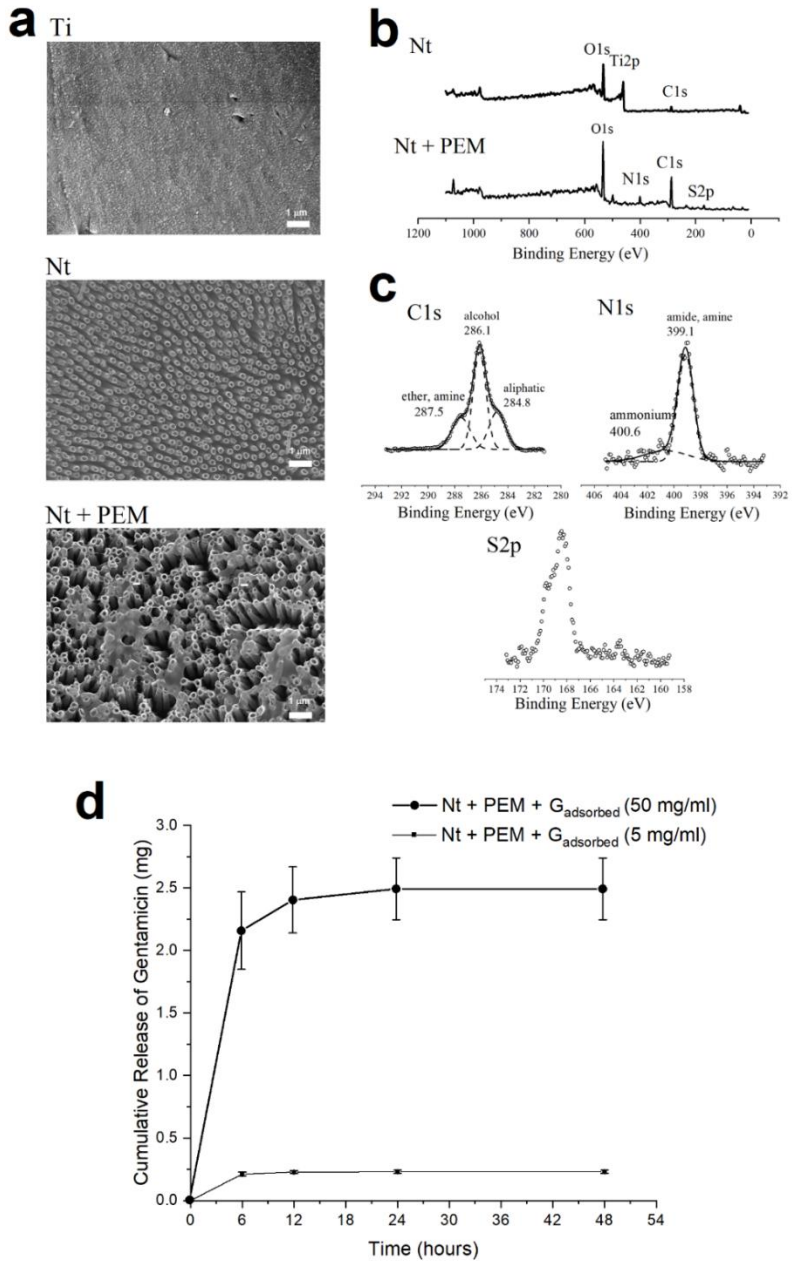

Figure 4.1. (a) Representative SEM images of surfaces. The flat titanium (Ti) image is a representative image of the flat titanium surface before anodization. The Nt image is a representative image of the titanium surface after anodization and the addition of nanotubes on the surface. The Nt + PEM image shows nanotubes surfaces after the addition of PEMs. (b) Full XPS survey spectra of Nt and Nt + PEM surfaces. O1, $Ti2p_{3/2}$, C1s, N1s, and S2p peaks are labeled. (c) High-resolution XPS spectra of C1s, N1s, and S2p for Nt + PEM surfaces.[81] (d) Cumulative release of gentamicin *in vitro* from Nt + PEM + $G_{adsorbed}$ surfaces (average ± SE). Ti, flat titanium; Nt, titania nanotubes; PEMs, polyelectrolyte multilayers; XPS, X-ray photoelectron spectroscopy; SEM, scanning electron microscopy.

4.3.3 Surface Response to *E. coli* and *S. aureus*

To test the antimicrobial activity of the surfaces loaded with 5 mg/mL gentamicin, the surfaces were exposed to gram-negative *E. coli* and gram-positive *S. aureus* for up to 24 h and the percent area of live and dead bacteria were calculated. After 6 h, Nt + PEM + $G_{adsorbed}$ had significantly less live *E. coli* than Nt surfaces (**Figure 4.2**). By 24 h, all surface types had significantly different amounts of live *E. coli* on the surface when compared to each, other with PEM + $G_{adsorbed}$ samples having the lowest amount. This suggests that by 6 h, the gentamicin modified surface prohibit live *E. coli* from attaching to the surface when compared to nanotubes, and by 24 h perform better than the Nt + PEM surfaces as well. There was no significant difference in the amount of dead *E. coli* on the surfaces at 6 h, and by 24 h there were significantly more dead *E. coli* on the Nt + PEM samples compared to the other two surfaces. The dead bacteria stained is only the bacteria on the surface of the samples, and is less than 0.4% of the surface area for all samples. The reduction in live bacteria on the gentamicin-modified surfaces suggests that *E. coli* does not bind to and survive on this surface. This would explain the limited dead bacteria on the Nt + PEM + $G_{adsorbed}$ samples.

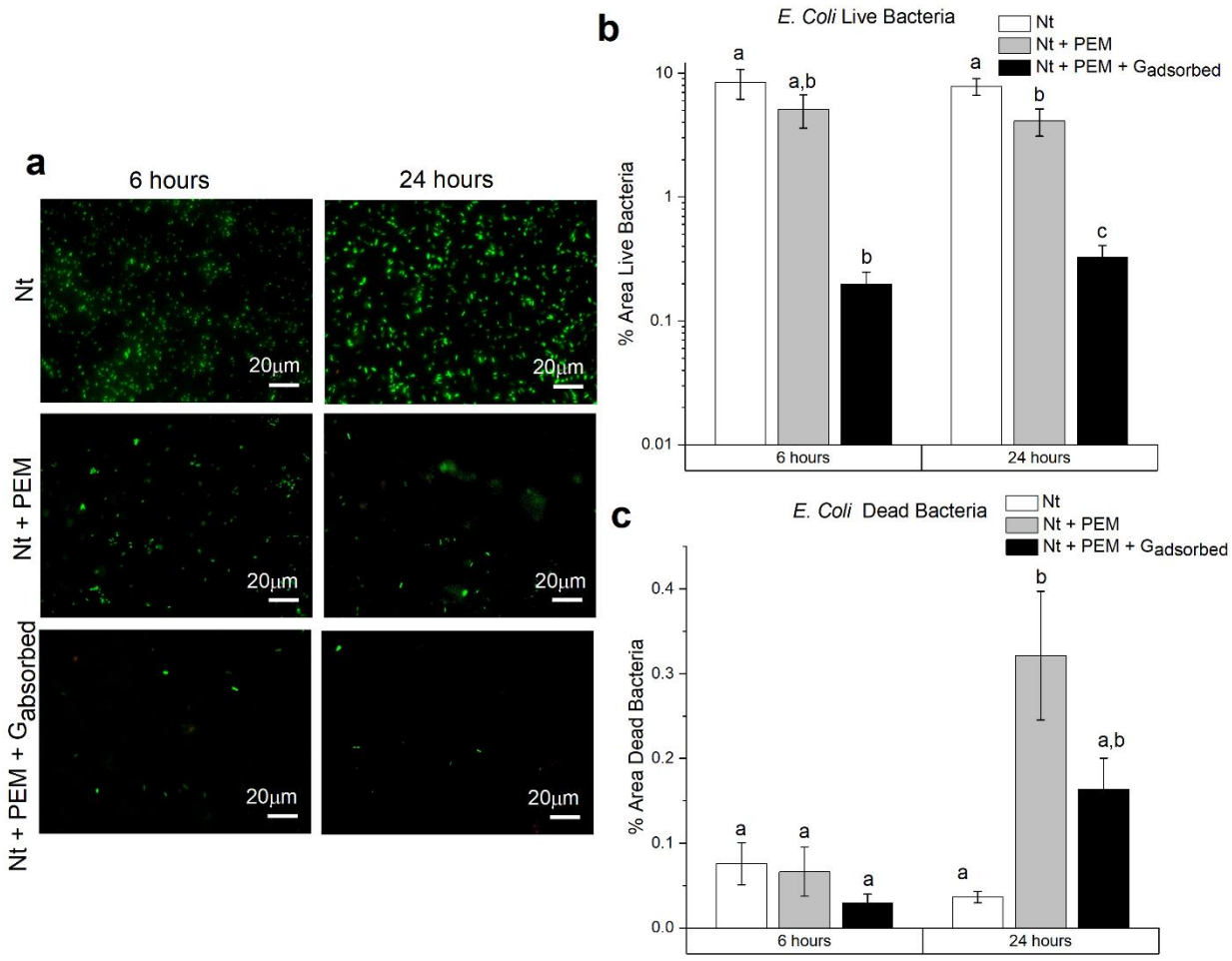

Figure 4.2. (a) Representative fluorescent images (original magnification is 20×) of *E. coli*. Live *E. coli* are stained green and dead are stained red. (b) Percent area of bacteria (mean ± SE) calculated at 6 and 24 h. (c) Percent area of dead bacteria (mean ± SE) calculated at 6 and 24 h. Means for (b) and (c) that share a letter are not significantly different ($p > 0.05$). Means were compared at each time point separately, so letters only correspond to that time point. Nt, titania nanotubes; PEMs, polyelectrolyte multilayers; G, gentamicin; *E. coli*, *Escherichia coli*.

After 6 h there was significantly less live *S. aureus* on Nt + PEM and Nt + PEM + $G_{adsorbed}$ surfaces, compared to Nt surfaces (**Figure 4.3**). There was significantly more dead *S. aureus* on Nt + PEM + $G_{adsorbed}$ samples compared to the other two samples. By 24 hours Nt + PEM samples had significantly more live *S. aureus* than the other two surfaces. There is significantly less dead *S. aureus* on Nt + PEM samples compared to the other two surfaces. Similarly to *E. coli*, this suggests that *S. aureus* does not survive on the gentamicin-modified surfaces.

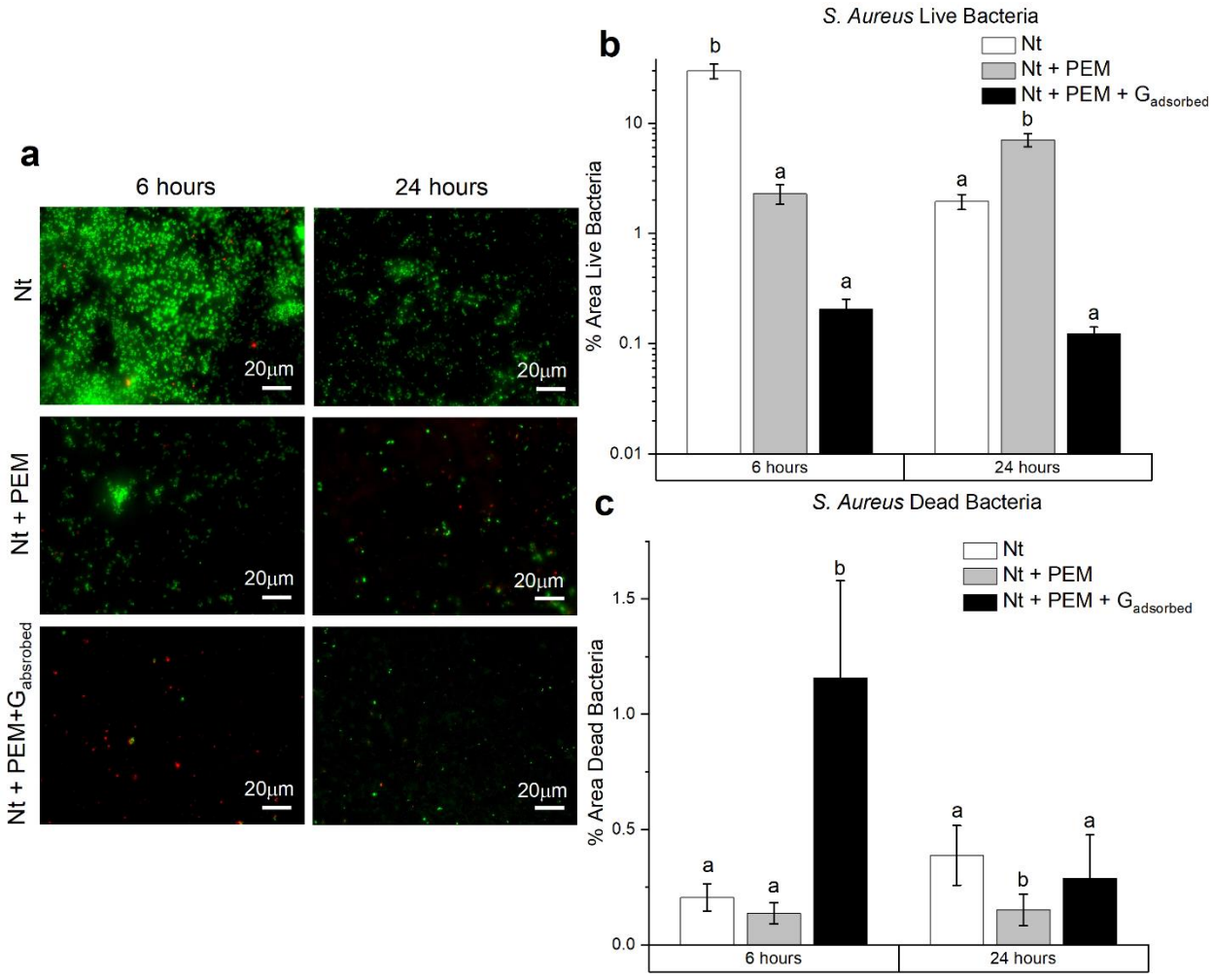

Figure 3.3. (a) Representative fluorescent images (20×) of *S. aureus* (n = 5). Live *S. aureus* are stained green and dead are stained red. (b) Percent area of bacteria (mean ± SE) calculated at 6 and 24 h (n=5). (c) Percent area of dead bacteria (mean ± SE) calculated at 6 and 24 h (n = 5). Means for (b) and (c) that share a letter are not significantly different (p > 0.05). Means were compared at each time point separately, so letters only correspond to that time point. Nt, titania nanotubes; PEMs, polyelectrolyte multilayers; G, gentamicin; *S. aureus*, *Staphylococcus aureus.*

Morphology of the bacteria on samples was assessed using SEM (**Figure 4.4**). When untreated *S. aureus* have smooth contours and spherical shapes in grape-like clusters.[44] This morphology and the grape like clusters are seen on the Nt and Nt+ PEM samples. On the Nt + PEM + $G_{adsorbed}$ there are very few *S. aureus*, compared to other samples. While there are a few

small clusters of the bacteria present on the surface most were singular and not in clusters. *E. coli* is a gram-negative rod-shaped bacteria.[45] There are several of these rod-shaped bacteria on the Nt and Nt + PEM samples. There were very few *E. coli* on the Nt + PEM + $G_{adsorbed}$ samples.

These experiments agree with previous experiments conducted using gentamicin-modified surfaces. The study by Escobar *et al* used poly-L-lysine (PLL) and complexes of poly(acrylic acid) (PAA) to absorb gentamicin onto glass surfaces. These surfaces had a burst release of gentamicin and were more effective than glass at preventing proliferation of *S. aureus*.[96] The study by Moskowitz *et al.* used PEMs composed of poly 1, a poly(β-amino ester), and Poly(acrylic acid) to absorb gentamicin on flat titanium surfaces, where lower infection rate of *S. aureus* was found on coated samples compared to non-coated samples.[32]

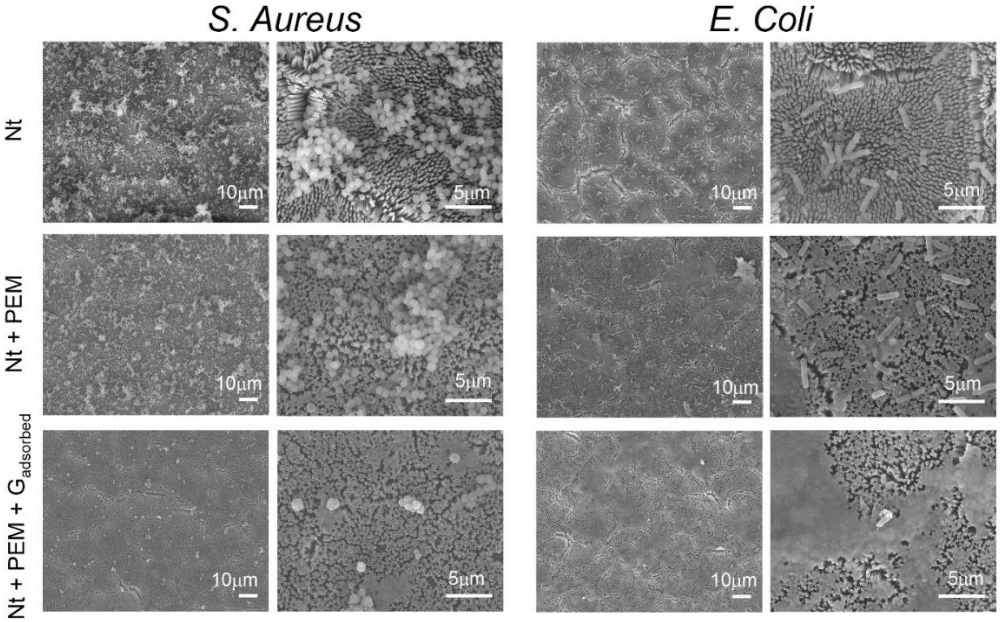

Figure 4.4. Representative SEM images of bacteria on samples. There are two images per sample and bacteria type. The image on the left for each bacteria is at low magnification (1000× original magnification) and the image on the right is from the same area at higher magnification (5000× original magnification). Nt, titania nanotubes; PEMs, polyelectrolyte multilayers; G, gentamicin; *S. aureus*, *Staphylococcus aureus;* SEM, scanning electron microscopy.

3.3.4 Responses of co-cultured hADSCs and S. Aureus to surfaces

To determine the ability for cells to attach to the surfaces while testing the antimicrobial properties of our surfaces, *S. aureus* and hADSCs were co-cultured on the surfaces. In this study, a positive control for gentamicin delivery in solution was included (Nt + $G_{solution}$). Samples were fluorescently stained and the percent area of hADSC nuclei and bacteria was calculated (**Figure 4.5**). At day one there was significantly less bacteria on Nt+ $G_{solution}$ and Nt + PEM + $G_{adsorbed}$ samples, compared to Nt and Nt + PEM samples. At day four there was still significantly less bacteria Nt + $G_{solution}$ and Nt + PEM + $G_{adsorbed}$ samples compared to Nt and Nt + PEM samples; however, there was also a significant difference in bacteria between Nt and Nt + PEM samples. At day seven Nt samples had significantly more bacteria than all the other samples. This suggests that gentamicin is effective against *S. aureus* both in solution and adsorbed on the samples. This agrees with the results from the monoculture of *S. aureus*, reported above.

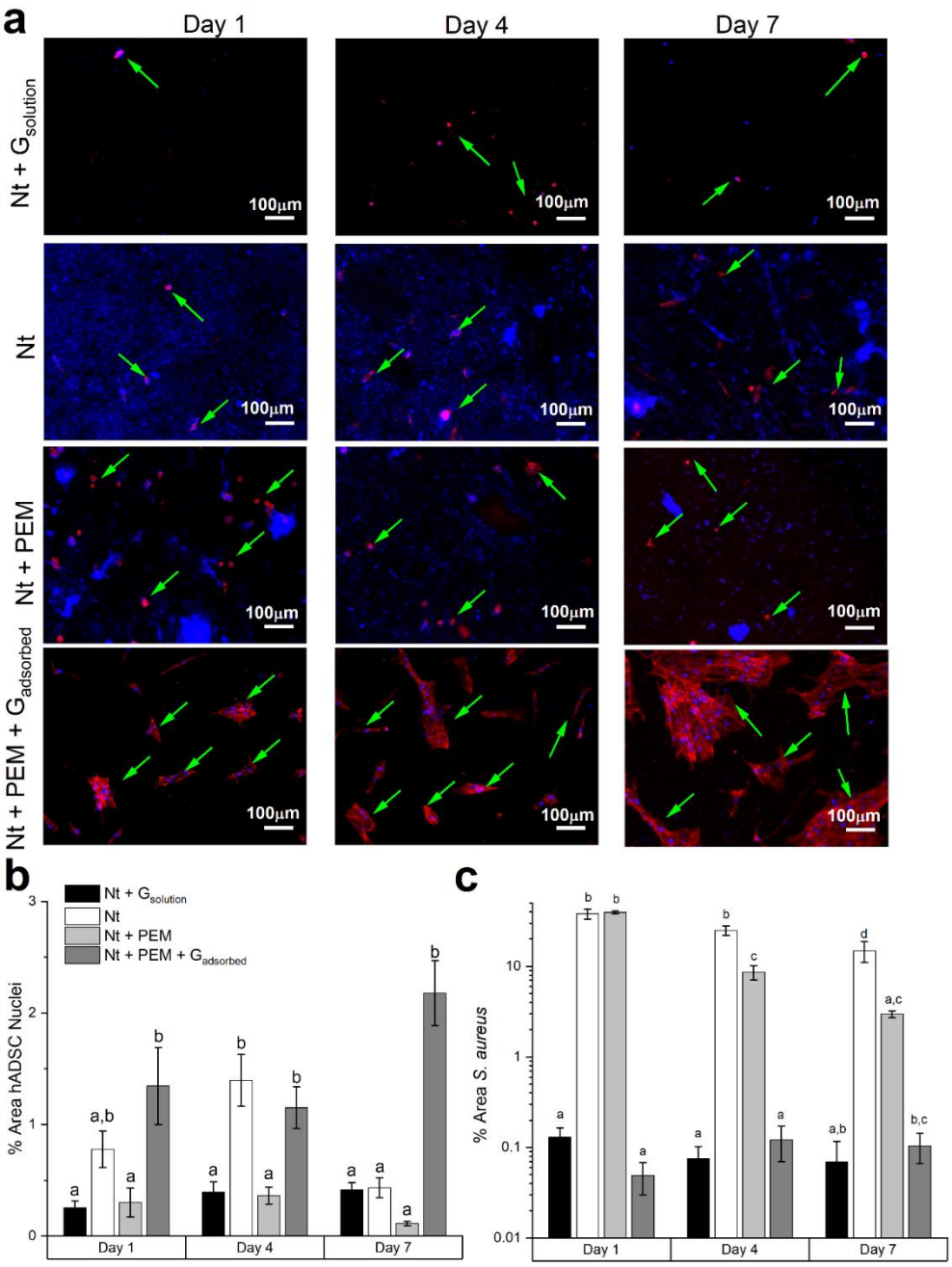

Figure 4.5. (a) Representative fluorescent images (10×) of *S. aureus* and hADSCs on Nt surfaces (n = 5). hADSC nuclei and bacteria (blue) and actin (red). Green arrows point to hADSCs as determined by surrounding actin stain. (b) Percent area of *S. aureus* (mean ± SE) at 1, 4, and 7 d (n = 5). (c) Percent area of hADSC nuclei (mean ± SE) at 1, 4, and 7 d (n = 5). Means for (b) and (c) that share a letter are not significantly different ($p > 0.05$). Means were compared at only to other conditions at the same time point, so letters only correspond to that time point. Nt, titania nanotubes; PEMs, polyelectrolyte multilayers; G, gentamicin; *S. aureus*, *Staphylococcus aureus;* hADSCs, human adipose-derived stem cells.

At day one and four there were significantly more hADSC nuclei on Nt + PEM + $G_{adsorbed}$ samples than on Nt + $G_{solution}$ and Nt + PEM samples. By day seven there were significantly more cell nuclei on Nt + PEM + $G_{adsorbed}$ then the other three samples. So, while Nt with gentamicin in solution and nanotubes modified with gentamicin and PEMs performed equally against *S. aureus* by day 7, the modified surfaces performed significantly better with respect to cell attachment. By day 7 there is no significant difference in the amount of *S. aureus* on the surface of the PEM-modified samples, suggesting the PEMs help reduce bacteria attachment. However, there is significantly more *S. aureus* on the Nt + PEM samples compared to the gentamicin-modified surface. This suggests that the bacteria wins "the race to the surface" on the Nt + PEM surface, because by day 7 there is significantly less hADSCs compared to Nt + PEM + $G_{adsorbed}$ samples. While this is a similar result to the previously mentioned study by Moskowitz *et al.*, where it was found that the coatings were nontoxic to MC3T3-E1 murine preosteoblast; however, the main difference in the *in vitro* portion of the Moskowitz study and this study, is that *S. aureus* was co-cultured with the mammalian cells in this study.[32]

Mammalian and bacteria cell morphology was assessed using SEM (**Figure 4.6**). hADSCs and *S. aureus* can be seen on all samples from day one to seven. On samples with PEMs there are also extracellular matrix (ECM) deposits present around the cells. The ECM deposits on the PEM samples were consistent with what was observed when cells were previously grown on PEM surfaces by this group.[6] From day one to seven there is very little *S. aureus* present on samples with gentamicin. There are grape like clusters of *S. aureus* present on the samples without gentamicin. This is consistent with what was found when the bacteria were cultured on the surfaces without hADSCs. The main difference was that the bacteria clusters were found on the cells or protein-like structures of the samples. Although both the gentamicin samples had less bacteria, the

gentamicin in solution had fewer cells and there was a notable difference in the morphology of the mammalian cells. The mammalian cells on the Nt + $G_{solution}$ were round and not spread out, while cells on the Nt + PEM + $G_{adsorbed}$ maintained a spread shape for up to 7 days. The cell shape is important, because hMSCs adopt a spread morphology before differentiating into osteoblasts, while cells that maintain a round shape tend to differentiate into adipose tissue.[46,47]

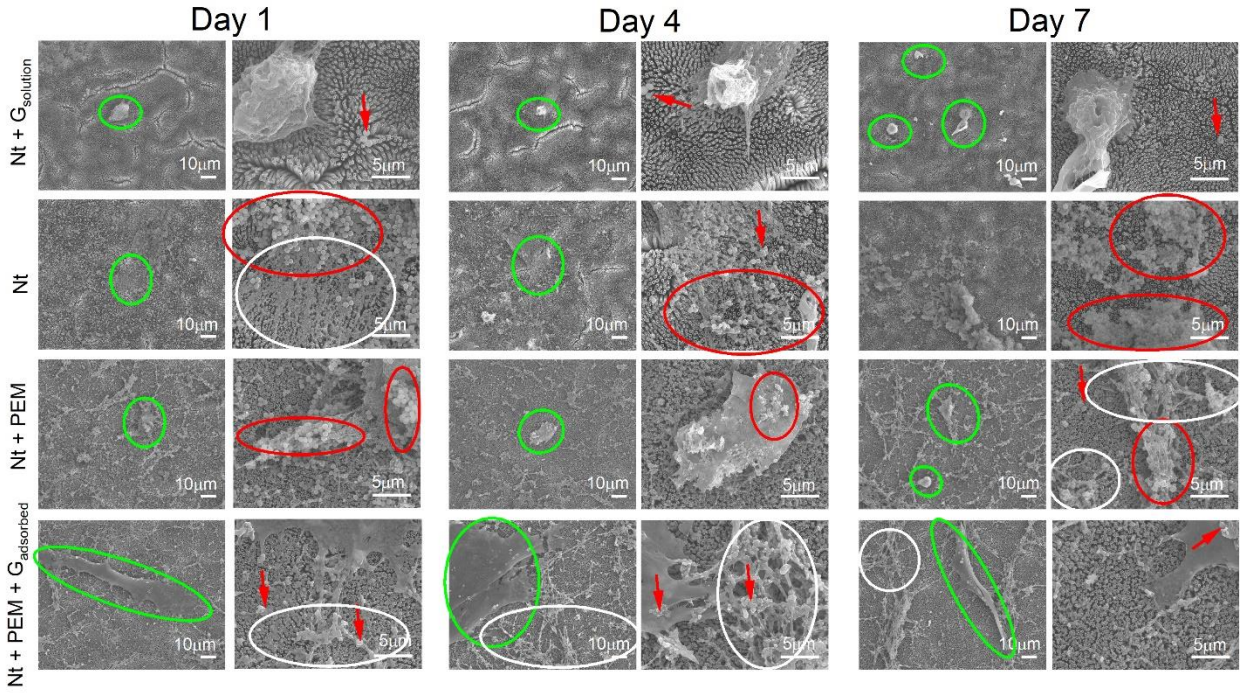

Figure 4.6. Representative SEM images of *S. aureus* cultured with hADSC. There are two images per sample and time point. The image on the left for each time point is at an original magnification of 1000× and the one on the right is of the same area at an original magnification of 5000×. Green circles on the 1000× image are hADSCs. Red are clusters of *S. aureus* and red arrows point to single bacteria not in clusters. White circles are examples of ECM deposits present on PEM samples. Nt, titania nanotubes; PEMs, polyelectrolyte multilayers; G, gentamicin; *S. aureus*, *Staphylococcus aureus;* hADSCs, human adipose derived stem cells; SEM, scanning electron microscopy.

These results agree with previous studies, in which gentamicin-modified surfaces reduce *S. aureus* growth, while still promoting cell attachment and proliferation.[32,34] Harris *et al.* modified titania nanotube surfaces with gentamicin, and found that it was effective against *S. aureus* while

still promoting the attachment of human marrow-derived mesenchymal stem cells (hMSC). The hMSCs were cultured separately from the bacteria and in antibiotic-containing media.[34] The innovation of our work is the combination of gentamicin delivery with nanotopography and PEMs to bind and stabilize gentamicin, while not effecting cell growth and attachment when co-cultured with bacteria. Our novel gentamicin-modified surfaces were shown to be effective against *S. aureus* and promote cell adhesion, when the two cell types were grown together in media deprived of antibiotics. This mode of gentamicin delivery is superior to delivering gentamicin in solution, as it achieves equally effective antibacterial activity, while not inhibiting hADSC growth and spreading.

4.4 Conclusion

Improving the antimicrobial properties of surfaces for orthopedic implants while maintaining the ability for cells to attach to the surface, is still a major problem. In this study gentamicin was successfully adsorbed onto Nt surfaces via PEMs. Surfaces modified with gentamicin can successfully reduce the amount of *S. aureus* while also promoting hADSC attachment, when the two are co-cultured together. When compared to Nt surfaces, the gentamicin-modified surfaces had significantly less live *S. aureus* on the surfaces at 6 h, and significantly less *E. coli* at 6 and 24 h. When *S. aureus* was co-cultured with hADSCs the gentamicin-modified surfaces had significantly fewer *S. aureus* and significantly more hADSC nuclei at 7 d, when compared to Nt samples without antibiotics. While there was no significant difference in the amount of *S. aureus* on the surface of Nt + $G_{solution}$ compared to Nt + PEM + $G_{adsorbed}$, there were significantly more hADSC nuclei on the gentamicin-modified surfaces compared to those with gentamicin in solution. Furthermore, the morphology of the hADSCs on the Nt + PEM + $G_{adsorbed}$ was more consistent with stem cells that eventually differentiate into osteogenic linage. This

unique presentation of gentamicin on surfaces provides increased antimicrobial activity while still maintaining the ability for mammalian cells to attach to the surface. By using co-culture to test antimicrobial activity, the "race to the surface" between the bacteria and mammalian cells could be evaluated. On the gentamicin-modified surfaces, the adipose-derived stem cells won the race to the surface against *S. aureus*. This provides a promising approach for antimicrobial surfaces used in orthopedic implants.

REFERNCES

1. Ethgen, O., Bruyère, O., Richy, F., Dardennes, C. & Reginster, J.-Y. Health-Related Quality of Life in Total Hip and Total Knee Arthroplasty. *J. Bone Jt. Surg.* 86, 963–974 (2004).

2. Raphel, J. *et al.* Engineered protein coatings to improve the osseointegration of dental and orthopaedic implants. *Biomaterials* 83, 269–282 (2016).

3. Etkin, C. D. & Springer, B. D. The American Joint Replacement Registry the first 5 years. *Arthroplast.* Today 3, 67–69 (2017).

4. Kurtz, S., Ong, K., Edmond, L., Mowat, F. & Halpern, M. Projections of Primary and Revision Hip and Knee Arthroplasty in the United States from 2005 to 2030. *J. Bone Jt. Surg.* 89, 780 (2007).

5. Campoccia, D., Montanaro, L. & Arciola, C. R. The significance of infection related to orthopedic devices and issues of antibiotic resistance. *Biomaterials* 27, 2331–2339 (2006).

6. Wigmosta, T. B., Popat, K. C. & Kipper, M. J. BMP -2 Delivery from Polyelectrolyte Multilayers EnhancesOsteogenic Activityon Nanostructured Titania . *J. Biomed. Mater. Res. Part A* 1–10 (2020).

7. Vacheethasanee, K. & Marchant, R. E. Surfactant polymers designed to suppress bacterial (Staphylococcus epidermidis) adhesion on biomaterials. *J. Biomed. Mater. Res.* 50, 302–312 (2000).

8. Trujillo, N., Popat, K., Trujillo, N. A. & Popat, K. C. Increased Adipogenic and Decreased Chondrogenic Differentiation of Adipose Derived Stem Cells on Nanowire Surfaces. *Materials (Basel)*. 7, 2605–2630 (2014).

9. Arciola, C. R., Radin, L., Alvergna, P., Cenni, E. & Pizzoferrato, A. Heparin surface treatment of poly(methylmethacrylate) alters adhesion of a Staphylococcus aureus strain: utility of bacterial fatty acid analysis. *Biomaterials* 14, 1161–1164 (1993).

10. Tavaria, F. K. *et al.* Chitosan: antimicrobial action upon staphylococci after impregnation onto cotton fabric. *J. Appl. Microbiol.* 112, 1034–1041 (2012).

11. Mansilla, A. Y. *et al.* Evidence on antimicrobial properties and mode of action of a chitosan obtained from crustacean exoskeletons on Pseudomonas syringae pv. tomato DC3000. *Appl. Microb. Cell Physiol.* 97, 6957–6966 (2013).

12. Stigter, M., Bezemer, J., De Groot, K. & Layrolle, P. Incorporation of different antibiotics into carbonated hydroxyapatite coatings on titanium implants, release and antibiotic efficacy. *J. Control. Release* 99, 127–137 (2004).

13. Radin, J. S., Campbellt, J. T., Ducheyne, P. & Cuckler+, J. M. Calcium phosphate ceramic coatings as carriers of vancomvcin. *Biomoteriols* 18, 777–782 (1997).

14. Lin, T. L. *et al.* Antimicrobial coatings: a remedy for medical device-related infections. *Artic. Med. device Technol.* (2001).

15. Stigter, M., De Groot, K. & Layrolle, P. Incorporation of tobramycin into biomimetic hydroxyapatite coating on titanium. *Biomaterials* 23, 4143–4153 (2002).

16. Lee, D. W., Yun, Y. P., Park, K. & Kim, S. E. Gentamicin and bone morphogenic protein-2 (BMP-2)-delivering heparinized-titanium implant with enhanced antibacterial activity and osteointegration. *Bone* 50, 974–982 (2012).

17. Campos, M. G. N. *et al.* In vitro gentamicin sustained and controlled release from chitosan cross-linked films. *J. Mater. Sci. Mater. Med.* 20, 537–543 (2009).

18. Tam, V. H., Kabbara, S., Vo, G., Schilling, A. N. & Coyle, E. A. Comparative Pharmacodynamics of Gentamicin against Staphylococcus aureus and Pseudomonas aeruginosa. Antimicrob. *Agents Chemother.* 50, 2626–2631 (2006).

19. Miglioli, P. A., Silini, R., Carzeri, O., Grabocka, E. & Allerberger, F. Antibacterial activity of gentamicin and ciprofloxacin against gram-negative bacteria: Interactions with pig and calf sera. *Pharmacol. Res.* 39, 321–323 (1999).

20. Kovacik, A. *et al.* In Vitro Assessment of Gentamicin Cytotoxicity on the Selected Mammalian Cell Line (Vero cells). *Adv. Reserach Life Sci.* 1, 111–116 (2017).

21. Isefuku, S., Joyner, C. J. & Simpson, A. H. R. W. Gentamicin may have an adverse effect on osteogenesis. *J. Orthop. Trauma* 17, 212–216 (2003).

22. Duewelhenke, N., Krut, O. & Eysel, P. Influence on mitochondria and cytotoxicity of different antibiotics administered in high concentrations on primary human osteoblasts and cell lines. Antimicrob. *Agents Chemother.* 51, 54–63 (2007).

23. Ince, A., Schütze, N., Karl, N., Löhr, J. F. & Eulert, J. Gentamicin negatively influenced osteogenic function in vitro. *Int. Orthop.* 31, 223–228 (2007).

24. Ballo, A., Agheli, H., Lausmaa, J., Thomsen, P. & Petronis, S. Nanostructured model implants for in vivo studies: influence of well-defined nanotopography on de novo bone formation on titanium implants. *Int. J. Nanomedicine* 6, 3415–3428 (2011).

25. Bjursten, L. M. *et al.* Titanium dioxide nanotubes enhance bone bonding in vivo. J. Biomed. *Mater. Res. Part A* 92, 1218–1224 (2009).

26. Dalby, M. J. *et al.* The control of human mesenchymal cell differentiation using nanoscale symmetry and disorder. *Nat. Mater.* 6, 997–100 (2007).

27. Biggs, M. J. P. *et al.* The use of nanoscale topography to modulate the dynamics of adhesion formation in primary osteoblasts and ERK/MAPK signalling in STRO-1+ enriched skeletal stem cells. *Biomaterials* 30, 5094–5103 (2009).

28. Fiedler, J. *et al.* The effect of substrate surface nanotopography on the behavior of multipotnent mesenchymal stromal cells and osteoblasts. *Biomaterials* 34, 8851–8859 (2013).

29. Alenezi, A. *et al.* Characteristics of 2 Different Commercially Available Implants with or without Nanotopography. *Int. J. Dent.* 2013, (2013).

30. Popat, K. C., Leoni, L., Grimes, C. A. & Desai, T. A. Influence of engineered titania nanotubular surfaces on bone cells. *Biomaterials* 28, 3188–3197 (2007).

31. Lin, W. *et al.* Inhibited bacterial biofilm formation and improved osteogenic activity on gentamicin-loaded titania nanotubes with various diameters. *Int. J. Nanomedicine* 9, 1215–1230 (2014).

32. Moskowitz, J. S. *et al.* Biomaterials The effectiveness of the controlled release of gentamicin from polyelectrolyte multilayers in the treatment of Staphylococcus aureus infection in a rabbit bone model. *Biomaterials* 31, 6019–6030 (2010).

33. Escobar, A. *et al.* Antibacterial Layer-by-Layer Films of Poly(acrylic acid)–Gentamicin Complexes with a Combined Burst and Sustainable Release of Gentamicin. *Adv. Mater. Interfaces* 6, 1–9 (2019).

34. Harris, L. G., Tosatti, S., Wieland, M., Textor, M. & Richards, R. G. Staphylococcus aureus adhesion to titanium oxide surfaces coated with non-functionalized and peptide-functionalized poly(L-lysine)-grafted- poly(ethylene glycol) copolymers. *Biomaterials* 25, 4135–4148 (2004).

35. Simon-Walker, R. *et al.* Glycocalyx-inspired nitric oxide-releasing surfaces reduce platelet adhesion and activation on titanium. *ACS Biomater. Sci. Eng.* 3, 68–77 (2017).

36. Liao, Y.-H. *et al.* Osteogenic differentiation of adipose-derived stem cells and calvarial defect repair using baculovirus-mediated co-expression of BMP-2 and miR-148b. *Biomaterial*s 35, 4907–4910 (2014).

37. Martínez-Pérez, M. *et al.* The "Race for the Surface" experimentally studied: In vitro assessment of Staphylococcus spp. adhesion and preosteoblastic cells integration to doped Ti-6Al-4V alloys. *Colloids Surfaces B Biointerfaces* 173, 876–883 (2019).

38. Martinez-Perez, M. *et al.* Evaluation of bacterial adherence of clinical isolates of Staphylococcus sp. using a competitive model: An in vitro approach to the 'race for the surface' theory. *Bone Jt. Res.* 6, 315–322 (2017).

39. Foss, B. L., Ghimire, N., Tang, R., Sun, Y. & Deng, Y. Bacteria and osteoblast adhesion to chitosan immobilized titanium surface: A race for the surface. *Colloids Surfaces B Biointerfaces* 134, 370–376 (2015).

40. Gristina, A. G. Biomaterial-Centered Infection : Microbial Adhesion Versus Tissue Integration. *Science* (80-.). 237, 1588–1595 (1987).

41. Almodóvar, J., Bacon, S., Gogolski, J., Kisiday, J. D. & Kipper, M. J. Polysaccharide -Based Polyelectrolyte Multilayer Surface Coatings can Enhance Mesenchymal Stem Cell Response to Adsorbed Growth Factors. *Biomacromolecules* 10, 2629–2639 (2010).

42. Frutos, P., Torrado, S., Perez-lorenzo, M. E. & Frutos, G. A validated quantitative colorimetric assay for gentamicin. *J. Pharm. Biomed. Anal.* 21, 1149–1159 (2000).

43. Sabino, R. M. *et al*. Enhanced hemocompatibility and antibacterial activity on titania nanotubes with tanfloc/heparin polyelectrolyte multilayers. *J. Biomed. Mater. Res. - Part* A 108, 992–1005 (2020).

44. Nishino, T. & Nakazawa, S. Cephalexin-Induced Morphological Alterations in the Surface Structures of Staphylococcus aureus and Escherichia coli Demonstrated by Scanning Electron Microscopy. *Jpn. J. Microbiol.* 17, 383–392 (1973).

45. Nanninga, N. Morphogenesis of Escherichia coli. *Microbiol. Mol. Biol. Rev.* 62, 110–129 (1998).

46. Park, I. S. *et al*. The correlation between human adipose-derived stem cells differentiation and cell adhesion mechanism. *Biomaterials* 30, 6835–6843 (2009).

47. McBeath, R., Pirone, D. M., Nelson, C. M., Bhadriraju, K. & Chen, C. S. Cell shape, cytoskeletal tension, and RhoA regulate stem cell lineage commitment. *Dev. Cell* 6, 483–495 (2004).

CHAPTER 5: CONCLUSIONS AND FUTURE DIRECTIONS

Overview: The work discussed previously focused on the development of biomimetic surfaces that increase bone mineralization and antimicrobial surfaces that also promote cell attachment and proliferation. The first chapter focuses on the motivation behind the work and previous strategies used. Chapter 2 found that the unique presentation of BMP-2 on nanostructured surfaces provides an increase in osteogenic properties of bone marrow cells. Chapter 3 found that gentamicin-modified surfaces provide a favorable template for adipose-derived stem cells to win the race to the surface against *S. aureus*. Chapter 4 found that PEMs composed of *iota*-carrageenan, pectin, and chitosan, can prevent deposition and growth of *S. aureus* and *P. aeruginosa* and can also provide efficient cell culture surface with a high cell growth rate. These strategies provide promising approaches to enhance bone healing and improve orthopedic implants.

Throughout this work, we developed biomimetic surfaces that increase bone mineralization and antimicrobial surfaces that also promote cell attachment and proliferation. This is explored in detail in the previous 3 chapters (chapters 2 through 4). While these are presented in order, the work is interconnecting and overlapping, not sequential. How the previously mentioned chapters are connected is outlined in **Figure 5.1**.

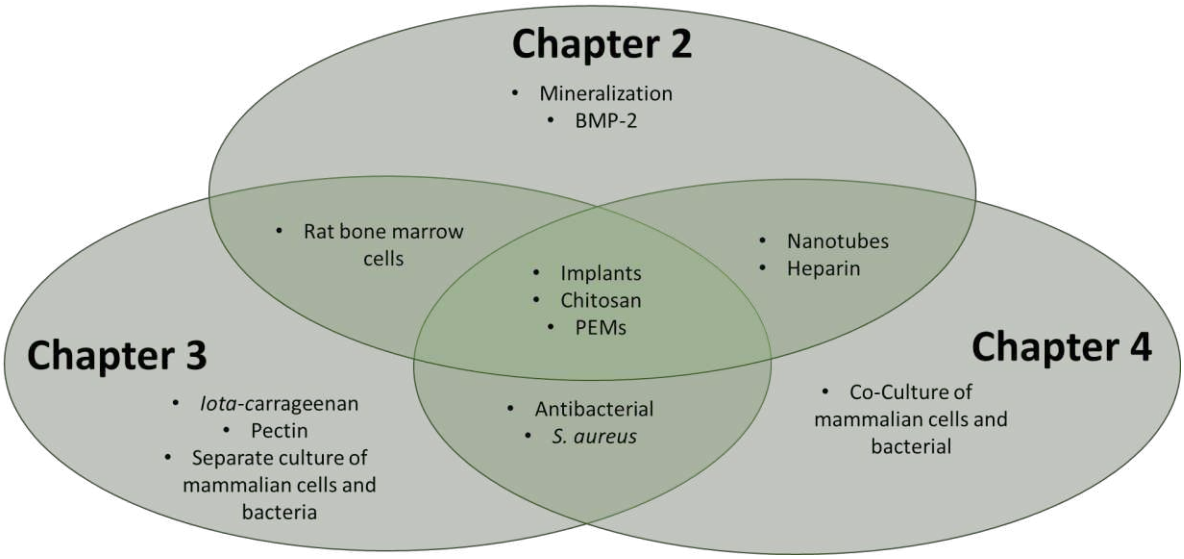

Figure 5.1: Overview of how chapters 2, 3, and 4 connect, overlap, and differ.

All three chapters address surfaces for implants while focusing on different objectives. Chapter 2 focuses on increasing mineralization of surfaces, while chapters 3 and 4 focus on antimicrobial properties of the surface. However, to accomplish these objectives, all three chapters use polyelectrolyte multilayers (PEMs), and the same polycation, chitosan, in the PEMs. This was due to PEMs providing a tunable surface for drug delivery, and chitosan's biocompatible and antimicrobial properties.[1-6] The focus of chapter 2 was to increase osseointegration of the surface, by testing the surface's ability to induce mineralization markers of rat bone marrow cells. To accomplish this BMP-2 is delivered from nanotube surfaces because it has been shown to promote bone formation and is currently used in commercial products.[7-10] The polyanion heparin is used in

the PEMs, BMP-2 has a binding site for heparin that modulates its bioactivity; in the presence of heparin, degradation of BMP-2 is blocked and the half-life in culture media is prolonged by nearly 20-fold.[11,12] Nanotubes increase cell attachment, proliferation, and mineralization markers *in vitro*, and were therefore used for this surface.[13,14] Increased antimicrobial properties and increased mammalian cell attachment and proliferation was the aim of chapters 3 and 4. Chapter 3 uses two polyanions, *iota*-carrageenan and pectin. The negative functional groups of the polyanions make them both hydrophilic and antimicrobial. Hydrophilicity has been shown to increase mammalian cell attachment and antimicrobial properties.[15] The antimicrobial and mammalian cell attachment properties were tested separately on these surfaces. While the aim of chapter 4 was to increase antimicrobial properties and mammalian cell attachment, it was tested by co-culturing mammalian cells with bacteria to determine which would win the "race to the surface." Chapter 4 used the polyanion heparin, because of its antimicrobial and hydrophilic properties, and ability to interact with gentamicin.[16–21] Gentamicin is a broad-spectrum antibiotic effective against the most common pathogens found in infect orthopedic implants.[6,18,22-26] To test the antimicrobial properties of the surfaces in chapters 3 and 4, both used S*taphylococcus aureus* (*S. aureus*), as it is the most common pathogen found in infected implants. Although each chapter focused on a unique aim and different methodologies, all are intertwined through materials and final goals.

The first chapter summarized the motivation and previous strategies used to increase osseointegration and antimicrobial properties of nanostructured biomimetic orthopedic implant surfaces. The first chapter concluded with a shift in hypothesis testing, outlining three different hypotheses: 1) surface modification(s) increased cytocompatibility and the osteogenic properties of mammalian bone cells; 2) surface modification(s) reduced bacterial adhesion, proliferation, and infection rate, without decreasing cytocompatibility; and 3) surface modification(s) provided a

favorable environment in which mammalian cells can beat bacterial cells and colonize the surface first, thus increasing the osteogenic and antimicrobial properties of the surface. The testing of these hypotheses was explored in chapters 2 through 4.

The second chapter explored the hypothesis 1) BMP-2 released from chitosan/heparin PEM-coated titania nanotubes surfaces induce an osteogenic response from rat bone marrow cells. Improving surfaces for orthopedic implants by creating surfaces that promote bone growth is still a major problem. In this study, BMP-2 was successfully absorbed onto Nt surfaces via PEMs and remained on the surfaces for up to 28 d in PBS. Our results showed that Nt surfaces modified with BMP-2 can increase osteogenic markers in bone marrow cells including osteocalcin and calcium content by 28 d in culture. Previous studies using BMP-2 use high concentrations of BMP-2 or lower concentrations on flat titanium or non-organized topographies. Our study combined organized nanotopographic surfaces with BMP-2 and heparin. This unique presentation of BMP-2 on surfaces provided an increase in osteogenic properties of bone marrow cells.[27]

Chapter 3 explored hypothesis 2) *iota*-carrageenan/chitosan and pectin/chitosan PEMs have antimicrobial properties against *Pseudomonas aeruginosa* (*P. aeruginosa*) and *S. aureus*, and support rat bone marrow cell adhesion and proliferation. The PEMs successfully reduced the number of both gram-negative and gram-positive bacteria on the surface. Furthermore, both surfaces are shown to have suitable microenvironments to support the bone marrow stem cells (BMSCs) adhesion, proliferation, and spreading after 7 days of cell culture. The work in this chapter showed for the first time that commercial CA and PC could be associated with CS in a weak acid condition (pH 5.0) to produce PEMs with antimicrobial and antiadhesive activities and desirable properties to act as coatings for biomedical materials and tissue engineering scaffolds.

PEMs composed of CA and CS can prevent the deposition and growth of *S. aureus* and *P. aeruginosa* and could also provide efficient cell culture with a high cell growth rate.[15]

Finally, chapter 4 explored hypothesis 3) gentamicin released from titania nanotubes coated with chitosan/heparin PEMs influences the "race to the surface" in favor of mammalian cells. In this study, gentamicin was successfully adsorbed onto Nt surfaces via PEMs. Surfaces modified with gentamicin successfully reduce the amount of *S. aureus* while also promoting hADSC attachment, when the two are co-cultured together. When *S. aureus* was co-cultured with hADSCs, the gentamicin-modified surfaces had significantly fewer *S. aureus* and significantly more hADSC nuclei at 7 d, when compared to Nt samples without antibiotics. While there was no significant difference in the amount of *S. aureus* on the surfaces with gentamicin in solution compared to gentamicin-modified surfaces, there were significantly more hADSC nuclei on the gentamicin-modified surfaces compared to those with gentamicin in solution. Furthermore, the morphology of the hADSCs on the gentamicin-modified surfaces was more consistent with stem cells that eventually differentiate into osteogenic linage. This unique presentation of gentamicin on surfaces provides increased antimicrobial activity while still maintaining the ability for mammalian cells to attach to the surface. By using co-culture to test antimicrobial activity, the "race to the surface" between the bacteria and mammalian cells could be evaluated. On the gentamicin-modified surfaces, the adipose-derived stem cells won the race to the surface against *S. aureus*.

Improving the antimicrobial properties of surfaces for orthopedic implants while maintaining the ability for cells to attach to the surface, is still a major problem. Throughout this work we looked at the problem of increasing mineralization, finding that BMP-2-modified nanostructured surfaces can help to increase osseointegration of the surfaces. When looking at

antimicrobial surfaces, we found that *iota*-carrageenan/chitosan and pectin/chitosan create a surface environment favorable to mammalian cell attachment and proliferation while also inhibiting bacterial growth. Finally, we found that gentamicin-modified titania nanotubes influenced the race to the surface between *S. aureus* and hADSCs in favor of the mammalian cells. These surfaces, or a combination of them, could be applied to support and enhance healing of orthopedic implants. Dual-functioning antimicrobial surfaces that promote osteogeneses could dramatically reduce implant failure and the need for corrective surgery.

Future directions of this work start with the combination of chapters 2 and 4, by combining BMP-2 and gentamicin modified titania nanotubes surfaces. These surfaces should be tested under similar co-culture conditions of chapter 4 of bacteria and mammalian cells while testing the antimicrobial and mineralization properties of these surfaces. These surfaces will also likely experience environments different from those studied in this work. This includes future work on co-culturing multiple mammalian cells with the bone marrow cells.

Vascularization is imperative to healthy bone.[28] Inclusion of vascular cells in co-culture with bone cells to study interactions between cells as well as surfaces influence on both cells types, could lead to surfaces that even better increase osseointegration.[28] Currently during total knee replacements tendons are cut to accommodate the implant.[29] While an increase in osseointegration is the goal, there is a chance of fibroblast cells colonizing the surface and the potential for scar instead of bone tissue formation.[30] Co-culturing fibroblast cells with bone cells, can better represent the environment and cell types the implants will encounter when implanted in the body, and the potential for scar tissue formation. Studying these cellular and surface interactions may better predict how the surface will perform *in vivo*. Finally, while nanotubes provide a suitable surface for studying *in vitro* and very small implants *in vivo* animal studies, it would be difficult

to scale up the anodization process for whole implant surfaces. Future work will need to be conducted on how to create nanotubes on a larger scale for human implant use.

REFERENCES

1. Mohammadi, M. *et al.* Fabrication of hybrid scaffold based on hydroxyapatite-biodegradable nanofibers incorporated with liposomal formulation of BMP-2 peptide for bone tissue engineering. *Nanomedicine Nanotechnology, Biol. Med.* **14**, 1987–1997 (2018).

2. Jeon, O., Song, S. J., Kang, S. W., Putnam, A. J. & Kim, B. S. Enhancement of ectopic bone formation by bone morphogenetic protein-2 released from a heparin-conjugated poly(l-lactic-co-glycolic acid) scaffold. *Biomaterials* **28**, 2763–2771 (2007).

3. Yamamoto, M., Takahashi, Y. & Tabata, Y. Controlled release by biodegradable hydrogels enhances the ectopic bone formation of bone morphogenetic protein. *Biomaterials* **24**, 4375–4383 (2003).

4. Hu, Y. *et al.* Regulation of the differentiation of mesenchymal stem cells in vitro and osteogenesis in vivo by microenvironmental modification of titanium alloy surfaces. *Biomaterials* **33**, 3515–3528 (2012).

5. Lai, M. *et al.* Surface Functionalization of TiO 2 Nanotubes with Bone Morphogenetic Protein 2 and Its Synergistic Effect on the Differentiation of Mesenchymal Stem Cells. *Biomacromolecules* **12**, 1097–1105 (2011).

6. Lee, D. W., Yun, Y. P., Park, K. & Kim, S. E. Gentamicin and bone morphogenic protein-2 (BMP-2)-delivering heparinized-titanium implant with enhanced antibacterial activity and osteointegration. *Bone* **50**, 974–982 (2012).

7. Bishop, G. B. & Einhorn, T. A. Current and future clinical applications of bone morphogenetic proteins in orthopaedic trauma surgery. *Int. Orthop.* **31**, 721–727 (2007).

8. Hustedt, J. W. & Blizzard, D. J. *The Controversy Surrounding Bone Morphogenetic Proteins in the Spine: A Review of Current Research*. *YALE JOURNAL OF BIOLOGY AND MEDICINE* **87**, (2014).

9. Ong, C. T., Choon, D. S. K., Cabrera, N. P. & Maffulli, N. The treatment of open tibial fractures and of tibial non-union with a novel external fixator. *Injury* **33**, 829–834 (2002).

10. U.S. Food and Drug Administration. *Infuse bone graft Important Medical Information*.

11. Zhao, B. *et al.* Heparin Potentiates the in Vivo Ectopic Bone Formation Induced by Bone Morphogenetic Protein-2 *. (2006). doi:10.1074/jbc.M511039200

12. Ruppert, R., Hoffmann, E. & Sebald, W. Human bone morphogenetic protein 2 contains a heparin-binding site which modifies its biological activity. *Eur. J. Biochem.* **237**, 295–302

(1996).

13. Popat, K. C., Leoni, L., Grimes, C. A. & Desai, T. A. Influence of engineered titania nanotubular surfaces on bone cells. *Biomaterials* **28**, 3188–3197 (2007).

14. Ballo, A., Agheli, H., Lausmaa, J., Thomsen, P. & Petronis, S. Nanostructured model implants for in vivo studies: influence of well-defined nanotopography on de novo bone formation on titanium implants. *Int. J. Nanomedicine* **6**, 3415–3428 (2011).

15. Martins, A. F. *et al.* Chitosan/iota-carrageenan and chitosan/pectin polyelectrolyte multilayer scaffolds with antiadhesive and bactericidal properties. *Appl. Surf. Sci.* **502**, 144282 (2020).

16. Vacheethasanee, K. & Marchant, R. E. Surfactant polymers designed to suppress bacterial (Staphylococcus epidermidis) adhesion on biomaterials. *J. Biomed. Mater. Res.* **50**, 302–312 (2000).

17. Trujillo, N., Popat, K., Trujillo, N. A. & Popat, K. C. Increased Adipogenic and Decreased Chondrogenic Differentiation of Adipose Derived Stem Cells on Nanowire Surfaces. *Materials (Basel).* **7**, 2605–2630 (2014).

18. Campoccia, D., Montanaro, L. & Arciola, C. R. The significance of infection related to orthopedic devices and issues of antibiotic resistance. *Biomaterials* **27**, 2331–2339 (2006).

19. Arciola, C. R., Radin, L., Alvergna, P., Cenni, E. & Pizzoferrato, A. Heparin surface treatment of poly(methylmethacrylate) alters adhesion of a Staphylococcus aureus strain: utility of bacterial fatty acid analysis. *Biomaterials* **14**, 1161–1164 (1993).

20. Tavaria, F. K. *et al.* Chitosan: antimicrobial action upon staphylococci after impregnation onto cotton fabric. *J. Appl. Microbiol.* **112**, 1034–1041 (2012).

21. Mansilla, A. Y. *et al.* Evidence on antimicrobial properties and mode of action of a chitosan obtained from crustacean exoskeletons on Pseudomonas syringae pv. tomato DC3000. *Appl. Microb. Cell Physiol.* **97**, 6957–6966 (2013).

22. Tam, V. H., Kabbara, S., Vo, G., Schilling, A. N. & Coyle, E. A. Comparative Pharmacodynamics of Gentamicin against Staphylococcus aureus and Pseudomonas aeruginosa. *Antimicrob. Agents Chemother.* **50**, 2626–2631 (2006).

23. Miglioli, P. A., Silini, R., Carzeri, O., Grabocka, E. & Allerberger, F. Antibacterial activity of gentamicin and ciprofloxacin against gram-negative bacteria: Interactions with pig and calf sera. *Pharmacol. Res.* **39**, 321–323 (1999).

24. Kovacik, A. *et al.* In Vitro Assessment of Gentamicin Cytotoxicity on the Selected Mammalian Cell Line (Vero cells). *Adv. Reserach Life Sci.* **1**, 111–116 (2017).

25. Stigter, M., Bezemer, J., De Groot, K. & Layrolle, P. Incorporation of different antibiotics into carbonated hydroxyapatite coatings on titanium implants, release and antibiotic efficacy. *J. Control. Release* **99**, 127–137 (2004).

26. Campos, M. G. N. *et al.* In vitro gentamicin sustained and controlled release from chitosan cross-linked films. *J. Mater. Sci. Mater. Med.* **20**, 537–543 (2009).

27. Wigmosta, T. B., Popat, K. C. & Kipper, M. J. BMP -2 Delivery from Polyelectrolyte Multilayers EnhancesOsteogenic Activityon Nanostructured Titania . *J. Biomed. Mater. Res. Part A* 1–10 (2020). doi:10.1002/jbm.a.37109

28. Ngel, A. ´ *et al.* Vascularization in Bone Tissue Engineering Constructs. *Ann. Biomed. Eng.* **43**, 718–729 (2015).

29. Engh, G. A., Holt, B. T. & Parks, N. L. A Midvastus Muscle-splitting Approach for Total Knee Arthroplasty. *J. Arthoplasty* **12**, 322–331 (1997).

30. Cohen, A., Liu-Synder, P., Storey, D. & Webster, T. J. Decreased fibroblast and increased osteoblast functions on ionic plasma deposited nanostructured Ti coatings. *Nanoscale Res. Lett.* **2**, 385–390 (2007).

APPENDIX A: SUPPLEMENTAL FIGURES FOR CHAPTER 3

.

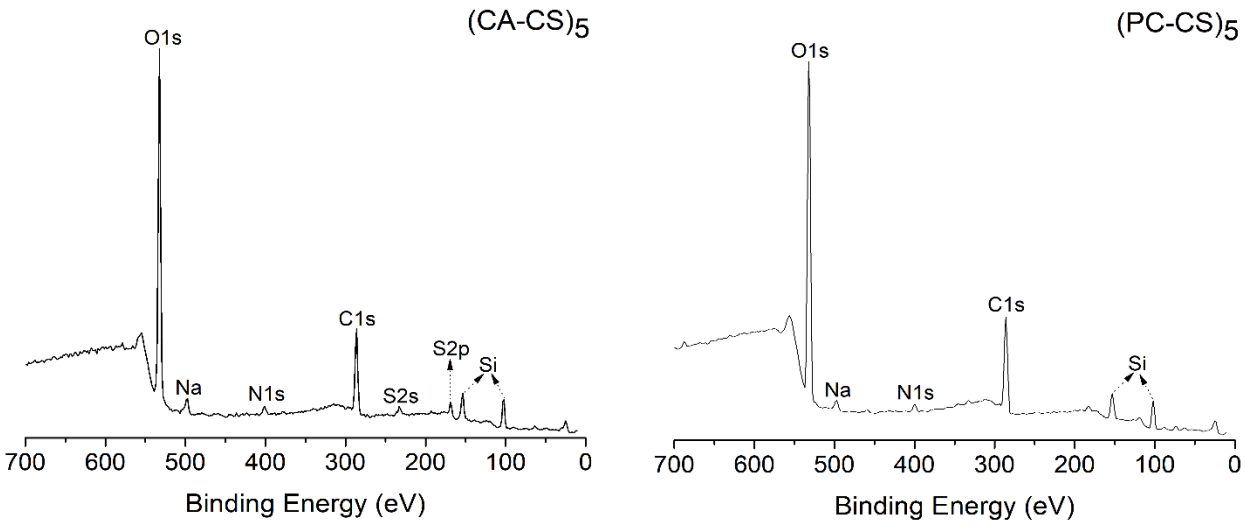

Figure A1. Survey XPS spectra of the PEMs build up with 5-layers.

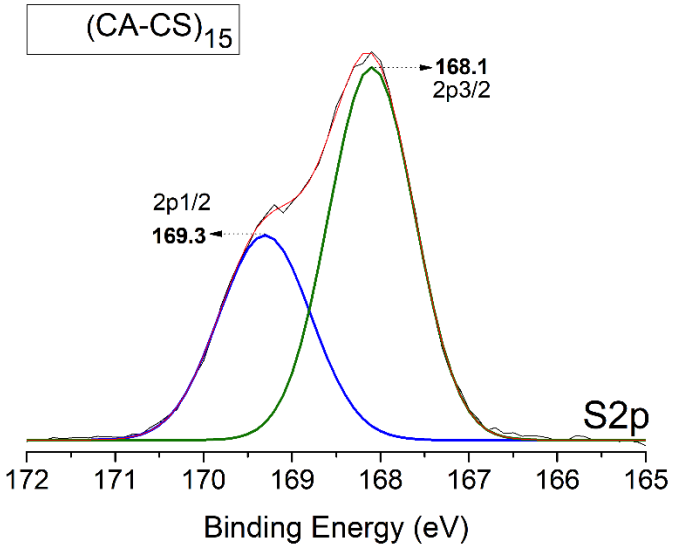

Figure A2. High resolution XPS spectra of the sulfur envelope (S2p).

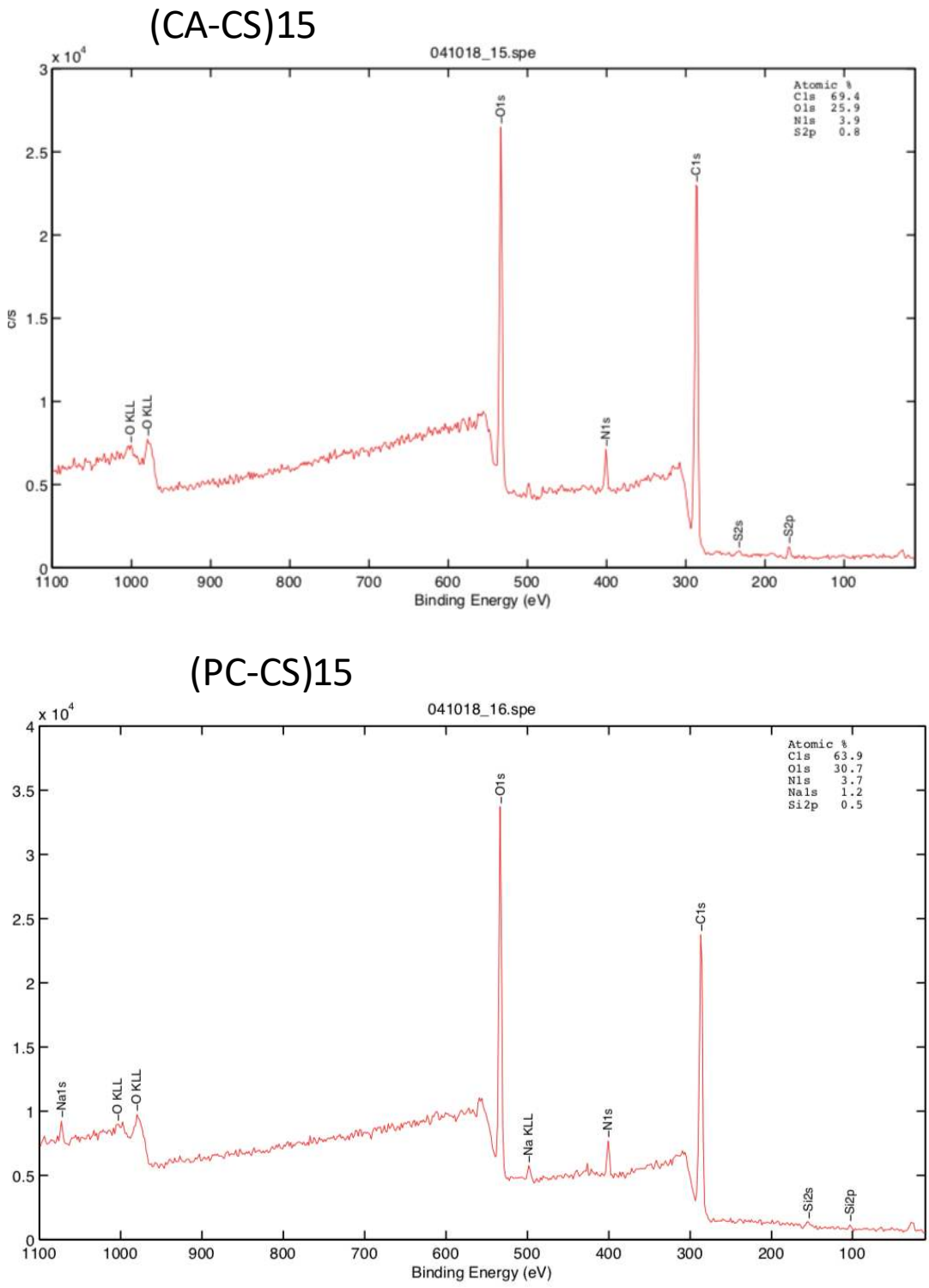

Figure A3. Survey XPS spectra of the PEMs obtained after stability test in PBS.

APPENDIX B: ANALYSIS OF BACTERIA AND MAMMALIAN CELL NUCLEI.

To determine the amount of bacteria and mammalian cells on samples, the percent area of total blue was calculated. Then percent area blue of the mammalian cell was calculated and subtracted from the total blue, to determine the amount of area the bacteria nuclei took up. This was done using 10× images, but the example here is on a 20× to better illustrate the process (Figure S1). First in ImageJ the red image (image A) was converted to a 32-bit image (image B). Then the brightness was increased (Image C). This was repeated with the blue image (image D) to get image F. Then image A and F were combined to get the new image with a more robust red (image G). Blue in the red areas was determined to be hADSC nuclei not bacteria. The threshold for image F was adjusted to produce image H. Then the measure tool was used to calculate the total percent area of the image. Then the same measure tool was used on the red areas in image H. These areas were added up and considered the % area hADSC nuclei. This was subtracted from the total area to determine the % area *S. aureus* nuclei.

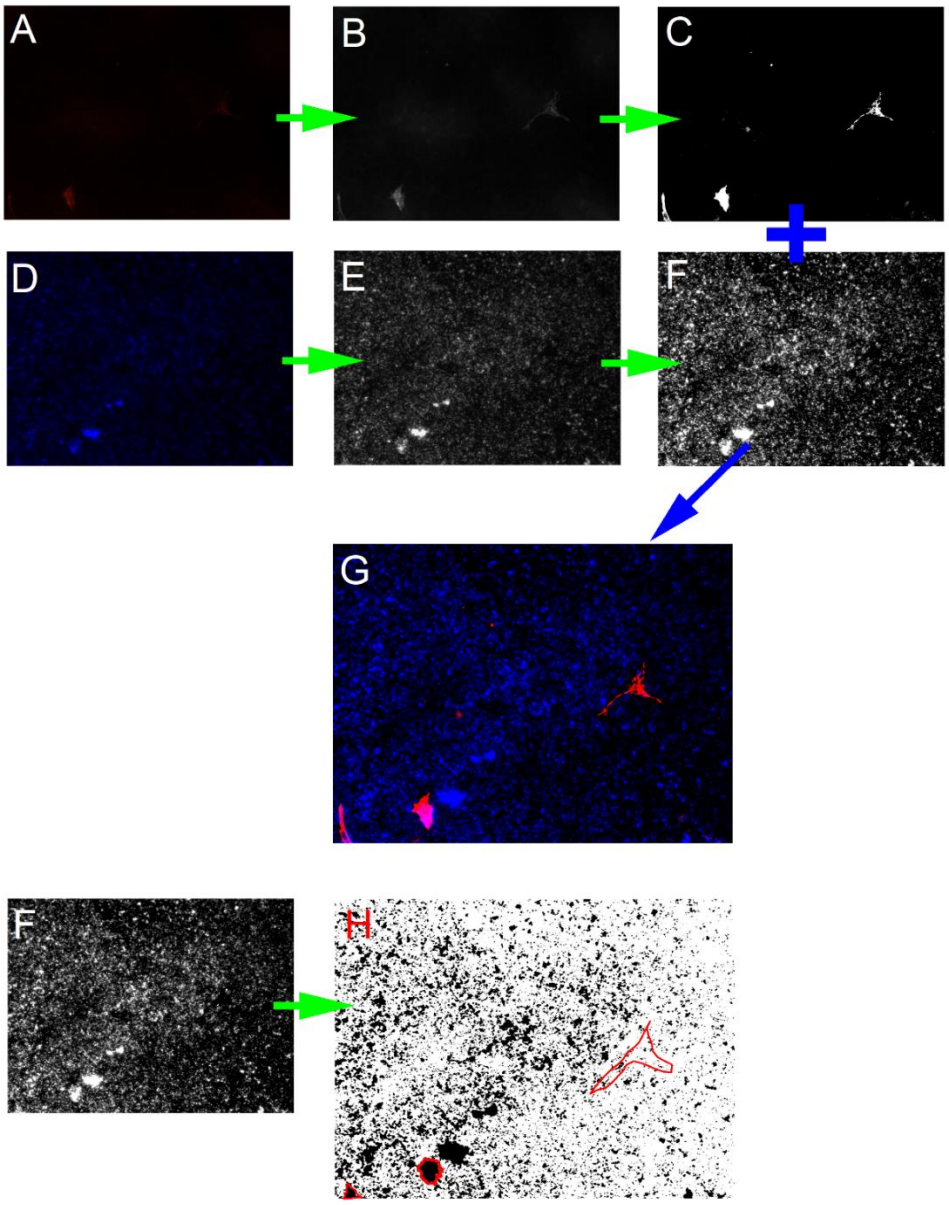

Figure B1. Example 20× image of a Nt samples. Image A and D are the original red and blue images respectively. Image B and E are image A and D respectively converted to 32-bit images. Images C and F are images B and E respectively with the brightness and contrast adjusted. Image G is the combination of C and F. Image H is image F after the threshold has been adjusted, the red areas represent areas that had red stain in image G. Nt, nanotubes.